Urban Water Research Association of Australia

Modelling and Design of Reservoir Aeration Destratification Systems

D.P.Lewis, J.C.Patterson, J.Imberger, R.P.Wright & S.G.Schladow
Centre for Water Research
University of Western Australia

Research Report No.23
April 1991

Published for the Urban Water Research Association by the Melbourne and Metropolitan Board of Works.

ISBN 1 875298 23 1

Cover design by Gregory R Smith

FOREWORD AND ACKNOWLEDGEMENTS

This report is based on UWRAA Research Projects No WS-2 and No WS-15: 'Evaluation of Aeration/Destratification of Reservoirs, Stages 1 and 2 (respectively)'.

The report is the second of three scheduled reports on these projects. The first report "Review of Artificial Destratification of Water Storages in Australia" was prepared by the Water Authority of Western Australia (WAWA) and published in December 1989 as UWRAA Research Report No 9. The third and final report, presently being prepared by WAWA, will describe detailed water quality studies of the implementation of aeration/destratification strategies in a reservoir with water quality problems.

Organisational responsibility for the project reported herein was as follows:

Sponsoring Authority	:	Water Authority of Western Australia
Research Agency	:	Coastal and Hydraulic Engineering Laboratory Centre for Water Research University of Western Australia
Project Officer	:	Mr D Lewis Centre for Water Research
Principal Researchers	:	Mr D Lewis Associate Professor J Patterson Professor J Imberger Ms R Wright Dr S G Schladow Centre for Water Research
Review Panel	:	Dr B Kavanagh Water Authority of Western Australia Professor J Imberger Centre for Water Research

The projects were funded by the Urban Water Research Association of Australia, the Water Authority of Western Australia, and by the Centre for Environmental Fluid Dynamics and the Centre for Limnological Modelling at the University of Western Australia.

SYNOPSIS

This report describes the results of a study programme directed at improving design methods for air bubbler destratification systems for reservoirs. The study consisted of laboratory and field investigations; further development of the bubble plume algorithm installed in the reservoir simulation model DYRESM; validation of the model against specific laboratory data and against field data from the Harding Dam in the northwest of W.A.; formulation of a design procedure; design of an aeration system for Harding Dam; monitoring of the aerator performance and validation of the simulation algorithm against this field data; and recommendations regarding future operation of the system in Harding Dam in the light of the observed and simulated bubbler performance.

The laboratory investigations identified a parameter, the plume number, for which the efficiency of destratification was a maximum. This plume number includes the effects of the stratification, the air flow rate and the reservoir depth, based on the performance of a single source bubble plume. If the plume number is larger than the optimum value, there is insufficient air flow for the water from the deep part of the reservoir to be carried to the surface; if the number is smaller than the optimum value, there is more air supplied than is required. In either case, the efficiency of energy conversion from that input by the air flow to mixing is not optimal. For each stratification and water depth, there is therefore an optimum air flow rate. Plume theory also indicates that the total entrainment from a number of sources is greater than that for a single source with the same total air flow rate.

The bubble plume simulation algorithm included in the reservoir simulation model DYRESM was validated against the laboratory data and limited field data obtained in Wungong and Harding Dams in W.A. The model was used to design an aeration system for Harding Dam, based on principles that are applicable for all reservoirs. Most designs will depend, however, on the operating criteria specified by the operating authority. These could include maintenance of a destratified condition over seasonal time scales, rapid destratification of an initially stratified reservoir, or maximising the efficiency of energy conversion to achieve these or other goals.

The Harding Dam aerator was installed and monitored during 1989. The design was partially successful in destratifying the reservoir, and after evaluation and modification of the model using the intensive data set gathered during the period of operation, modification of the design was recommended. The modified aeration model was shown to be a reliable tool for designing reservoir destratification systems. The model is a significant improvement over current design methodologies as it allows the designer to evaluate alternative design strategies under temporally varying conditions. The model makes it possible for the operator to adjust the aeration strategy to suit the changing conditions so that increased destratification efficiencies may be achieved.

TABLE OF CONTENTS

LIST OF TABLES

LIST OF FIGURES

CHAPTER 1

INTRODUCTION

The vertical density stratification observed in most Australian lakes and reservoirs is a natural occurrence resulting from solar radiation penetrating the water surface during the summer months. This creates a temperature and density structure characterised by a surface mixed layer separated from the deeper hypolimnion waters by a strong gradient in both temperature and density. This gradient zone is known as the metalimnion. The metalimnion acts as a barrier preventing active exchange between the surface and the hypolimnion, leading to seasonal deoxygenation of the hypolimnion, and thereby contributing to the deterioration of the quality of the hypolimnion waters. This deterioration may be reflected in the increased release of undesirable substances from the sediments of the reservoir (such as iron and manganese) or increased algae populations.

Artificial destratification of the water column is a common means of addressing these water quality problems, with the most popular method of destratification being aeration. In this method, a source of compressed air is pumped to the bottom of the reservoir and released through some form of diffuser pipe. The resultant buoyant plume carries relatively heavy water towards the surface to be ejected at a level at which it is negatively buoyant, causing local mixing as it falls back through the density field. In this way, the density structure of the water column is dismantled allowing oxygenation of the bottom waters of the storage as the hypolimnion waters are mixed and exchanged with water in the surface mixed layer. The application of the compressed air in itself does not transfer any significant amount of oxygen to the bottom waters of the storage.

Artificial destratification of reservoirs by aeration was introduced into Australia in the mid-1960's. Aeration has since been used as a water quality management technique in many storages throughout Australia. As part of this research project, McAuliffe and Rosich (1989) carried out a review of artificial destratification of water storages, carefully documenting over 50 applications of destratification in Australia. McAuliffe and Rosich (1989) concluded that, for the most part, artificial destratification in Australia has had only limited success in alleviating water quality problems.

The effectiveness of artificial destratification through aeration is measured not only in terms of the method's success in overcoming a specified water quality problem but also in terms of the cost associated with implementing the method as compared to alternative management options. Both of these issues are critically dependent upon the effectiveness and efficiency of the destratification procedure which, in turn, are dependent upon the degree of stratification, the buoyancy input to the storage via the aerator, and the efficiency with which the buoyant plume entrains the hypolimnetic water.

Existing design procedures and operational strategies for aeration systems are inadequate. The design rules in general use (for example, those given by Davis, 1980) are empirically based on energy considerations. They place little emphasis on the dynamics of the buoyant air-water plume mixture or how the energy is transferred from buoyancy to a change in the potential energy of the water column. These design rules assume some mean efficiency of destratification which ignores the changing conditions in the reservoir. The method proposed by Davis, for example, assumes a constant 5% efficiency. This has been shown by Patterson and Imberger (1989) to be, at times, substantially lower than the efficiencies capable of being developed by carefully designed and operated aerators.

The aim of this component of the research project "Aeration/Destratification of Reservoirs" was to address this shortcoming in the existing procedures for the design of reservoir aeration destratifications systems. The work described by Patterson and Imberger (1989) showed that a simple model of the dynamics of a bubble plume incorporated in the one dimensional reservoir dynamics simulation model DYRESM allowed the design of aeration systems with efficiencies approaching 15%.

This report is titled "Modelling and design of reservoir aeration destratification systems". The work was separated into two stages, each comprising two major components. Stage 1A, set out in Chapter 2, describes the implementation of the bubble plume model in DYRESM and a recommended procedure for the design of aeration systems. Although much of this work is based on the previous results of Patterson and Imberger (1989), further laboratory and numerical experiments examining the dynamics of buoyant plumes in stratified environments are described. Stage 1B of the project (Chapter 3) describes the application of the model to the design of an aerator for installation in Harding Dam in the north-west of Western Australia. This dam was used as a test site through the course of the study for the application and assessment of the model. Chapter 4 sets out the results of Stage 2A of the project. This essentially consisted of the evaluation of the aeration model with subsequent modification of the model to overcome various shortcomings identified during the evaluation process. Stage 2B (Chapter 5) describes the application of the modified model to improve the design of the Harding Dam aerator. A number of recommendations relating to the future operation of the system are discussed.

The study describes the formulation, implementation, evaluation and modification of a model incorporating the effects of a buoyant bubble plume in a stratified reservoir. The model is structured to allow simple application to the design of aeration systems. The model is a significant improvement over existing design methodologies as it allows the designer to evaluate alternative aeration strategies based on data appropriate to the reservoir in question. The model makes it possible for the operator to adjust the aeration strategy to suit changing conditions so that destratification efficiencies of up to 15% may be achieved.

CHAPTER 2

STAGE 1A : IMPLEMENTATION OF THE AERATION MODEL FOR DESIGN

Stage 1A of the research project consisted of three activities aimed at verifying the existing aeration model for the design of efficient reservoir aeration systems. A series of laboratory experiments were carried out to determine the efficiency of energy conversion associated with bubble plumes rising through linearly stratified and layered water bodies. The aeration algorithm installed in the one-dimensional DYRESM model was then reviewed and validated against existing data to check its accuracy in simulating the behaviour of a bubble plume. Finally, a procedure was presented for the design of efficient aeration systems based on the one-dimensional simulation model.

2.1 Laboratory Experiments

A series of laboratory experiments investigating the behaviour of bubble plumes in stratified conditions were completed in 1988 and 1989 by Dr. Takashi Asaeda, of the University of Tokyo, under the direction of Professor Jörg Imberger. The experiments aimed first, to explain the changes in plume flow behaviour under varying aeration configurations and degrees of stratification; and second, to describe the variation in the efficiency of energy conversion from the input of buoyancy to changing the potential energy of the water column. The experiments were initially carried out in a one metre square glass tank containing water to a depth of 80 cm. These experiments are described in detail in Asaeda and Imberger (1990). Further experiments completed in 1989 used a two metre square tank with a water depth of 1.8 metres. These experiments aimed to describe the effects of bubble size and bubble concentration on the flow behaviour and efficiencies observed in the smaller scale tests. The results of the second set of experiments are described by Asaeda, Ikeda and Imberger (1990).

2.1.1 Bubble plumes in a linearly stratified water body

Air bubbles released into a linearly stratified water body (i.e. a water column with a constant density gradient) have been shown to entrain the surrounding water and carry it up as an air-water mixture. At some level, the increased negative buoyancy flux of the entrained water leads to detrainment of water outwards, away from the rising plume. This detrained water forms an annular downward flow immediately outside the inner upward moving plume. This downdraft continues to

plunge downwards until it reaches a level of neutral buoyancy, whereupon a horizontal intrusion forms. The inner core of the plume continues to rise towards the surface, with the air bubbles still supplying positive buoyancy. Additional sub-surface intrusions may form if the stratification is sufficiently strong. At the water surface, the flow spreads outward to a certain radius at which point the heavier water plunges. This submergence is the beginning of a falling plume that again propagates downwards to a level of neutral buoyancy where another intrusion is formed (see Fig. 2.1).

Three types of intrusions were shown to form from the plunging downdrafts: a single intrusion, multiple intrusions and unsteady intrusions (Asaeda and Imberger, 1990); the form of the intrusion is dependent upon the plume number P_N, and the bubble Reynolds number Re, defined as:

$$P_N = \frac{N^3 H^4}{Q_B g} , \tag{2.1}$$

$$Re = \frac{W_s^3}{g\nu} , \tag{2.2}$$

given that

$$N^2 = - \frac{g}{\rho_o} \frac{d\rho}{dz} , \tag{2.3}$$

where N is the Brunt Vaisala frequency, ρ_o is the water density, H the total water depth, Q_B the air flow rate (at atmospheric pressure), W_s the rise velocity of air bubbles in still homogeneous water, g the gravitational acceleration, ν the fluid kinematic viscosity, and z the upwards direction.

For the generalised case, Schladow and Patterson (1990) have shown that the plume number must include an additional term accounting for air bubble compression. This term is dependent upon the depth of water above the buoyancy source relative to atmospheric pressure, with the plume number then being defined :

$$P_N^* = \frac{N^3 H^4}{Q_B g} \left(\frac{H + h_a}{h_a} \right) \tag{2.4}$$

where h_a is the atmospheric pressure head (approximately 10.2 metres).

The total water depth H in the laboratory experiments was sufficiently small (ranging from 0.6 to 1.8 metres) that the air bubble compression term$\{(H + h_a) / h_a\}$ could be ignored. Asaeda and Imberger (1990) then showed that for a constant bubble size of around 1.0 mm, the flow behaviour and plume shape in the shallow laboratory experiments were dependent primarily on the plume

number P_N. In these experiments, both the air flow rate, Q_B, and the buoyancy frequency, N, were varied.

For very large air flow rates a single horizontal intrusion was observed at the surface (Fig. 2.1). As the air flow rate was decreased, however, the buoyancy flux became too small to carry the lower fluid to the surface and multiple intrusions were observed to form, exiting the downdraft region at equally spaced intervals. At very low air flow rates the intrusions became unsteady and poorly defined. It was shown that, in the limit of small Reynolds numbers, single intrusions formed when P_N was less than 300; multiple intrusions formed when P_N was in the range 300 to around 2000; while the intrusions were poorly defined for P_N greater than 2000. Figure 2.2 shows how the flow types vary with the dimensionless parameters P_N and Re. The right-hand side of the figure (where P_N is large) represents the condition in which the stratification is strong relative to the buoyancy input, while for small P_N (the left-hand side of the figure), the flow in the bubble plume is energetic relative to the stratification.

2.1.2 Bubble plumes in a two-layered water body

An additional set of experiments was carried out with a bubble plume released into a two layer water body with a sharp density interface. The air bubbles again had a diameter of about 1.0 mm. Two distinct flow regimes were observed; first, where the lower layer plume penetrated the interface and continued to the surface; and second, where the lower layer plume did not fully penetrate the density interface.

It was evident that when the air flow rate was high relative to the degree of stratification, the air-water mixture penetrated the interface and rose to the free surface, forming a column of rising and falling water in the upper layer (Fig 2.3a). The column in this upper layer consisted of many large eddies which entrained the surrounding water. On the other hand, with a low air flow rate relative to the stratification, the lower layer water formed a dome-like swell at the interface as the upward momentum induced by bubbling was insufficient to penetrate the interface (Fig. 2.4a).

Following similar arguments as those used for linear stratification, the flow in the shallow two layer case may be described by the parameter:

$$P_\Delta = \frac{g'^{3/2} h_l^{3/2}\, H}{g\, Q_B} \left(\frac{h_u}{H}\right)^3 , \qquad (2.5)$$

where h_l and h_u are the lower and upper layer depths respectively, H is the total depth and g' is the reduced acceleration due to gravity, where

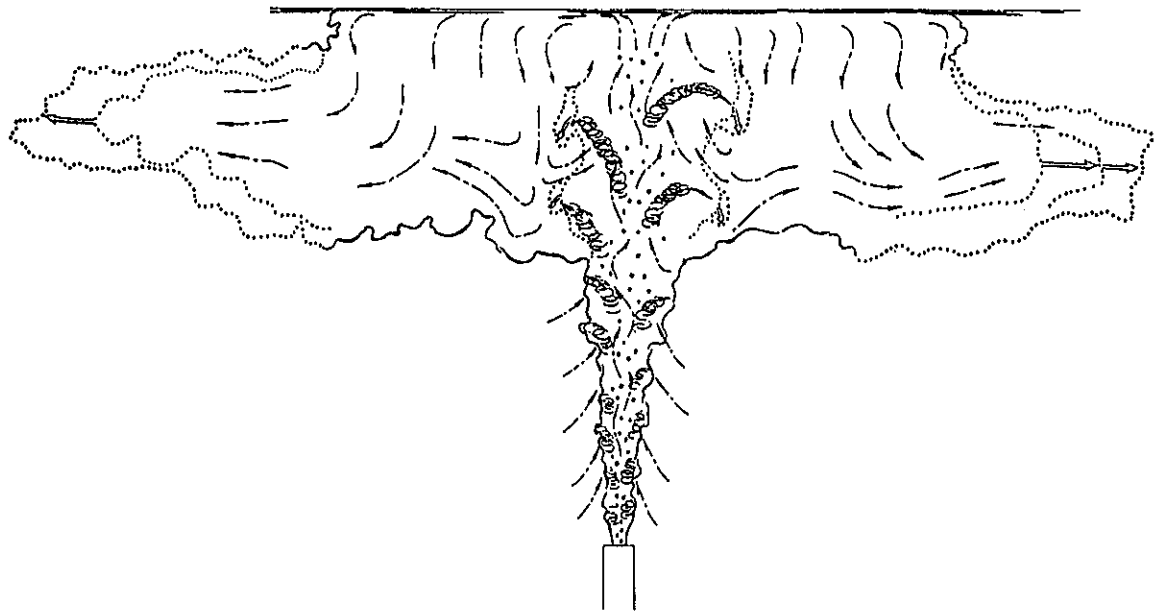

Figure 2.1 Typical flow pattern associated with a rising air-water mixture ($P_N < 300$).

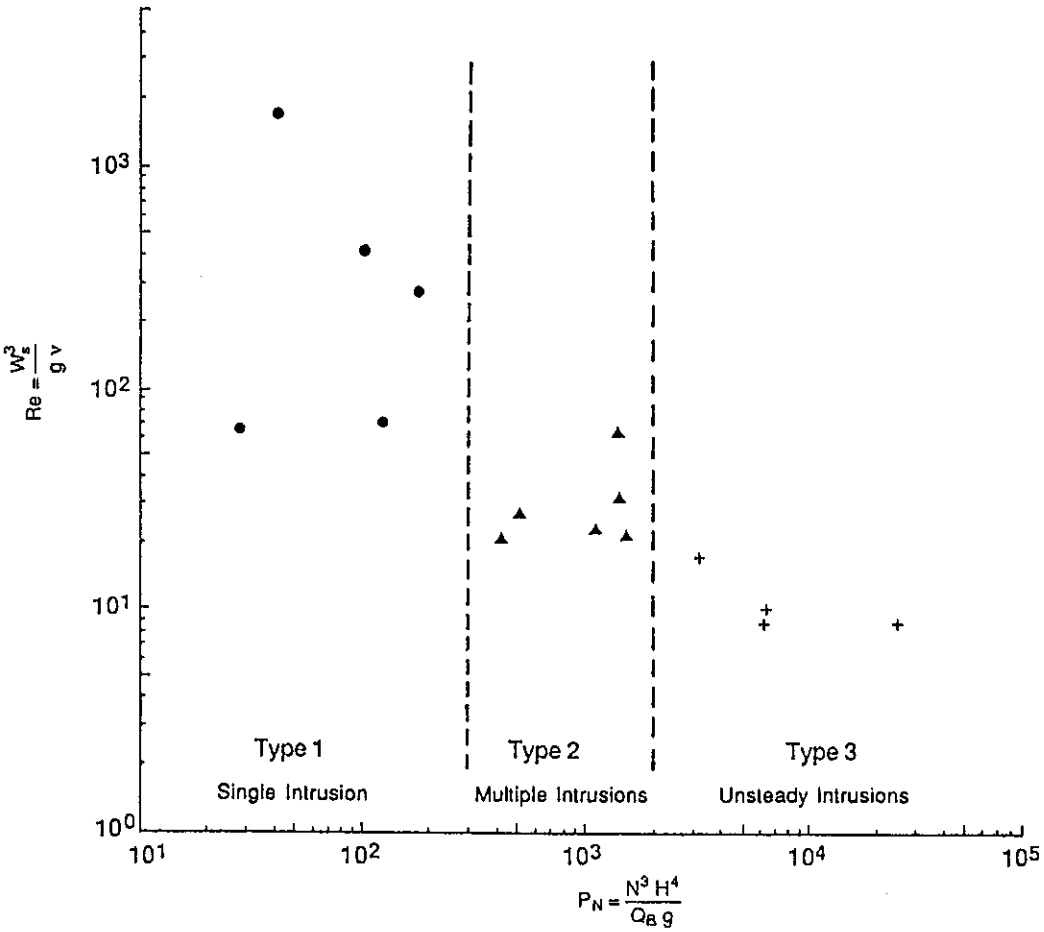

Figure 2.2 Distribution of flow types in linearly stratified conditions (expressed in terms of the non-dimensional parameters P_N and Re).

$$g' = \left(\frac{\rho_l - \rho_u}{\rho_l}\right) g \tag{2.6}$$

and ρ_l and ρ_u are the upper and lower layer densities respectively. As before, the plume number P_Δ must include the air bubble compression term when the bubbles are released in deep water bodies.

The boundary between the two flow regimes described above occurred when P_Δ was approximately 30. When P_Δ was less than 30 (the condition of high air flow and weak stratification) the flow structure appeared as illustrated in Fig. 2.3a. In this case, the bubble plume broke through the interface, and actively mixed with the water from the upper layer. The mixture was carried to the free surface, where it spread horizontally and ultimately plunged back towards the interface. The intrusion created by this flow propagated across the tank immediately above the interface. The thickness of the intrusion in the two-layer stratified case was smaller and propagated faster than was observed in the linear stratification experiments. The corresponding changes in the density profile, shown in Fig. 2.3b, demonstrated a relatively uniform density change in the upper layer, indicating extensive mixing, with the interface broadening with time as the intrusion propagated over the interface.

Figure 2.4a illustrates the flow pattern for P_Δ greater than 30 where the air flow rate was low relative to the degree of stratification. The plume generated by the rising air bubbles formed many dome-like eddies immediately above the interface. Fragments of the lower fluid were occasionally torn off from the domes by the rising bubbles. These were rapidly mixed with the surrounding fluid as they were lifted to the surface. The amount of fluid mixed in this way increased with increasing air flow. Additional mixing was caused by the dome-like eddies rising slightly above the interface and entraining some of the upper layer fluid. The amount of water entrained in this manner was much smaller than the previous case, so the horizontal intrusion formed by this mixed water propagated underneath the interface and produced a broad layer of intermediate water within the lower layer. The area near the dome was a region of flow divergence, leading to a general spreading of the bubble core. Above the interface, the bubble core contracted again, re-establishing a well defined rising plume (see Fig. 2.4a). As shown in Fig. 2.4b, the rate of change of the density structure was small, highlighting the very weak exchange between the two layers.

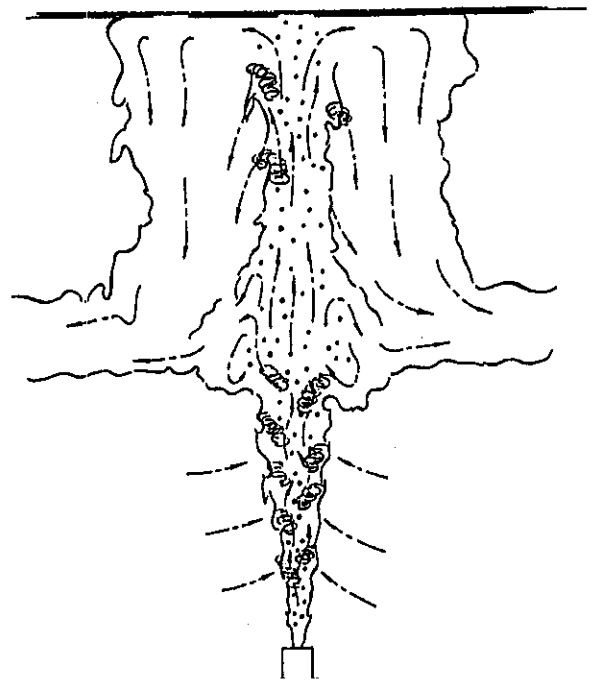

Figure 2.3a Typical flow pattern for $P_{\Delta} < 30$ (high air flow rate; weak stratification).

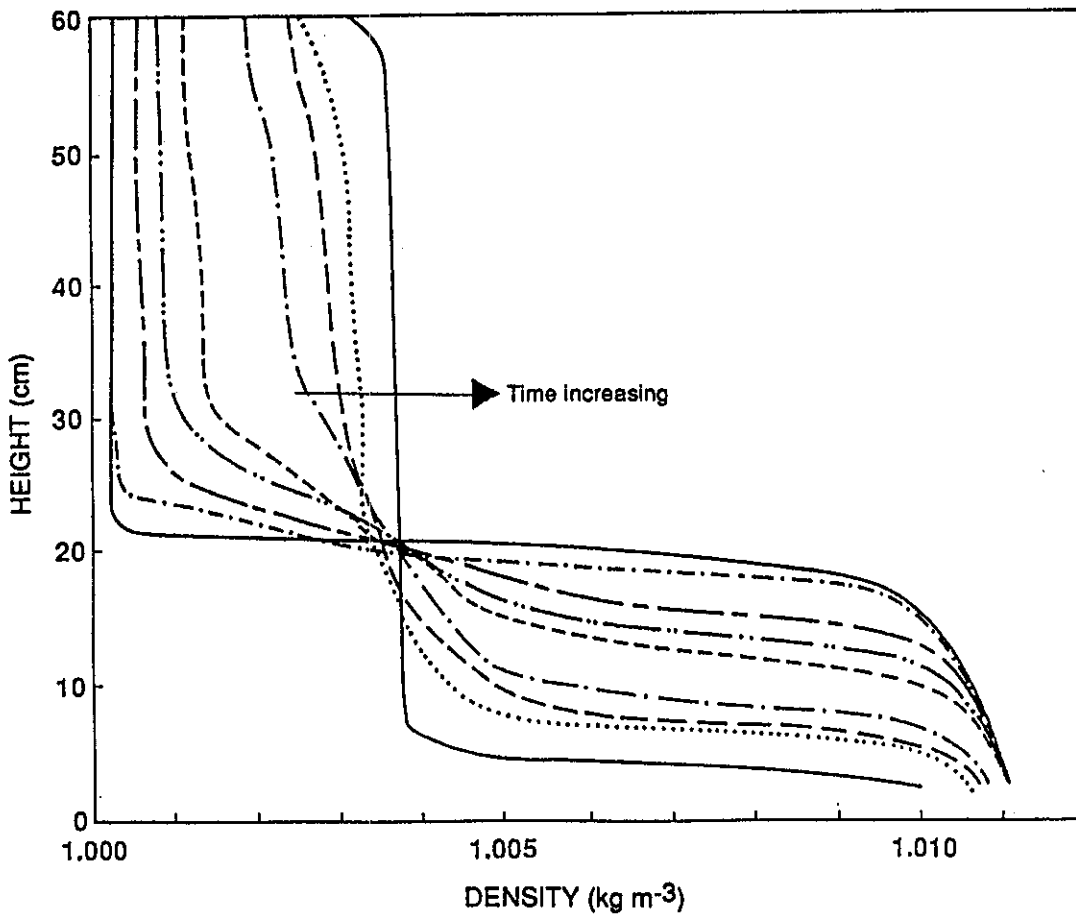

Figure 2.3b Variation of the density profile with time for $P_{\Delta} < 30$.

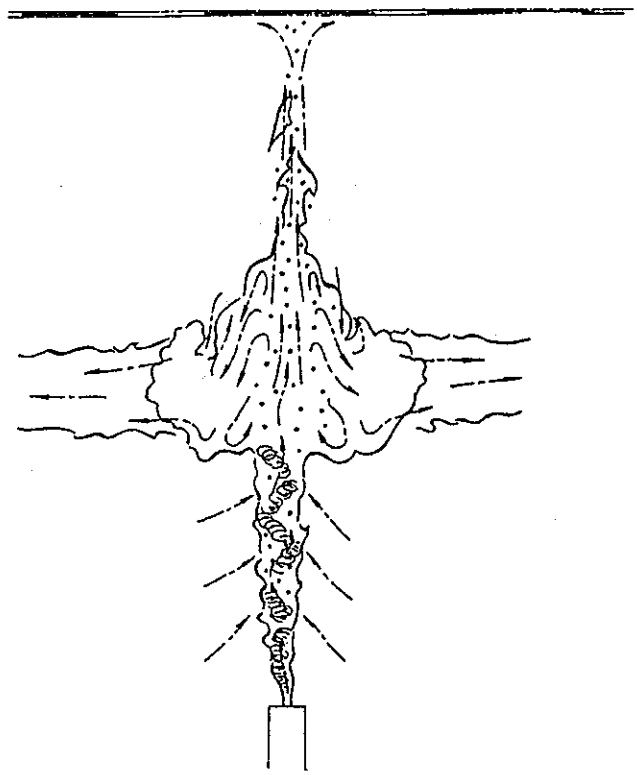

Figure 2.4a Typical flow pattern for $P_{\Delta} > 30$ (low air flow rate; strong stratification).

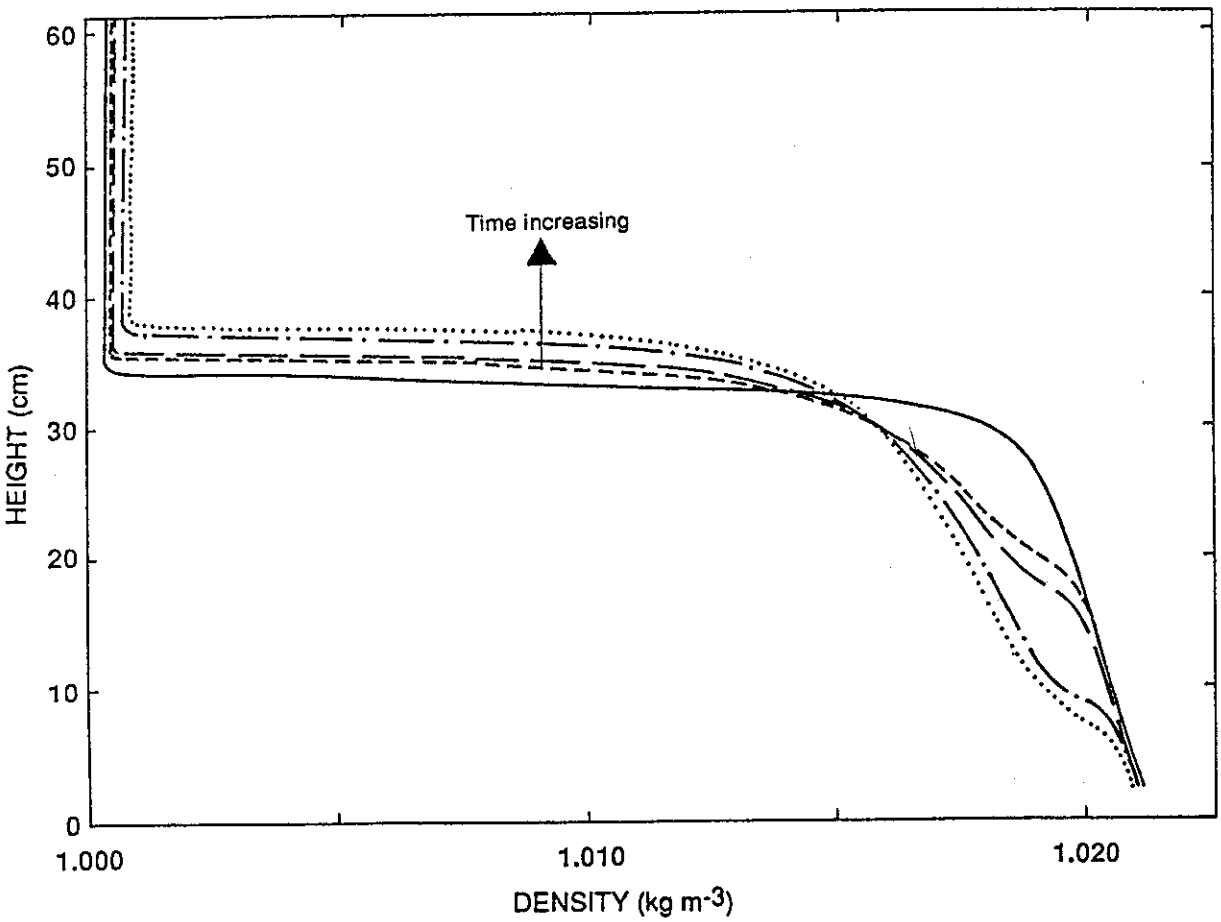

Figure 2.4b Variation of the density profile with time for $P_{\Delta} > 30$.

2.2 Implementation of the Aeration Algorithm in DYRESM

The one dimensional dynamic reservoir simulation model DYRESM is a numerical model used for the prediction of the vertical distribution of temperature and salinity in lakes and reservoirs of medium size (see Imberger and Patterson, 1981). The model is based on a Lagrangian layer scheme in which the lake is represented by a series of horizontal layers each of uniform property but variable thickness. The position, and therefore the thickness of the layers, may change as inflow or outflow modify the lake volume. Individual layer thicknesses are determined to give a resolution appropriate to the process acting on the layers at each time step. The time step itself is variable between 15 minutes and 12 hours, depending on the time scale of the process operating. Thus, the model is able to resolve time scales down to 15 minutes and length scales down to a few centimetres. The model utilises such fine resolutions only when and where necessary, thus providing an accurate yet computationally efficient simulation model.

In DYRESM, surface layer deepening is energised by penetrative convection, wind stirring at the surface, and shear induced turbulence at the base of the surface layer. Turbulent transport in the hypolimnion is modelled using a diffusion-like process with eddy diffusivities based on the local density gradient and the rate of dissipation of turbulent kinetic energy. Inflow and outflow are confined to narrow regions adjacent to the insertion and offtake levels. Imberger and Patterson (1981) provide a detailed description of the parameterization of these processes and a general description of the model. The conditions for which the one dimensional assumption is applicable are discussed by Patterson *et al.*, (1984).

An algorithm describing the behaviour of bubble plume aerators, patterned on a simple integral plume model, was recently incorporated into DYRESM. The initial development of the algorithm was in the context of the one dimensional model and its application to Myponga Reservoir, as described by Patterson and Imberger (1989). The model closely reproduced the thermal structure of the reservoir over a year long simulation, indicating that the algorithm successfully captured the fundamental dynamics of the buoyant plume and its interaction with the other mixing processes controlling the thermal structure of the reservoir. Although this original algorithm has been upgraded during the course of this research project (see Chapter 4), the fundamental concepts remained unchanged.

The algorithm is based on the assumption that the rising bubbles from each hole in the aerator may be considered as a source of buoyancy, and that each plume may be modelled as a simple buoyant plume with a density equal to the density of the air-water mixture (McDougall, 1978). As the plume rises through the decreasing density of the ambient stratification, it entrains water from the environment, increasing the air-water mixture density. This causes the plume water to slow down until it reaches a level at which the mixture can no longer rise and, as observed in the laboratory

experiments, the plume detrains. The detrained water no longer contains the air and is therefore locally heavy; it falls to the level of neutral buoyancy and intrudes horizontally. The level of intrusion will be above the aerator level as the plume has entrained lighter water from above the aerator and the detrained water density is therefore less than that at the level of the aerator. The reader is referred to Patterson and Imberger (1989) for further details describing the aeration algorithms.

The accuracy of the bubble plume algorithm has recently been further reviewed and validated by Schladow and Patterson (1990). To validate the algorithm it was separated from the DYRESM model so that the bubble plume dynamics could be studied in isolation from the other reservoir mixing processes embodied in the model. As a first step, the effect of bubble expansion was removed from the algorithm, thus converting the bubble plume into a simple, buoyant plume. A considerable body of theoretical and experimental results are available describing the behaviour of such plumes. In the first test, the bubble plume was released into a homogeneous water column. The rate of entrainment of ambient fluid (and hence the plume diameter) matched the theoretical result that the plume diameter was approximately 1.2 α times the height of rise of the plume, where α is the plume entrainment coefficient. In the second test, the bubble plume was released into a linearly stratified water column. Morton *et al.* (1956) derived a dimensionless height of rise of the entrained water X_1, dependent upon the initial buoyancy flux F_0 (given by the air flow rate Q_B) and the stratification N:

$$X_1 = 2^7 \frac{\pi^{0.25} \alpha^{0.5} N^{0.75}}{F_0^{0.25}} \tag{2.7}$$

Schladow and Patterson (1990) showed that the bubble plume algorithm matched the experimental result described by Equation (2.7), and that the height of rise X_1 was proportional to $(P_N^*)^{-1/4}$.

These first two tests confirmed that the plume number P_N^* could be used to classify the effect of an aerator when air bubble expansion was ignored. Bubble expansion was included in the algorithm for the third set of tests and the algorithm then run for a range of air flow rates, stratifications and water depths. Little theoretical or experimental data exist to test the model under these conditions, however, the results did follow the trends indicated by the modelling work of McDougall (1983).

The model showed that, under certain circumstances, the effect of bubble expansion on the buoyancy flux can be very important, with the detrainment height of the plume having a significant impact on the efficiency of energy conversion. This efficiency has been shown to be a critical factor in the design of bubble plume destratification systems. It is defined as the ratio of the change in potential energy (ΔE) of the water column over time (Δt) divided by the buoyancy energy supplied by the air bubbles :

$$\eta = \frac{\Delta E}{\rho Q_B g H \Delta t} \tag{2.8}$$

When the water depth H is small (i.e. the effect of bubble expansion may be ignored), the linearly stratified experiments described by Asaeda and Imberger (1990) showed that the efficiency of energy conversion varies as a function of the plume number P_N and the bubble diameter (Fig. 2.5). For 1.0 mm diameter bubbles, the efficiency appeared to increase with P_N until the plume number approached 2000 whereupon the efficiency decreased with increasing P_N. For the larger diameter bubbles (around 4.0 mm), the efficiency maximum occurred at a smaller value of P_N, around 300. The peak efficiency in the experiments appeared to approach 15% for the smaller diameter bubbles and 10% for the larger diameter bubbles.

These laboratory results indicated that the bubble diameter is likely to have some influence on the efficiency of destratification. This influence is reflected in the aeration model through the entrainment coefficient α. For a simple, single phase buoyant plume (i.e. with no air bubbles), α is generally assumed to be 0.0833 (List, 1982). This entrainment coefficient appears to be a satisfactory approximation except when the air-water mixture includes extremely large bubbles, where the entrainment coefficient tends towards zero.

Figure 2.6 plots two sets of simulation results encompassing the range of the laboratory experiments described in Fig. 2.5. To realistically simulate the laboratory conditions, both the bubble slip velocity and the effect of bubble expansion were ignored in the simulation runs. A large range of air flow rates were then simulated, starting with a fixed linear stratification. Each test result is denoted with a separate symbol in Fig. 2.6, where the efficiency of destratification (as defined by Equation 2.8) is plotted against the plume number.

The curve denoted by the open squares was generated using an entrainment coefficient of 0.0833. The other result was produced using an entrainment coefficient of 0.04. Comparing the laboratory and numerical results (Fig. 2.5 versus Fig. 2.6) shows that the numerical result using the higher entrainment coefficient (0.0833) gives a peak efficiency for a plume number around 300. This corresponds to the laboratory data for the 4.0 mm diameter bubbles except that the peak efficiencies differ very markedly (around 17% in the simulations compared to 10% in the laboratory experiments). The peak simulated efficiency using the lower entrainment coefficient (0.04) was predicted to occur at a plume number of around 1200. This matched the laboratory result for the 1.0 mm diameter bubbles quite well, with the magnitude of the peak efficiencies both being around 15%.

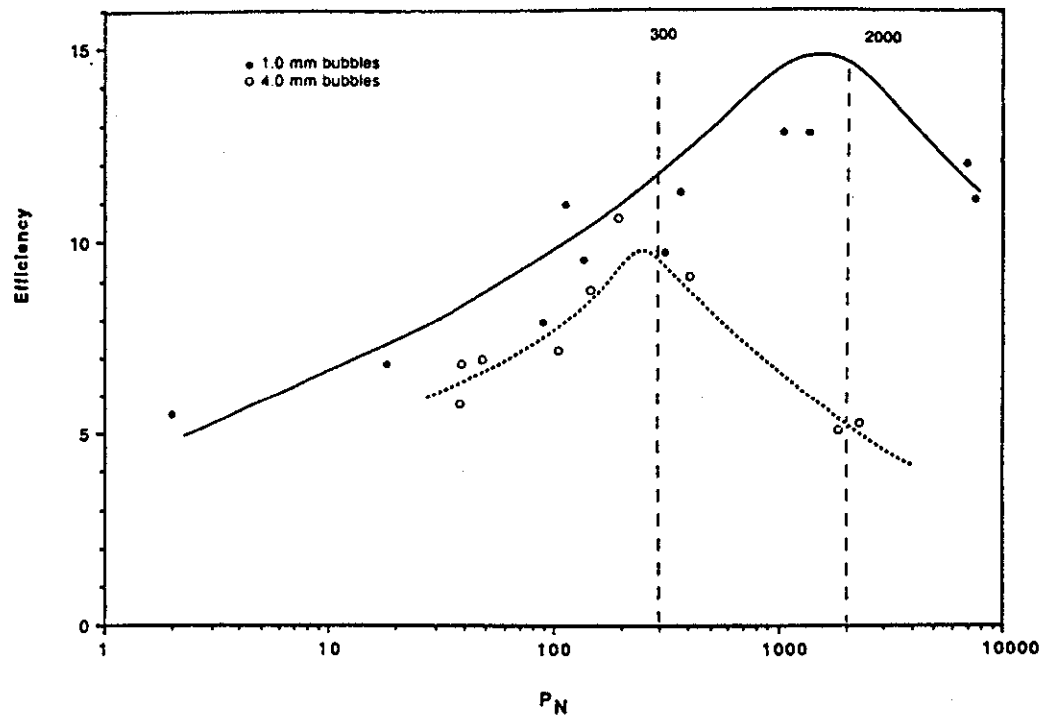

Figure 2.5 Measured efficiency of energy conversion versus plume number (linear stratification).

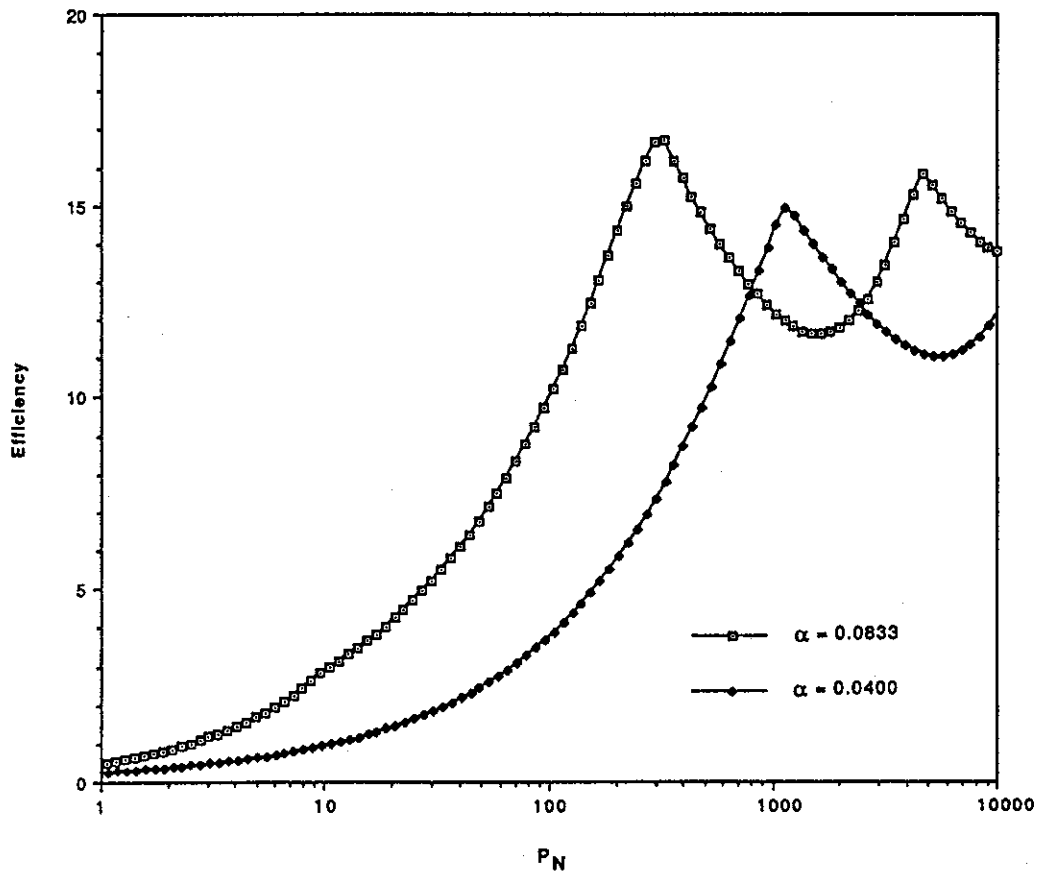

Figure 2.6 Simulated efficiency of energy conversion versus plume number (linear stratification).

The discrepancy between the observed and simulated peak efficiencies for the 4 mm diameter bubbles (α = 0.0833) can be attributed to the small number of data points collected in the experiment. The simulated efficiency peaks were much sharper than believed at the time of the laboratory work and it now appears that the point of maximum efficiency was simply not sampled. The curve fit to the experimental data (Fig. 2.5) also tends to smooth out the efficiency peaks. This "undersampling" would also explain the differing trends between the laboratory and numerical results at high plume numbers where secondary efficiency peaks were predicted to occur in the simulations. The discrepancy between the laboratory and numerical results at very low plume numbers, where the simulated efficiencies tend towards zero, was most likely the result of the turbulence generated by the plume in the small laboratory tank. The model does not account for such boundary effects which naturally result in additional mixing, and higher destratification efficiencies, at the relatively high air flow rates used in the laboratory tests.

Recent work has shown that the maximum efficiency of destratification occurs when the entrained water is ejected just as it reaches the water surface. At low plume numbers (i.e. too high air flow rates) excessive buoyancy is introduced and the efficiency falls (as shown in Figs. 2.5 and 2.6). At high plume numbers (i.e. low air flow rates), insufficient air is supplied and the plume detrains below the water surface with a reduced efficiency and a secondary plume forming where the previous plume detrained. The secondary efficiency peaks shown in Fig. 2.6 correspond to conditions under which this secondary plume is ejected just as it reaches the water surface. In principle, a succession of secondary efficiency peaks will be produced as each successive plume detrains under low air flow aeration, with each peak having a progressively lower efficiency.

2.3 Recommended Procedure for the Design of Reservoir Aeration Systems

The experimental and numerical results described above showed that a single air flow rate exists for a given stratification at which the efficiency of destratification is a maximum, with this efficiency being dependent upon the plume number and the entrainment coefficient. For example, in a weakly stratified water body, or given an air flow rate too strong relative to the stratification, the bubble plume reaches the water surface with the plume still positively buoyant; that is, more air than is required has been supplied. In a strongly stratified water body, or given a relatively low air flow rate, the plume has been shown to detrain at multiple depths with multiple secondary plumes forming; that is, insufficient air has been supplied. In either case, the mixing efficiency is not a maximum.

It is not possible to define a fixed air flow rate per source to maintain continuous operation of the aerator at peak efficiency since the stratification continually changes in response to the input

buoyancy and charging environmental conditions. Although feasible, existing destratification systems do not allow the real time adjustment of either the total air flow rate or the air flow per source to maintain a peak efficiency. The procedure described below was formulated, in part, for the design of the aerator installed in Harding Dam. The approach is applicable to most storages, with the general aim being to maintain a destratified storage at a minimum capital and operating cost.

The first step in the procedure is to select a hole diameter so that the entrainment coefficient α is likely to approach 0.0833. This is a difficult task since little literature is available describing the relationship between the hole diameter in a pipe, the air bubble size, the entrainment coefficient and the efficiency of destratification, however, it appears that a hole diameter of the order of 1.0 mm is appropriate. The second step is to run a large number of comparative simulations using the DYRESM model with various total free air flow rates and hole configurations, thus giving a range of options in terms of air flow per hole (or source).

In the case of the Harding Dam design, the total air flow rate was selected on the basis of a number of measures of the long term effectiveness of each system. These were derived by plotting the total number of days operation of the aerator per year against the number of holes in the aerator, or by plotting net efficiency of aeration against time (see Section 3.4). Patterson and Imberger (1989) showed that plotting either the net efficiency of aeration against the number of holes (e.g. Fig. 2.7) or the mean temperature difference between the water surface and the aerator against the number of holes (e.g. Fig. 2.8) could also be used to select the most effective aerator configuration for a given total air flow rate for long term operation.

The above approaches essentially describe the relative effectiveness of a range of air flow rates per source over the long term. Subsequent work by Schladow and Patterson (1990) introduced a procedure based on the maximum efficiency per source over short time scales. In this approach the aeration algorithm is used to define the air flow per source that achieves the maximum efficiency of destratification for a given density profile. To select the most appropriate profile it is important to recognise that the weaker the stratification in the reservoir the less air flow required to break down the stratification. If aeration commences at the first sign of seasonal stratification then a lower design air flow rate per source will be necessary. It is possible, however, that at some stage sufficient stratification will develop such that the aerator, designed to prevent the onset of stratification, may not have the capability to destratify the reservoir (for example, following mechanical breakdown of the aerator). The aerator should therefore be designed with sufficient capacity to not only maintain destratified conditions but also break down what may be termed a "worst case" stratification.

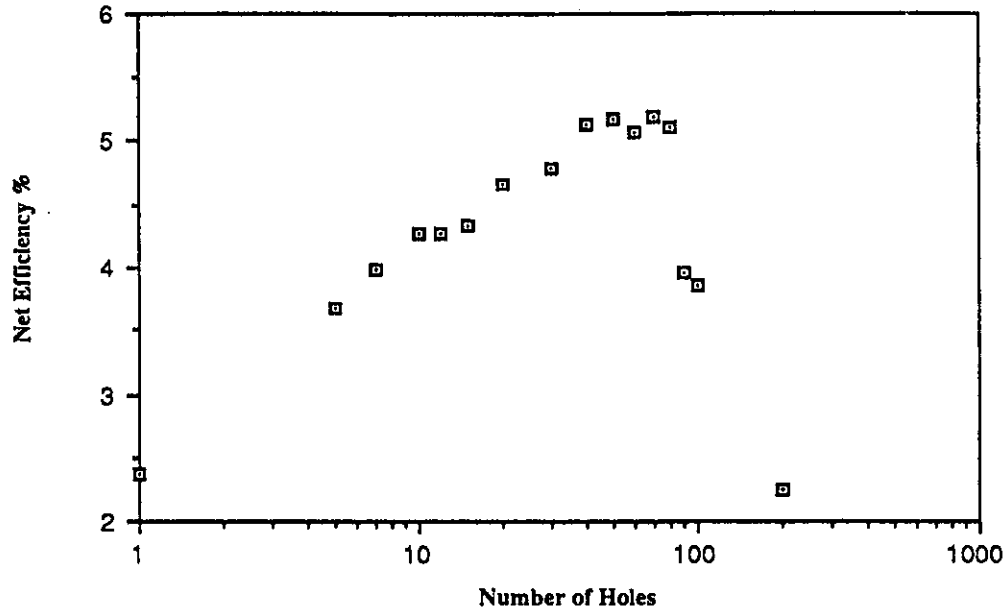

Figure 2.7 Simulated net efficiency of aeration versus number of holes : aerator activated when the surface to aerator temperature difference exceeds 1°C.

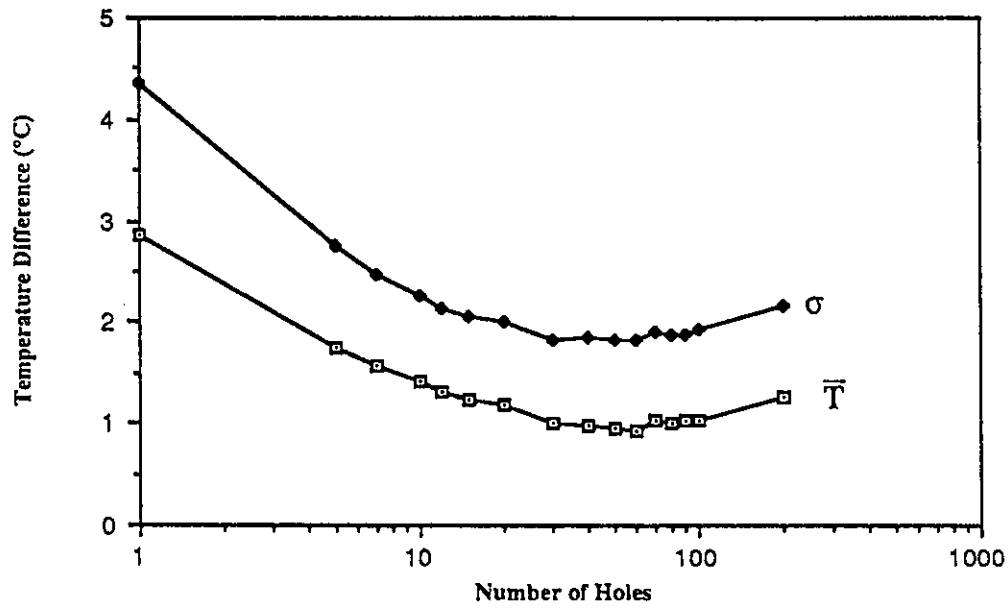

Figure 2.8 The mean $\overline{T}$ and standard deviation σ of the simulated temperature difference between the aerator and surface as a function of the number of holes : aerator activated when the surface to aerator temperature difference exceeds 1°C.

This "worst case" profile should be defined by the operator of the storage. It is dependent upon many factors, the most important being the time of installation of the aerator relative to the onset of stratification and the likelihood of extended non-aeration due to mechanical problems. It is also important that the operator specify a minimum time period for dismantling of the "worst case" profile. This depends upon the water quality problems in the storage and the preferred cost bias between capital and operating costs. Given a "worst case" profile and a minimum destratification period the aeration model can then be used to calculate the air flow rate required with each source operating around its optimum efficiency.

The next step in the modified design procedure is to define the total air flow rate required to maintain the storage in a destratified state over a summer. This is achieved by again running a number of comparative simulations with varying total free air flow rates. In this case, however, the number of holes should be selected to ensure the air flow per hole matches that specified previously to maintain maximum efficiency for the design density profile. As a final step, it remains essential that the design be tested over a full stratification period to ensure the storage is maintained in a destratified state at all times.

CHAPTER 3

STAGE 1B : DESIGN OF AN AERATION SYSTEM FOR HARDING DAM

Stage 1B of the research project set out to design and install an aeration system in Harding Dam, Western Australia so that the aeration algorithm in DYRESM could be validated against field data. The aerator design was based on a sparse data set using the version of the aeration algorithm described by Patterson and Imberger (1989). This aerator was installed in February 1989 and operated continuously through to early June 1989. Operation re-commenced in September 1989 with the onset of summer stratification in the storage.

3.1 Physical Characteristics of Harding Dam

Harding Dam is located on the Harding River, 23 km south of Roebourne in the north-west of Western Australia (Fig. 3.1). Commissioned in May 1985, the dam was constructed to augment water supplies for towns and industry in the West Pilbara Region previously served by water pumped from the Millstream Aquifer.

The Harding River forms part of the Port Hedland Coast river basin. The catchment is characterised by a semi-arid climate with very low winter rainfall. The average rainfall for the catchment is 330 mm per annum with most falls in late summer associated with cyclonic activity. Pan evaporation in the region is around 3500 mm per annum.

The river catchment area is 1060 km^2 extending some 80 kilometers from the main embankment south towards the Chichester National Park (see Fig. 3.1). The catchment primarily consists of high table lands and plains, comprised of loams and clay soils (Northcote *et al.*, 1967). There is no significant clearing of the catchment but considerable over-grazing has occurred on the valley plains. Around 50% of the area supports sheep and cattle grazing on pastoral leases, the remaining 50% of the catchment being National Park.

A river gauging station (Nº 709 211) on the Harding River was established at downstream Cooya Pooya by the Public Works Department in December 1965. The station was moved to upstream Cooya Pooya in November 1968 (Nº 709 001). Gauging ceased with the construction of Harding Dam. For the period 1965 to 1982 the mean annual flow at Cooya Pooya was 42.9 x 10^6 m^3, with February having the greatest mean monthly flow (9.9 x 10^6 m^3). Little flow has been recorded between August and January in any year, although the maximum instantaneous flow gauged between 1965 and 1982 was 1420 m^3 s^{-1} in April 1966.

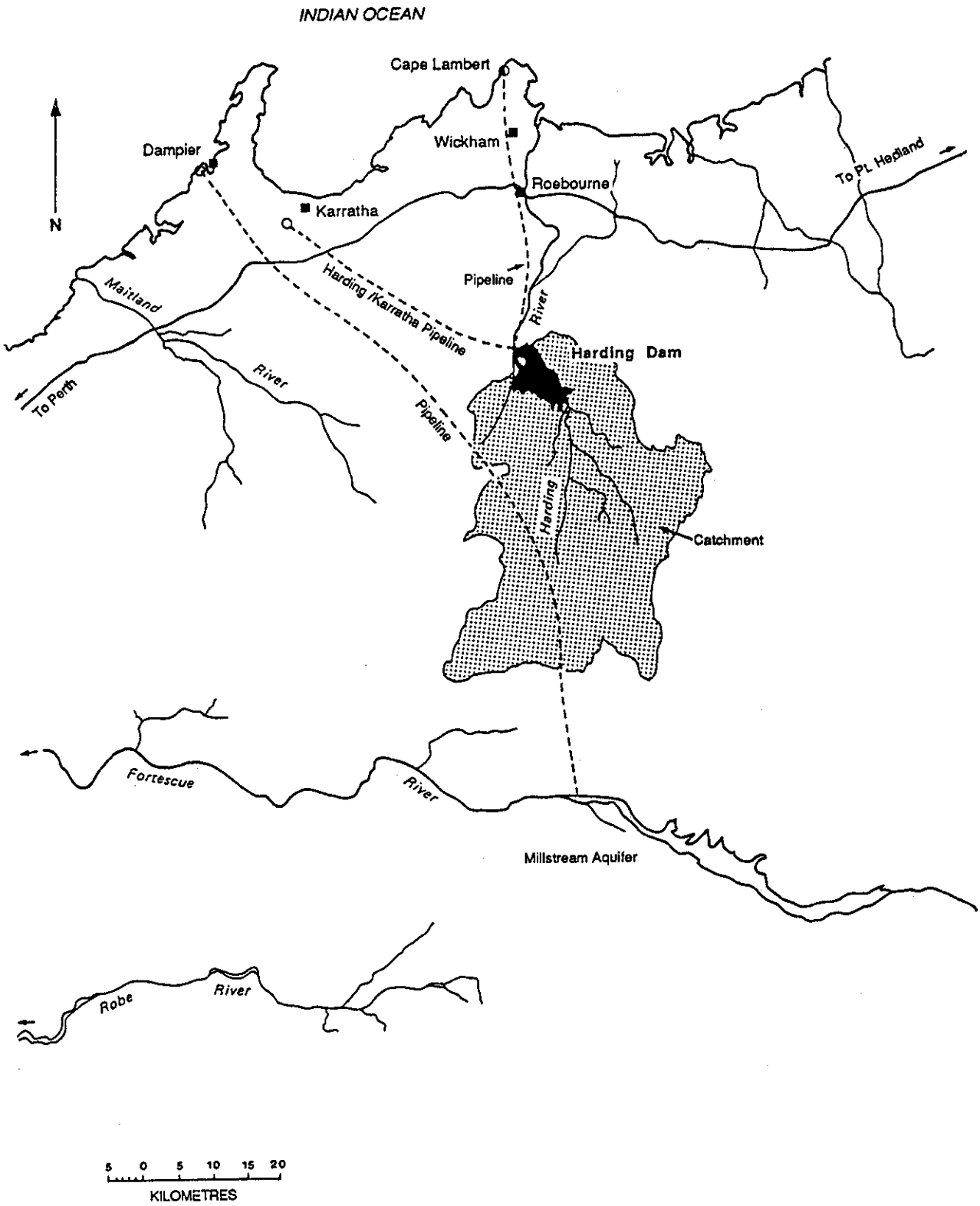

Figure 3.1 Location of Harding Dam and catchment.

The construction of the earth and rock fill main embankment of Harding Dam was completed in 1984. A small auxiliary embankment approximately 300 metres south of the main embankment was constructed to close off a saddle above the reservoir full supply level. The main spillway is an uncontrolled open channel located in a cutting through a rock ridge some 100 metres further south-west of the auxiliary embankment. It is 200 metres long with a design capacity of 7 360 $m^3 s^{-1}$. An auxiliary spillway, with a design flow capacity of 2 300 $m^3 s^{-1}$, is located in a natural saddle near Lockyers Gap.

The main embankment is 320 metres long at the crest (R.L. 77.0) and some 36 metres above the river valley floor. The maximum flood level is R.L. 76.0 metres, one metre below the embankment crest level. The maximum flood storage is 838.3×10^6 m^3 with a water surface area of 96×10^6 m^2. The full supply level is R.L. 60.0 metres (16 meters below the maximum flood level). The full supply storage is 63.8×10^6 m^3 with a water surface area of 14.1×10^6 m^2. Figure 3.2 illustrates the operating levels of the storage together with the outlet tower offtake levels.

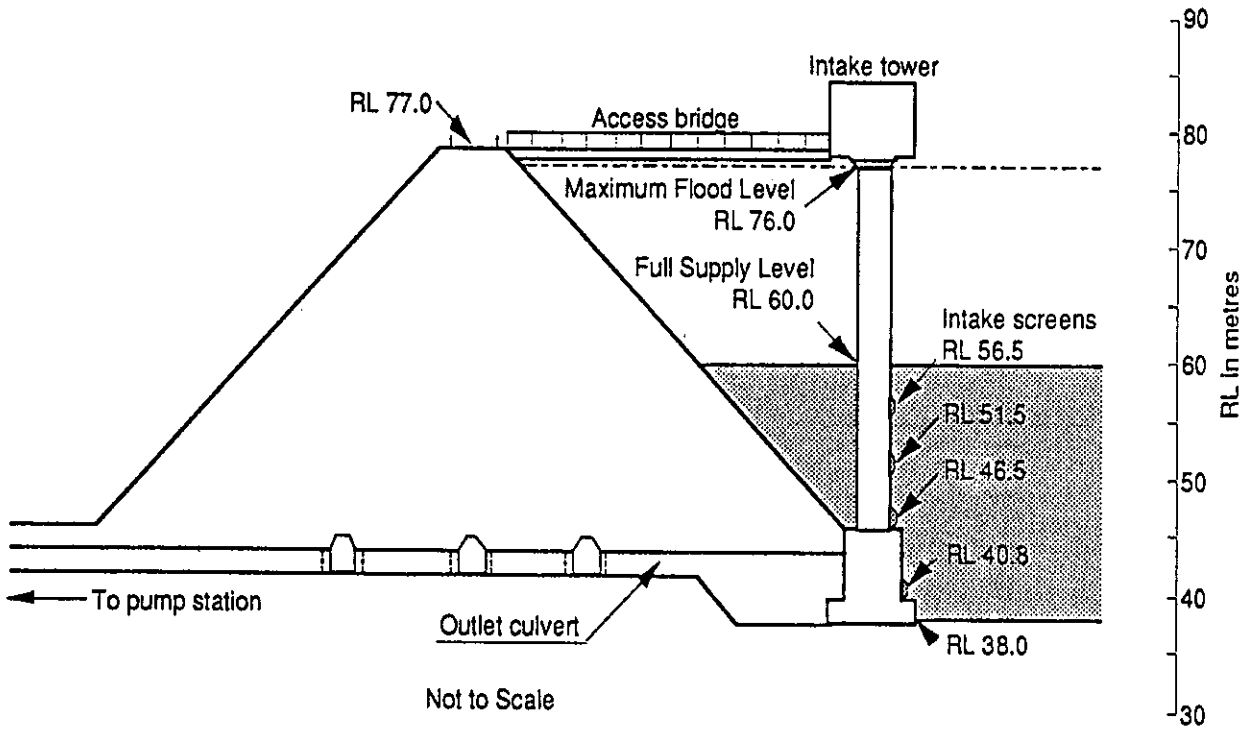

Figure 3.2 Operating supply levels at Harding Dam.

The outlet works is comprised of the intake tower, outlet culvert, scour outlet, pump station and the water treatment building. The intake tower is 49 metres high and contains 4 multi-level screen offtakes at R.L. 40.8, 46.5, 51.5 and 56.5 metres respectively. The outlet culvert consists of two 1.22 metre diameter steel pipes connected to the pump station and scour outlet. The pump station has a delivery capacity of 110 000 $m^3 d^{-1}$ and delivers water through two pipelines to distribution tanks located at Yannery and Plat (see Fig. 3.1).

Appendix A1 summarises the physical characteristics of the storage, the main and auxiliary spillways, and the main and auxiliary embankments at Harding Dam.

3.2 Aeration of Harding Dam

Three different aeration systems have been used in Harding Dam since its construction. The first aeration system operated from 14 April, 1986 to 16 June, 1988. The system consisted of a 36 metre long pipe laid parallel to the main embankment containing 36 holes, each 7 mm in diameter and spaced one metre apart. The air was transferred to the storage through ceramic diffuser heads containing high density foam intended to produce small discrete air bubbles. The aerator bar was initially located at R.L. 45.0 metres (5 metres above the bed) and approximately 138 metres in front of the main embankment. On 28 January, 1988 the aerator was lowered to R.L. 43.5 metres. The compressor delivered an air flow ranging from 0 to 175 Ls^{-1} with a gauge pressure capacity of 800 kPa. After some two years of operation the aerator was eventually removed after having limited success in reducing stratification in the storage. Table A2.1 in Appendix A2 summarises the operational details of the aeration system.

A second aeration system operated over the period 26 August, 1988 through 30 January, 1989. The system consisted of a 12 metre long pipe again laid parallel to the main embankment, with a total of 40 ceramic diffusers, spaced 0.3 metres apart. An electric compressor delivered air at a constant flow rate of 40 Ls^{-1} with gauge pressure capacity of 400 kPa. The aerator pipe was again located at R.L. 45.0 metres and approximately 138 metres from the main embankment. On 15 September, 1988 it was lowered to R.L. 42.8 metres. After four months operation, this second aeration system was removed, again after having little success in destratifying the reservoir. Table A2.2 in Appendix A2 details the operational history of the aerator.

The third aeration system commenced operation on 13 February, 1989. The system was designed as part of the research project described in this report (see sections 3.3 and 3.4 below). The performance of the aerator was monitored from the time of installation through spring 1989 (see Chapter 4), however, several periods of ungauged inflow and unreliable temperature data prevented

full verification of the achieved aerator efficiencies as compared to those predicted by the model. Although the aerator did not maintain the storage in a continuously destratified state, it did significantly reduce the impact of stratification in Harding Dam as reflected by the smaller number of consumer complaints about the quality of the water supply. Recommendations relating to the aerator's future operation are discussed in detail in Chapter 5.

3.3 Design Input Data

The DYRESM model requires meteorological data, inflow and outflow information, water clarity data, and an initial reservoir temperature and salinity profile. In addition, accurate temperature and salinity profiles throughout the period of simulation are necessary to validate the simulation results. The data described below were used first, to validate the model without aeration, and second, to specify the air flow rate and distribution system for the aerator.

3.3.1 Meteorological data

Meteorological data required by DYRESM include daily total values of short and long wave radiation and rainfall, and daily average values of air temperature, vapour pressure and wind speed. These data were not available at the dam site. The input data were thus estimated using information collected at Roebourne and Port Hedland over the period June 1980 to July 1981. Although not completely satisfactory, no alternative was available. Two meteorological stations have since been installed at the dam as from October 1988.

The Roebourne meteorological data consisted of isolated measurements of maximum and minimum air temperature, wet and dry bulb temperature, wind speed, total rainfall and cloud cover. The Port Hedland meteorological data also included total daily short wave radiation measurements. The techniques used to obtain daily totals and daily average values from these isolated measurements are summarised below.

Total daily short wave radiation at the Harding Dam, SW_{in}, was assumed identical to that recorded at Port Hedland. In the absence of measured data, total daily incoming long wave radiation, LW_{in}, was estimated using (3.1), with the observed cloud cover and air temperature recorded at 0900 and 1500 hours at Roebourne input as daily average values (Tennessee Valley Authority, 1972).

$$LW_{in} = clwin * \left\{1 + 0.17 *(cc)^2\right\} * (T_4)^6 \quad [J\, m^{-2}\, d^{-1}] \tag{3.1}$$

where clwin = 5.313×10^{-13},

cc = daily average cloud cover (0.0 to 1.0),

T_4 = daily average absolute air temperature (°K).

Total daily rainfall was measured directly at Roebourne, a distance of 23 km from the storage.

Average daily air temperatures were estimated by averaging the maximum and minimum temperatures recorded at Roebourne at 0900 and 1500 hours.

The average daily partial water vapour pressure of air, e_a, was estimated from wet bulb and dry bulb air temperatures measured twice daily at Roebourne (Tennessee Valley Authority, 1972):

$$e_a = e_{as} - 0.00066\left(1 + 0.00115\theta_D\right)P\left(\theta_w - \theta_D\right) \qquad (3.2a)$$

where e_{as} = saturation vapour pressure (mB),

θ_w = wet bulb air temperature (°C),

θ_D = dry bulb air temperature (°C),

P = atmosphere pressure (mB).

The saturation vapour pressure, e_{as}, at the wet bulb temperature, was given by the Magnus-Tetens equation (Tennessee Valley Authority, 1972) :

$$e_{as} = exp\left\{2.3026\left[\frac{a\theta'_a}{a\theta'_a + b} + c\right]\right\} \qquad (3.2b)$$

where a = 7.5

b = 237.3

c = 0.7858

Average daily wind speeds were assumed to be constant and equal to the averaged point wind speeds recorded at 0900 and 1500 hours at Roebourne. Point measurements are extremely variable and the maximum wind speed values recorded at Roebourne were much higher than the expected daily average values. The daily average wind speeds were therefore arbitrarily limited to 5 m s^{-1} for the simulation runs.

3.3.2 Inflow and outflow data

DYRESM requires daily inflow and outflow volumes and the average temperature and salinity of all inflows. Neither inflow nor outflow data was available for the period simulated (1980-81) as the

dam had yet to be constructed. Since most of the significant inflows to the Harding storage come from relatively infrequent and irregular cyclonic events of short duration, it was deemed reasonable to simulate the storage ignoring inflows. This approach was also conservative since these events cause extensive mixing of the reservoir and are, therefore, not critical in terms of the long term stratification, and hence aeration, of the storage. The design of the prototype aerator was therefore dependent upon long term meteorological forcing and independent of the influence of inflows. Total outflow from the storage for the design period was assumed to be zero.

3.3.3 Light penetration

The light attenuation coefficient, K, is used in the model to quantify the penetration of light into the water column, and consequently the heat transfer associated with incoming short wave radiation. In the field, a Secchi disk is usually used to estimate the depth of light penetration and thereby determine K using Beers Law :

$$\frac{I_z}{I_0} = e^{-Kz} \tag{3.3}$$

where I_z is the amount of light existing at the Secchi disk depth,
I_0 is the amount of light penetrating the surface,
z is the Secchi disk depth.

The amount of light reaching the Secchi disk depth may be assumed to be approximately 10% of the total light penetrating the surface (Cole, 1979); that is, $I_z/I_0 = 0.1$. The average Secchi disk depth measurement taken at Harding Dam during 1987 was 1.2 metres, thereby giving an average light attenuation coefficient, K, of 1.9 m^{-1}.

3.3.4 Initial profiles

As the period of the prototype design simulation (June 1980 to July 1981) was prior to the construction of the dam, a temperature profile for early June 1986 was used as the starting model profile.

In a similar fashion, the initial salinity profile had to be arbitrarily selected. On the basis of conductivity measurements taken in Harding Dam from 1985 to 1987, a uniform salinity profile was selected as representative of the storage. The conductivity over this period was quite low, of the order of 2×10^{-4} S m^{-1}, and approximately constant.

3.4 Aerator Design

The design of the third aeration system for Harding Dam was based on a very limited and inexact data set. Installation of the aerator early in stage 2 of the project was essential to allow detailed monitoring of the aerator's performance over a period during which a complete meteorological and water quality data set could be collected.

The design of the aerator aimed to maintain a destratified storage over a typical summer period at a minimum operating cost. The annual stratification pattern observed in the dam indicated that it would be inefficient to operate the aerator over the winter months. The initial simulations of the aerator therefore aimed to define the most efficient air flow rate and aeration configuration to destratify the storage with the aerator operating only in the presence of significant stratification (defined as a specified difference in water temperature between the surface and the aerator level). The aerator was assumed to be positioned 3 meters above the bottom of the storage (RL 43.0) so that suspension of bed material would be minimised.

Appendix A3 details the theoretical background used in the pneumatic design of aeration systems. Equation A3.7, reproduced below as Equation (3.4), defines the fundamental design parameters of a compressed air aeration system :

$$Q_{AT} = 0.063 \frac{P_1 D^2}{\sqrt{T_l}} \cdot \left[\left(\frac{P_2}{P_1}\right)^{1.43} - \left(\frac{P_2}{P_1}\right)^{1.71}\right]^{0.5} \times 10^{-3} \quad [L\,s^{-1}] \qquad (3.4)$$

where Q_{AT} is the free air flow rate per hole; P_1, the upstream absolute pressure; and D, the hole diameter. Given that:

(i) the free air flow rate per hole is defined by the total air delivery Q_T divided by the total number of holes N in the aerator line;

(ii) the maximum downstream pressure $P_2{}^M$ is defined by the maximum depth of the aerator, H^M; and

(iii) the upstream pressure P_1 is given by the sum of the downstream pressure P_2, the overpressure ΔP_o, and the pressure loss in the delivery pipelines (and therefore flow rate);

the design variables become:

ΔP_o = the over-pressure,
H^M = the maximum water depth,
D = the hole diameter,
Q_T = the total free air flow rate,
N = the total number of holes.

For the design of the Harding Dam system, the maximum water depth H^M was set to 10 metres and the hole diameter D was set to 1.5 mm. The hole diameter was selected as a compromise between maximum plume efficiency (i.e. approximately 1.0 mm diameter holes) and pneumatic considerations (i.e. flow rate per hole versus the required in-line pressure). Equation (3.4) shows that as the hole diameter decreases, the in-line delivery pressure required to achieve a fixed air flow rate through each hole must increase (non-linearly). The selection of 1.5 mm diameter holes for the Harding Dam aerator therefore aimed to result in reasonably efficient destratification whilst only requiring a moderately sized compressor.

3.4.1 Design simulations

Section 2.3 outlined a recommended procedure in developing a design strategy for an aerator with a number of issues requiring special attention. These included the time of installation relative to the onset of stratification, the likelihood of extended periods of non-aeration and the minimum time required to dismantle the stratification. The guidelines for the design of the Harding Dam aerator were straightforward. The aerator was to be installed before the development of strong stratification in the storage with the aerator monitored and maintained so as to minimise periods of non-aeration. The design was to maintain fully mixed conditions in the reservoir at a minimum capital cost and operating expense.

A wide range of simulations were carried out using a variety of total air flow rates and and air distribution configuration to define the aeration strategy. Given the designated flow and distribution, the pneumatic design of the system, and specification of the appropriate compressor, was then completed as per Equation (3.4) and is detailed in Appendix A4.

The operational strategy on which the aerator design simulations were based was a modification of the control strategy used with the previous aerator installed in Harding Dam. Specifically, the aerator was designed to be activated only when the temperature difference between the surface and the aerator exceeded a preset amount, and de-activated when the difference was less than some smaller preset amount. These preset values were arbitrary indicators of the stratification, and for the design exercise were initially set to 3°C and 1°C. Thus, the aerator came on if the temperature

difference exceeded 3°C, and was turned off when the difference fell below 1°C. the difference between the two amounts being necessary to prevent rapid cycling of the aerator.

The capital cost of the aerator may be minimised by specifying the smallest possible compressor capable of destratifying the reservoir with short delivery and aerator pipelines. The operating cost may be reduced by operating this compressor for the shortest possible period whilst maintaining the reservoir in a fully mixed condition. Although straightforward, these requirements are often contradictory since the stratification and water depth constantly vary, thereby changing the air flow rate and distribution required to maintain operation of the aerator at its peak efficiency.

Given all of the above, a reasonable measure of the efficient performance of the aerator design was assumed to be given by the predicted number of days of operation of the aerator per year required to meet the specified operational strategy. Figure 3.3 shows the number of days of operation for four different total air flow rates, as a function of the number of separate holes in the aerator pipeline. This figure assumed the entrainment coefficient α to be constant (0.0833).

Two important features were immediately evident in Fig. 3.3. First, as the total air flow rate was increased, the total number of days of aeration for a given number of holes decreased. This meant that, a specific number of holes could be selected for each air flow rate such that the number of days of operation was a minimum. Second, for the condition where the least number of days operation was required, there was little improvement in performance between the 50 Ls^{-1}, 100 Ls^{-1}, and 200 Ls^{-1} air flow rates, but the 25 Ls^{-1} rate was markedly less effective. The efficiency of energy conversion, as defined by Equation (2.8), varies with the degree of stratification in the storage since the mechanical energy input during any single simulation is fixed.

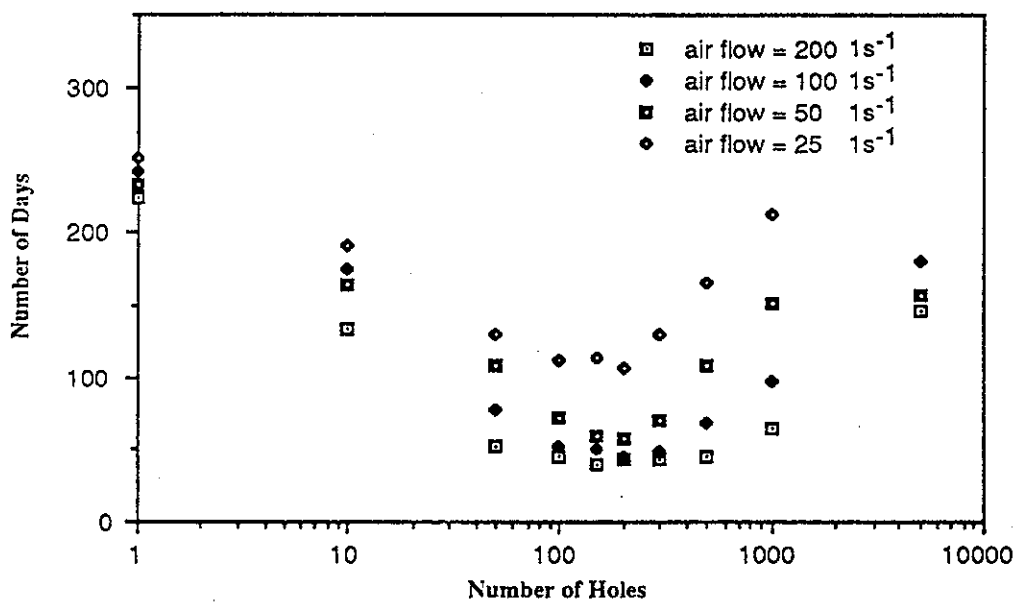

Figure 3.3 Simulated number of days of aerator operation per year versus number of holes (3 °C on/1 °C off).

This follows the experimental and numerical results showing that a bubble plume cannot be continually operated at peak efficiency as the plume number changes (Figs. 2.5 and 2.6). Figure 3.4 shows the efficiency of aeration versus time for two of the proposed aeration configurations (i.e. 50 Ls^{-1} and 100 holes, 100 Ls^{-1} and 100 holes).

Subsequent to the work completed above, the Water Authority of Western Australia indicated that the aerator operating criteria of 3°C on/1°C off was likely to result in dissolved oxygen levels in the storage being too low. Additional simulations were carried out with a 1.0°C on/0.5 °C off operational control. The result, shown in Fig. 3.5, demonstrated that although the number of operational days increased, the overall design specifications remained much the same, a total free air flow rate ranging from 50 Ls^{-1} to 200 Ls^{-1} with the total number of holes between 100 and 200.

3.4.2 Design specifications

The total air flow rate depends upon the extent of destratification required and the specified time taken to achieve that designated destratification. In turn, these requirements depend upon the water quality problems which the system is attempting to alleviate and a trade-off between operating and capital costs. As a basis for design, the maximum desirable temperature difference between the surface and the aerator was set to 1 °C with a breakdown of the 1 °C gradient taking of the order of several days once the aerator was re-activated. In addition, the design assumed an equal trade-off between operating costs (i.e. the total free air flow rate) and capital costs (i.e. total number of holes or aerator length). With these criteria in mind, the final design configuration was specified as :

Total free air flow rate, Q_T	=	50 Ls^{-1}
Total number of holes, N	=	100
Free air flow rate per hole, Q_{AT}	=	0.5 Ls^{-1}
Hole diameter, D	=	1.5 mm
Hole spacing, S	=	4.0 m.

The hole spacing was selected to be that required to minimise interaction between adjacent plumes. As a rule of thumb, the spacing should be no less than one-fifth the water depth above the aerator. The aerator line was then fixed at 400 metres in length, given a spacing of four metres between each hole. The line was laid by WAWA along the main river channel, perpendicular to the main embankment, and suspended approximately six metres above the deepest part of the storage. The delivery line to the aerator pipe was some 100 metres long running from the intake tower to the start of the aerator pipe. Both the aerator and delivery pipes were 50 mm inner diameter. The pneumatic design calculations are summarised in Appendix A4.

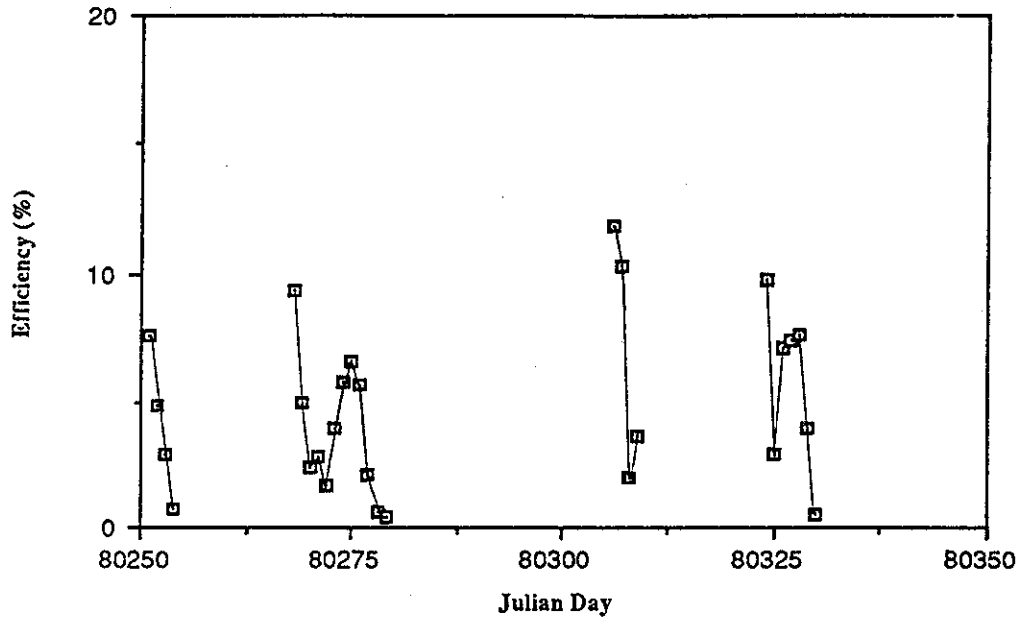

Figure 3.4a Efficiency of energy conversion for a total air flow rate of 100 Ls^{-1} and 100 holes versus Day number (3 °C on/1 °C off).

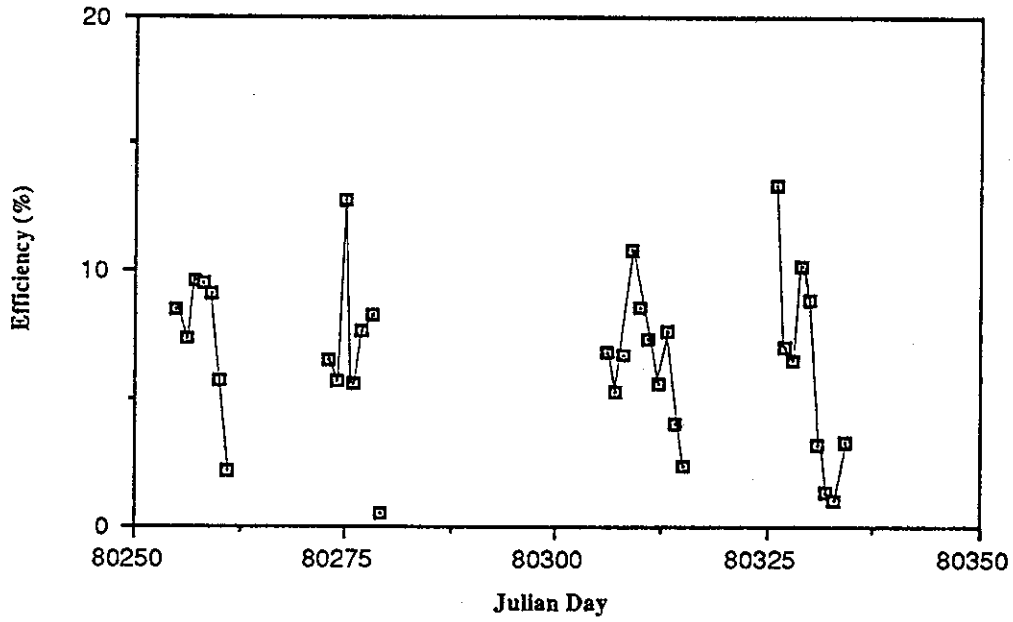

Figure 3.4b Efficiency of energy conversion for a total air flow rate of 50 Ls^{-1} and 100 holes versus Day number (3 °C on/1 °C off).

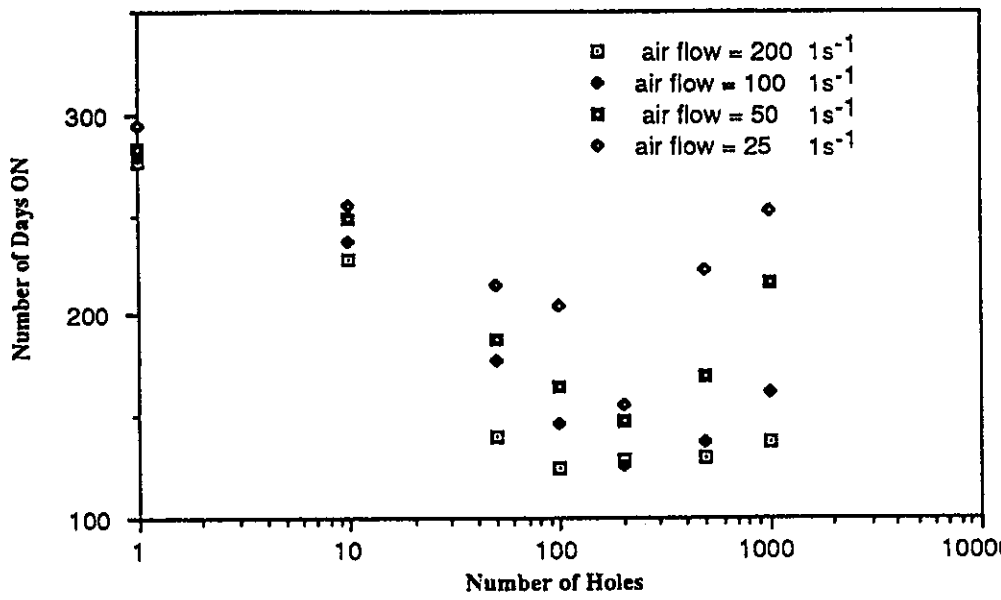

Figure 3.5 Simulated number of days of aerator operation per year versus number of holes (1 °C on/0.5 °C off).

The aeration system was commissioned on 13 February 1989. An electric rotary compressor was installed in the intake tower, with a maximum delivery pressure of 300 kPa gauge, running at a constant delivery air flow rate of around 40 Ls^{-1}. Each hole then delivered a free air flow rate of some 0.4 Ls^{-1}. Pressure measurements taken on 20 February 1989, when the water depth above the aerator was some 10 metres, defined a delivery pressure at the compressor of 175 kPa (gauge). Allowing for line losses in the delivery and aerator pipes of some 29 kPa, gave an overpressure, ΔP_o, of 47 kPa and a calculated free air flow rate of 0.39 Ls^{-1} per hole (see Appendix A4).

The system was designed to run using the temperature based operational strategy which turned the compressor on for 6 hours when the temperature difference between the surface and aerator was greater than 1.0 °C. The aerator was switched to manual operation on 25 February 1989 and was then run continuously through 26 June 1989. The aerator was re-activated on 22 September 1989 and operated throughout the 1989-90 summer period on a 24-hour basis. The aerator evidently operated at an efficiency less than that predicted in the design simulations. Chapter 4 and 5 detail the reasons behind this problem, describe the appropriate changes to the aeration algorithm and design assumptions, and then set out recommended changes to the aeration strategy for Harding Dam.

CHAPTER 4

STAGE 2A : EVALUATION AND MODIFICATION OF THE AERATION ALGORITHM

The first stage of the project aimed to verify the suitability of the existing aeration model for the design of reservoir destratification systems and then apply this model to design an aerator for installation in Harding Dam. The second stage of the project required a detailed assessment of the performance of the aerator, as compared to that predicted by the aeration model, so that the model could be modified as necessary. This task required the collection of a comprehensive set of data including meteorological, water balance, light attenuation and temperature and conductivity profile information. This chapter describes the monitoring program and the evaluation process and then details the required modifications to the aeration algorithm.

4.1 Field Monitoring Program

As noted previously, to simulate the changes in the physical water properties in Harding Dam, the numerical model DYRESM requires daily (or more frequently measured) meteorological data at the surface of the reservoir, accurate inflow and outflow information, water clarity data, and initial lake temperature and conductivity profiles. To verify the accuracy of the model's predictions, accurate temperature and conductivity profiles must also be measured at regular intervals during the period simulated . The collection of this data at Harding Dam was undertaken by the Water Authority of Western Australia, North West Region, with assistance from the Scientific Services Branch in Perth. A reasonably complete data set, including meteorological data, outflow information, and profile and water clarity data, was collected over the study period from November 1988 through October 1989.

4.1.1 Meteorological data

The meteorological data required by the model includes daily total values of incoming short and long wave radiation, and rainfall; and daily average values of air temperature, vapour pressure and wind speed. Since these data were not previously available at the dam site (see Section 3.3.1) two meteorological stations were installed on location at Harding Dam by WAWA in October 1988. The locations of the two stations are shown in Fig. 4.1, with the corresponding Australian Map Grid coordinates given in Table 4.1. Station 1 was located on an island within the main basin of the storage approximately 500 metres from the main embankment. Station 2 was sited

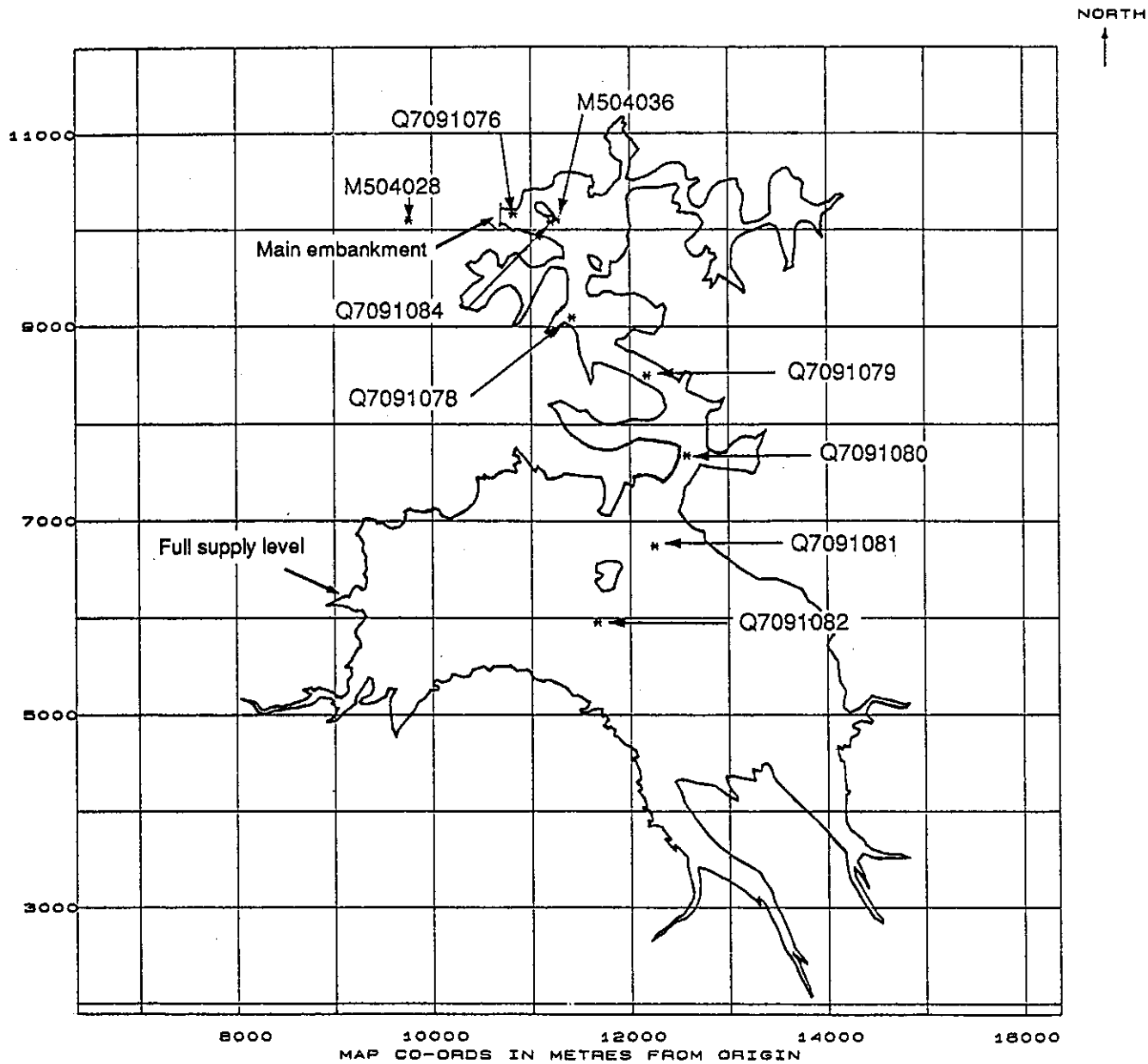

Figure 4.1 Location of meteorological stations and water quality profiling sites on Harding Dam.

approximately 1500 metres west of the main embankment at the base of the main range of hills. The data collected and the accuracy and range of each sensor are listed in Table 4.2.

TABLE 4.1

LOCATION OF THE HARDING DAM METEOROLOGICAL STATIONS

Station	AMG Coordinates (metres)	Distance from Embankment (kilometres)
M504028 (land)	509 770 E, 7 680 100 N	1.2
M504036 (island)	511 260 E, 7 680 110 N	0.5

TABLE 4.2

METEOROLOGICAL DATA RECORDED BY STATION 1 (ISLAND) AND STATION 2 (LAND) AND INSTRUMENT SPECIFICATIONS

Parameter	Description	Units	Accuracy	Range
T_A	air temperature	℃	± 0.1°C	-5° to 54.5°C
T_O	temperature under net radiance	℃	± 0.1°C	-5° to 54.5°C
R_H	relative humidity	%	± 3%	0 to 100%
WR	wind run	km	± 2%	0.5 to 67 ms^{-1}
SW_{in}	incoming short wave radiation	Wm^{-2}	± 5%	400 to 1200 nm
T_n	net total radiation	Wm^{-2}	± 3%	300 to 4000 nm

Both meteorological stations were set up to collect data over ten minute periods. The data were then stored on Unidata 8 bit Starloggers. The data were extracted from the loggers approximately every 4 weeks and a disk copy of the data then forwarded to CWR in ASCII format.

Upon receiving the raw meteorological data files, the land station file, denoted M504028.DAT, and the island station file, M504036.DAT, were renamed according to the following convention: HMSSYDDD.RAW, where:

SS was the station number (i.e. 28 or 36),

Y was the last digit of the year (i.e. 8 or 9),

DDD was the Julian Day of the start of the record.

The renamed raw data files were then processed using the program VALIDD.EXP. This routine carried out range and error checks, calculated the daily average wind speed, W_s, by dividing the wind run WR by 86.4; and then calculated the incoming long wave radiation, LW_{in}, from the net total and incoming short wave radiation recordings. That is:

$$LW_{in} = 5.67*10^{-8} * (T_O)^4 + T_n - SW_{in} \quad (4.1)$$

where T_O is the temperature measurement under the net radiance sensor (°C),

T_n is the net total radiation(Wm^{-2}),

SW_{in} is the incoming short radiation (Wm^{-2}).

The data files generated after processing then contained six channels, these being :

T_A : air temperature,

R_H : relative humidity,

W_S : wind speed,

SW_{in} : incoming short wave radiation,

T_n : net total radiation,

LW_{in} : calculated incoming long wave radiation.

The program VALIDD.EXP reported the number of errors found in each channel of each individual data file to a file denoted HMSSYDDD.REP. Each channel was then plotted against time. Any inconsistent or unusual data were then checked or edited and the final data file archived as HMSSYDDD.VAL.

The DYRESM model requires input of the following parameters as daily averages:

T_A : air temperature (°C),

V_{PP} : calculated vapour pressure (mB),

W_{SC} : corrected wind speed (ms^{-1}),

and the following parameters as daily total values:

SW_{in} : incoming short wave radiation (Wm^{-2}),

LW_{in} : incoming long wave radiation (Wm^{-2}),

$Rain$: rainfall (mm).

The meteorological data included in HMSSYDDD.VAL directly provided T_A, SW_{in} and LW_{in}. The values for V_{PP}, *Wsc* and *Rain* were then derived as described below.

The saturation vapour pressure, V_{PP}, was calculated from the relative humidity, R_H, and the air temperature, T_A, directly recorded on the storage, according to Equation (4.2) below:

$$Vpp = (R_H / 100) * exp\ [\{(7.5 + T_A) / (T_A + 273.3)\} + 0.7858] \qquad (4.2)$$

The recorded wind speed W_S was corrected to an equivalent wind speed at a height of 10 metres above the surface of the storage using Equation (4.3). That is :

$$W_{sc} = W_s\ ln\ (10/Z) / ln\ (m/Z) \qquad (4.3)$$

where: W_{sc} is the corrected wind speed at an elevation of 10 metres,
m is the height of the wind speed anemometer above the water surface,
Z = 10/exp[k/C_D],
k = 0.411
C_D = $(1.3 \times 10^{-3})^{0.5}$.

The daily rainfall was taken to be identical to the daily total rainfall recorded in Karratha. Table 4.3 shows the periods over which reliable meteorological data were obtained from the two stations between November 1988 and October 1989.

4.1.2 Inflow and outflow data

DYRESM requires quantification of all inflows and outflows, and the average temperature and salinity of each inflow. Discharge valve settings, together with any flow over the spillway, were used to define the total daily outflow volume (V_{OUT}) from the storage. Since no direct gauging of any inflow has been undertaken on Harding Dam, the total daily inflow volume (V_{IN}) was estimated from daily water balances using Equation (4.4) below:

$$V_{IN} = V_{OUT} + \Delta Storage + Evaporation - Precipitation \qquad (4.4)$$

where *ΔStorage* is the change in storage volume over the day (m^3),
Evaporation is the daily evaporation volume (m^3),
Precipitation is the daily rainfall volume (m^3).

Figure 4.2 plots the water surface elevation of the storage from October 1988 to October 1989, major inflow events occurring in late February, late April, and mid-June 1989.

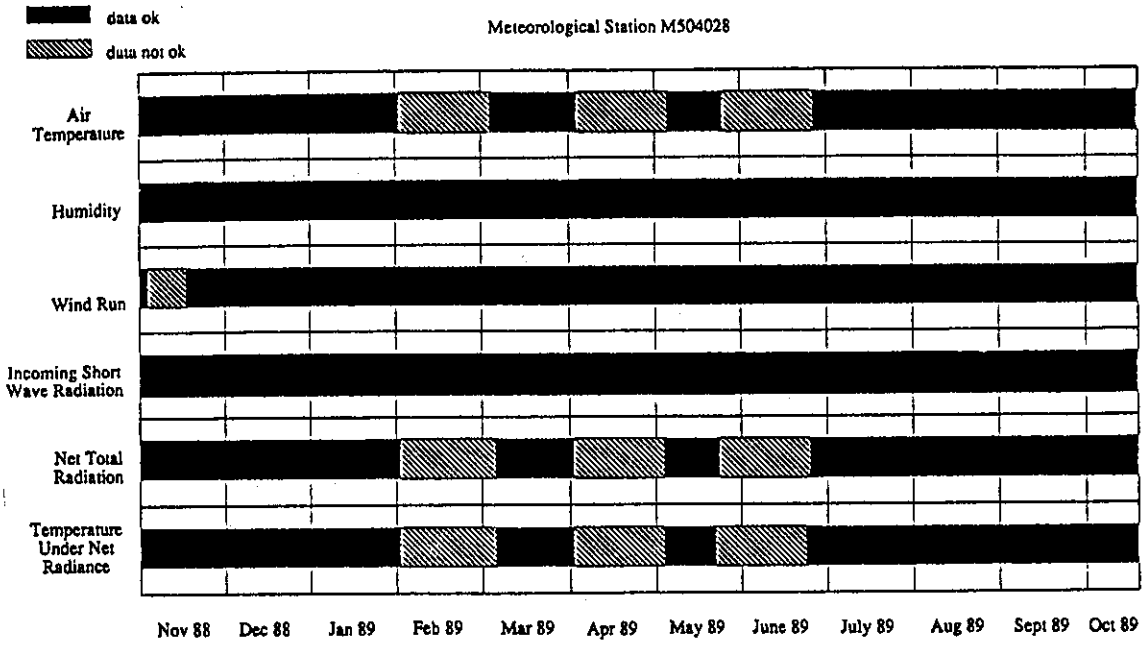

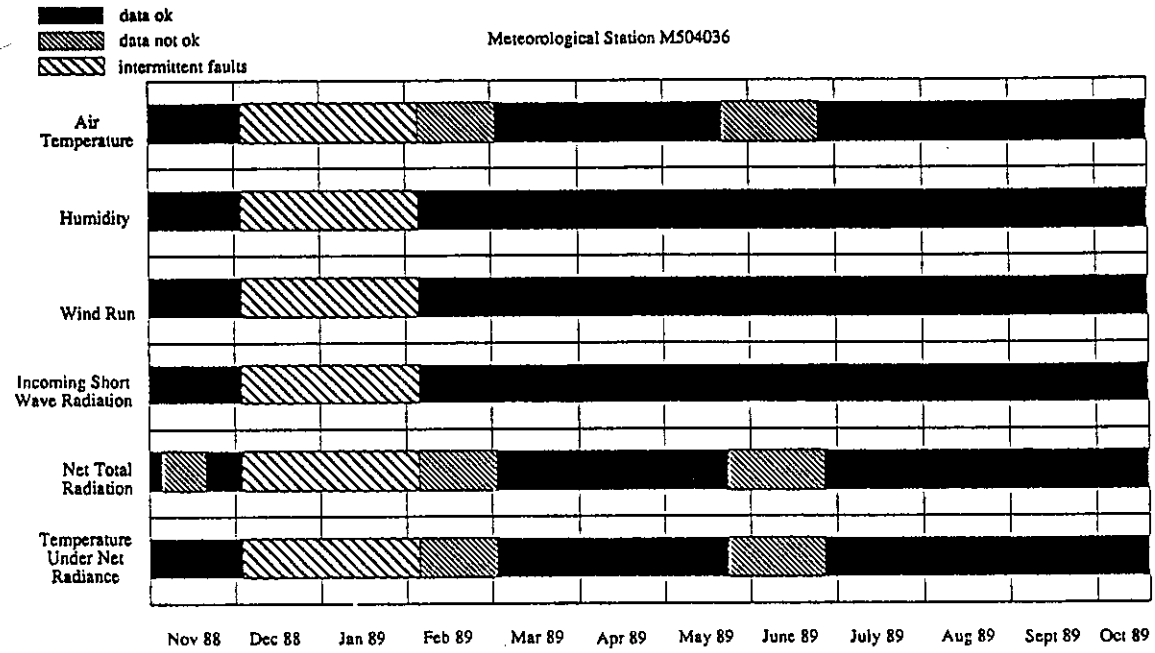

Table 4.3 . Periods of reliable meteorological data.

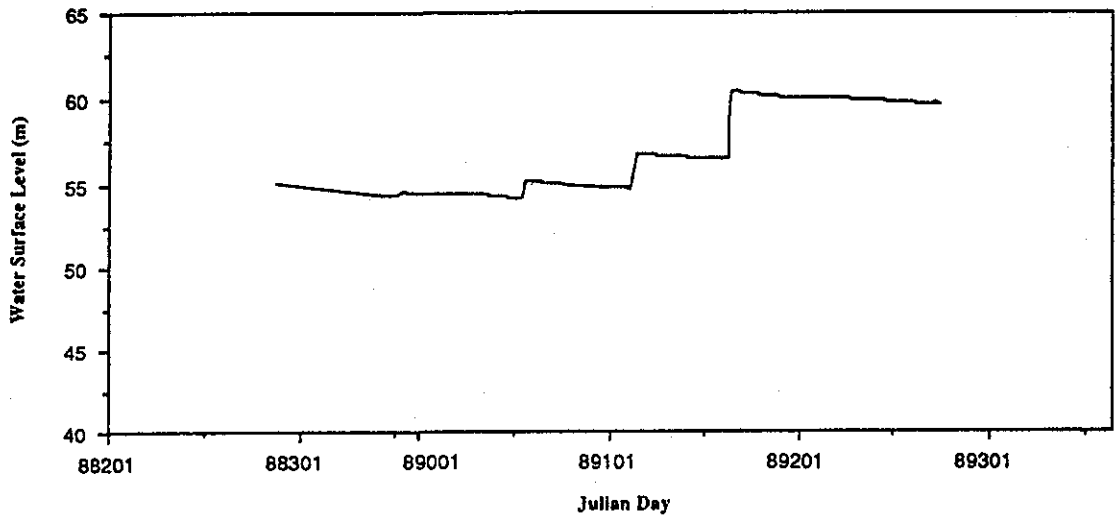

Figure 4.2 Harding Dam storage level 1988/1989.

As a first approximation, inflow temperatures were assumed equal to the air temperature, and conductivities were assumed to be constant at 1.6×10^{-4} S m^{-1}. These approximations, in combination with the estimate of inflow volume based on the water balance, led to a poor simulation of the thermal structure of the storage during periods of significant inflow. It was therefore decided that, as far as was practicable, further model simulations would only be carried out during periods of zero or very small inflow.

4.1.3 Light attenuation coefficient

Secchi disk depth measurements taken in Harding Dam over the period June 1988 to August 1989 ranged from 1.0 to 1.9. An average depth of 1.2 metres was used to calculate a light attenuation coefficient, K, of 1.9 m^{-1} as per Equation (3.3).

4.1.4 Water quality data

The Water Authority of Western Australia has carried out regular profiling of temperature, conductivity and dissolved oxygen since the dam was completed in 1985. Three-weekly sampling was carried out through 1989 at the stations shown in Fig. 4.1. Table 4.4 lists the location (AMG Coordinates) and the distance from the main embankment of each sampling site.

Temperature and dissolved oxygen profile data for stations Q7091076, Q7091084, Q7091078, Q7091079 and Q7091080 were contoured for the years 1986 to 1988 and are presented in Appendix A5. Data collected to October 1989 at the stations 0.1 km and 0.5 km from the dam wall are plotted in Figs. 4.3 and 4.4. The arrows in these plots indicate the dates on which data were collected. Some of the temperature data collected during this period were suspect due to inadequate calibration of sensors.

TABLE 4.4

LOCATION OF HARDING DAM WATER QUALITY PROFILING SITES

Site	AMG Coordinates (metres)	Distance from Embankment (kilometres)
Q7091076	510 825 E, 7 680 170 N	0.1
Q7091084	511 200 E, 7 680 085 N	0.5
Q7091086	- -	0.6
Q7091078	511 415 E, 7 679 100 N	1.5
Q7091079	512 175 E, 7 678 510 N	2.5
Q7091080	512 575 E, 7 677 690 N	3.5
Q7091081	512 250 E, 7 676 755 N	4.5
Q7091082	511 670 E, 7 675 965 N	5.5

In addition to the monitoring described above, WAWA also carried out regular profiling of a range of other water quality parameters at all stations. These data have been analysed by the Scientific Services Branch with the results described in Rosich and McAuliffe (1990) as a part of this research project.

4.2 Assessment of the Aeration Algorithm

The field monitoring program described above was used for short and long term validation of the simulation model. To examine the dynamics of the mixing generated by bubble plume aerators in greater detail, the Centre for Environmental Fluid Dynamics (CEFD) conducted a number of field investigations on Wungong and Harding Dams in Western Australia. The first two field trips focused on collecting microstructure data while the third, more intensive experiment, acquired a range of fine-scale and microstructure mixing information relevant to the aerator installed in Harding Dam. The results of these investigations, although still being analysed, were used by the Centre for Limnological Modelling (CLM) to modify the aeration algorithm installed in DYRESM.

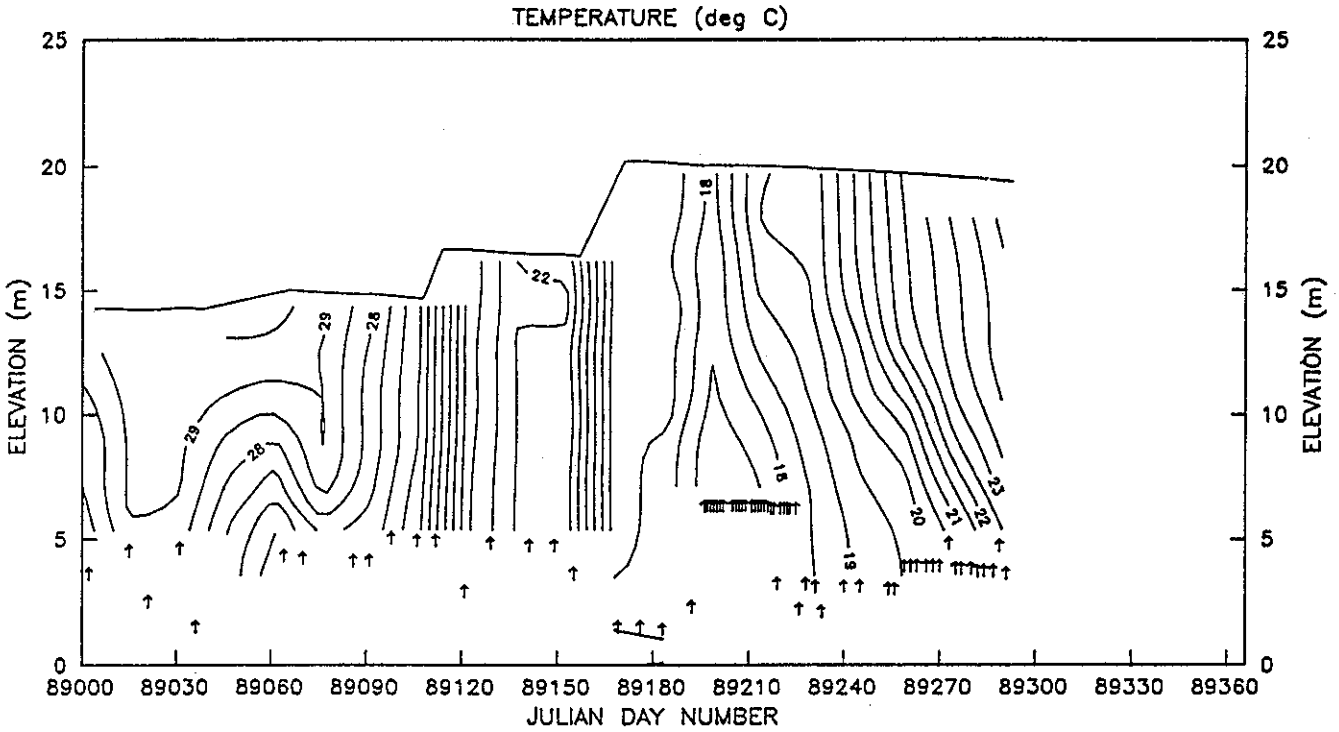

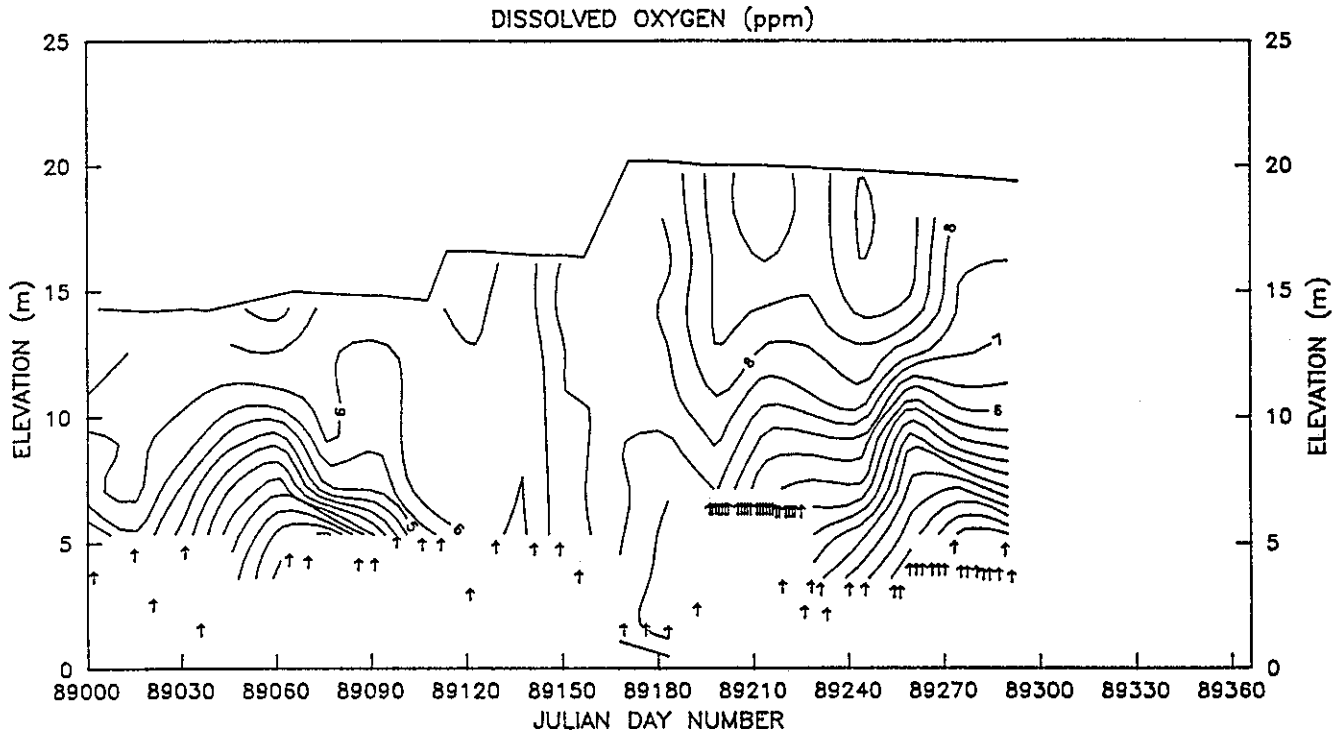

Figure 4.3 Temperature and dissolved oxygen contours of 1989 data at station Q7091076 (0.1 km from the dam wall). The aerator was operated at a total air flow rate of 40 Ls^{-1} through 100 holes from Day 89053 to Day 89177 and from Day 89265 to Day 89304.

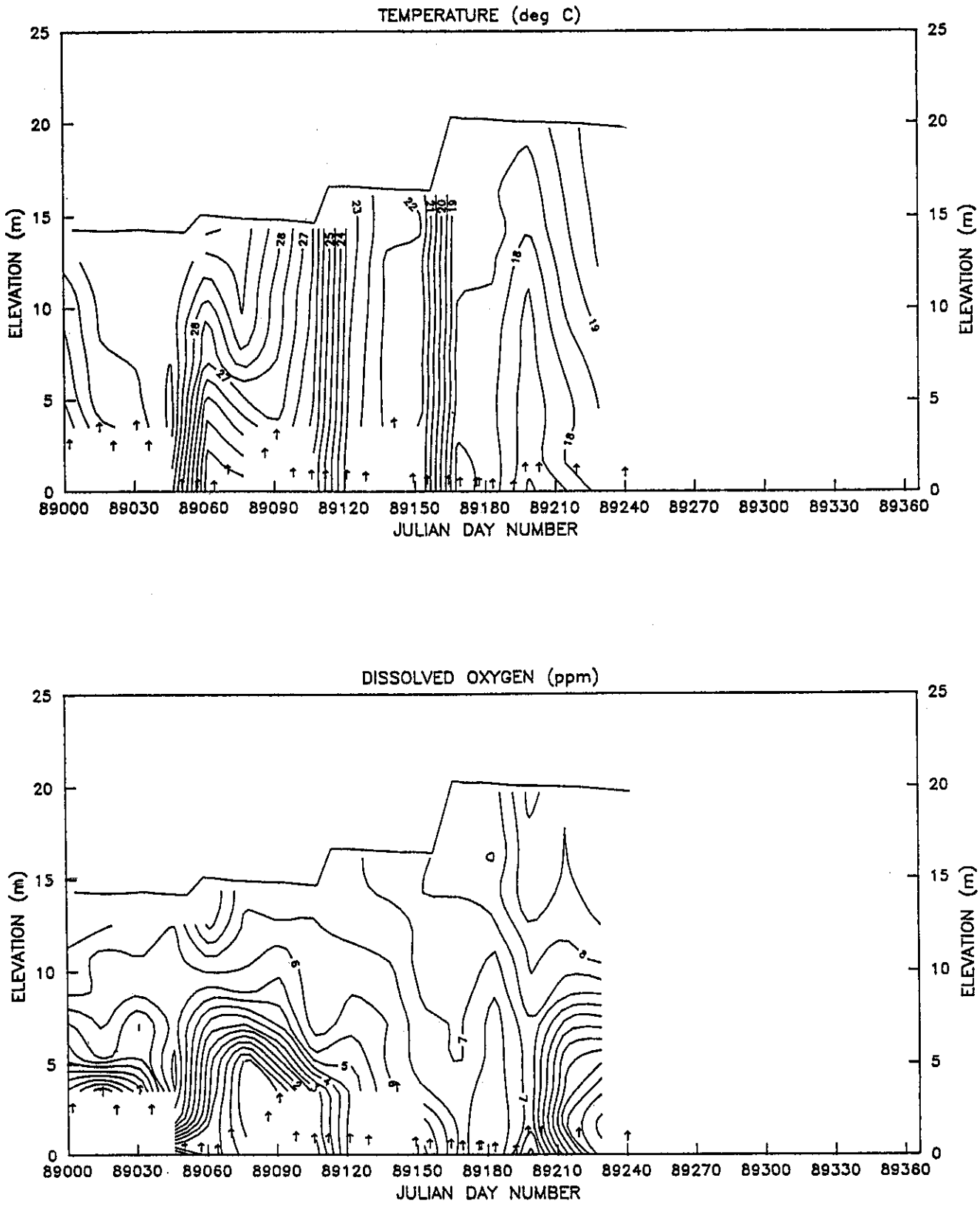

Figure 4.4 Temperature and dissolved oxygen contours of 1989 data at station Q7091084 (0.5 km from the dam wall). The aerator was operated at a total air flow rate of 40 Ls^{-1} through 100 holes from Day 89053 to Day 89177 and from Day 89265 to Day 89304.

The results of the field and numerical work are briefly summarised below but will be published in greater detail at a later date.

4.2.1 Summary of field investigations

In conjunction with the laboratory work described in Section 2.1, an initial field investigation of a single source bubble plume was completed on Wungong Dam in February 1988. The aim was to collect microstructure, fine-scale and basin-scale data to assess the flow field and the turbulence levels associated with the plume. Experiments were carried out with a flow rate both greater and smaller than the predicted critical value of the plume number required to form a single intrusion.

The field data indicated that when the flow rate was in excess of the critical value, as defined by plume number of around 2000, the bubble plume lifted cold water from the aerator level to the water surface, whereupon the water plunged to an intermediate level and then intruded horizontally into the reservoir approximately 10 metres below the surface. For small air flow rates, multiple intrusions were observed to form and the exchange of water was not from the aerator to the surface but to an intermediate depth in the water column. These characteristics were in general agreement with those observed in the laboratory experiments (Figs. 2.3 and 2.4).

Two further field experiments, aimed at collecting microstructure data within plume intrusions, were carried out on Harding Dam on November 26 and 27, 1988, and February 26 and 27, 1989. A more intensive field investigation, focusing on the dynamics of the plume formed by the aerator in Harding Dam, was conducted from 5 March to 12 March, 1989 (Julian days 89096 to 89103).

The results of this work illustrated the influence of stratification on the short term behaviour of bubble plume aerators. Figure 4.5 clearly shows the formation of a wide plume under weakly stratified conditions, and a tall, narrow plume under a strong stratification. The amount of entrainment appeared to be dependent upon the plume reaching the free surface. The data implied that additional entrainment, not given by the existing plume theory, takes place at the point of flow divergence as the plume plunges. A simple model of this entrainment was subsequently incorporated into the modified aeration algorithm (see Section 4.2.2). The amount of entrainment was also shown to be dependent on the diurnal stratification, confirmation of the laboratory result indicating the efficiency of destratification being determined, at least in part, by the plume number. To account for the influence of the diurnal stratification cycle, the time step in the model was reduced (see Section 4.2.2).

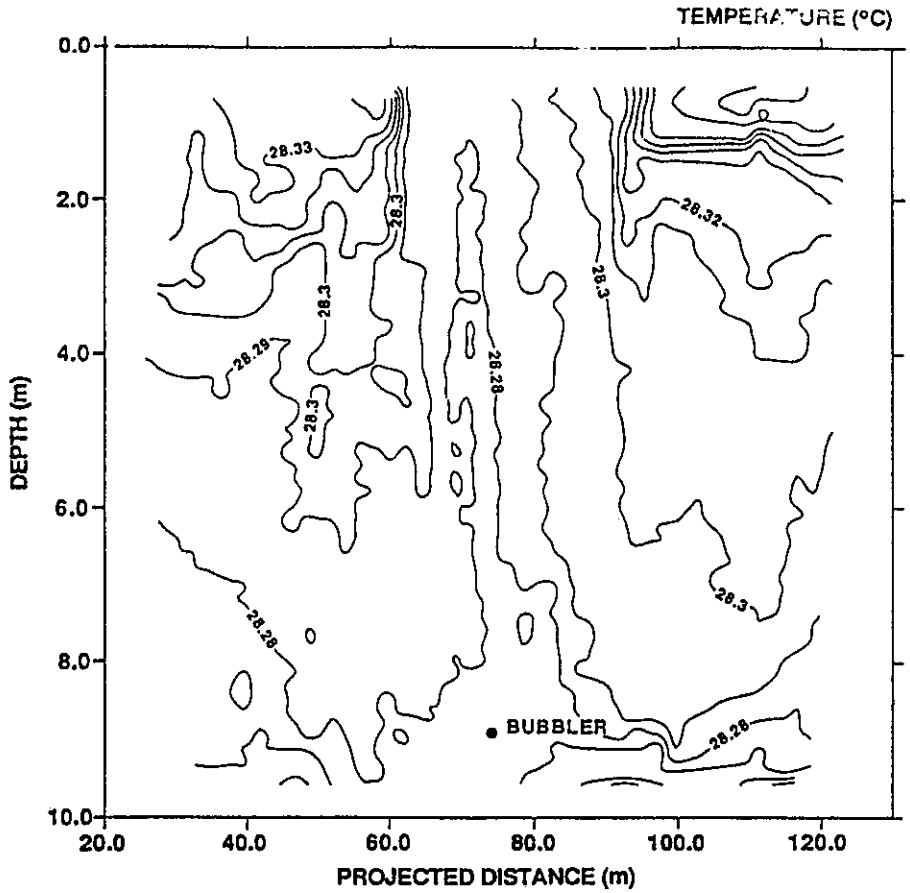

Figure 4.5a Transect across the centre of the aerator located at a depth of 9 metres in Harding Dam - morning transect with weak stratification.

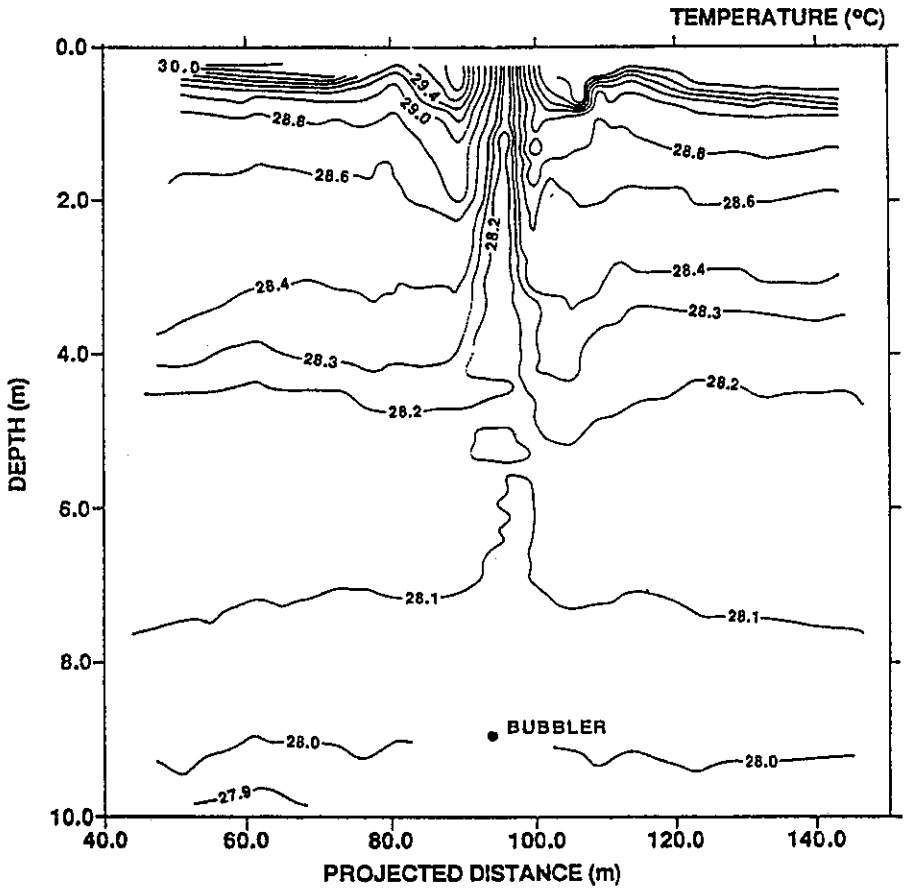

Figure 4.5b Transect across the centre of the aerator located at a depth of 9 metres in Harding Dam - afternoon transect with strong stratification.

4.2.2 Modifications to the aeration model

The aerator installed in Harding Dam was designed using DYRESM to provide an efficient system to maintain destratification in the storage. The design was based on the aerator algorithm described by Patterson and Imberger (1989), however, the laboratory and numerical experiments and the field investigations summarised in this report indicated that there were some deficiencies in the formulation and implementation of the aeration model. A number of modifications were then made to the model followed by validation against the field data described in Section 4.1.

First, the aeration algorithm was changed to more closely reproduce the dynamics associated with the plume interacting with the free surface. The field and laboratory data showed that the ejected plume plunged to the level of neutral buoyancy before intruding horizontally. The model had previously assumed that the ejected plume mixed with the surface water before plunging. The algorithm was modified to better reflect the entrainment occurring as the plume plunged.

Second, the algorithm was modified to allow interaction between the plume and the reservoir stratification on shorter time scales. The field experiment conducted on Harding Dam between Julian days 89095 (March 5) and 89102 (March 12) illustrated a very strong diurnal stratification cycle. The morning profiles showed the storage to be mixed down to the level of the aerator, stratified in the upper layers during the day, and then broken down by convective mixing during the night. These data indicated that the interaction between the aerator and the meteorological forcing occurred over quite short time scales. The influence of the diurnal stratification on the plume entrainment was taken into account by using sub-daily meteorological data and then incorporating the aeration algorithm into this sub-daily loop.

Traditionally, DYRESM has used daily input data to simulate those processes which occur over time scales much less than one day. As suggested above, a simple average value for meteorological data throughout the entire day may not be adequate to reproduce the effects of the aerator. Since ten minute meteorological data were available, DYRESM was modified to run using sub-daily meteorological data. In the modified sub-daily loop, average daily meteorological information was applied at smaller time intervals throughout the entire day except for short wave radiation, which was applied at the smaller time intervals for only 12 hours of the day.

Third, the time step of the model was reduced. In the aerator model used for the design of the Harding Dam aerator the plume algorithm was enacted once daily. In subsequent simulations, this time step appeared to result in excessive mixing of the hypolimnion. The long time step allowed numerical instabilities to develop requiring a change to a shorter step for the bubble plume

algorithm. The time step was set to a maximum of 10 minutes or the time required to entrain a volume equivalent to the model layer at the depth of the aerator.

4.2.3 Field validation of the modified aeration model

Application of the modified version of the DYRESM model confirmed the modifications provided an improved simulation of the behaviour of Harding Dam. All simulations after modification of the model used the sub-daily meteorological data with the reduced time step in the aeration algorithm. The simulations were based on the land station wind data, with a light attenuation coefficient of 1.9 m^{-1} and an entrainment coefficient of 0.0833.

Figure 4.6 plots the result of a simulation from Day 89258 to Day 89275, with the aerator activated on Day 89265. Although there were some discrepancies between the temperature profiles measured in the field and those predicted by the model, the model was reasonably successful in reproducing the stratification and mixing in Harding Dam. The model accurately predicted the depth of the surface mixed layer and the development of the strengthening thermocline over the period of the simulation. Figure 4.6 shows that the aeration algorithm, with an entrainment coefficient of 0.0833, predicted somewhat more rapid mixing of the water column than was observed, with the epilimnion water temperature predicted to be slightly lower than measured, the hypolimnion water temperature slightly greater than that measured and the predicted thermocline significantly sharper than that observed in the field. The more effective mixing of the storage predicted by the model, as compared to the field data, may have been the result of the entrainment coefficient being set too high. The laboratory experiments described in Chapter 2 showed that the entrainment is affected by the air bubble size in the rising plume. The numerical work (Fig. 2.6) indicated that this effect may be incorporated in the model by adjusting the entrainment coefficient α.

Figure 4.6 demonstrated the performance of the modified aeration model over a simulation period incorporating seven days without aeration followed by aeration of the storage for ten days. A number of data deficiencies, however, prevented a more complete model validation over a longer seasonal period because of :

(a) large inflows of unknown temperature and volume occurring at three times during the study period (see Fig. 4.3),

(b) the failure of both meteorological stations at various times through the study period limiting the length of the record for which data were available (as shown in Table 4.3),

(c) the temperature profile data being occasionally suspect, with probe calibration changing significantly at various times through the study period.

As a result of these deficiencies, the long-term validation period was set from Day 89198 to Day 89272 with the aerator being activated on Day 89265. This allowed the modified model to be tested over a period ranging from weakly to strongly stratified conditions with initiation of the aerator included in the simulation period.

The result of the simulation is plotted in Fig. 4.7. The plot shows that the model was partially successful in reproducing the thermal behaviour of Harding Dam, with the epilimnion water temperature being reproduced reasonably accurately but the predicted hypolimnion water temperature being consistently less than that observed. During the period of non-aeration of the storage (i.e. Day 89198 to Day 89265), the model predicted a significantly sharper and shallower thermocline compared to the field data. After activation of the aerator on Day 89265, the predicted and observed depth of the surface mixed layer matched closely although the thermocline was again predicted to be too sharp.

Figures 4.6 and 4.7 showed that the modified aeration model was reasonably successful in predicting the influence of the aerator on the thermal structure of Harding Dam. It was concluded that the model was a suitable (and improved) tool for the design of reservoir aeration systems.

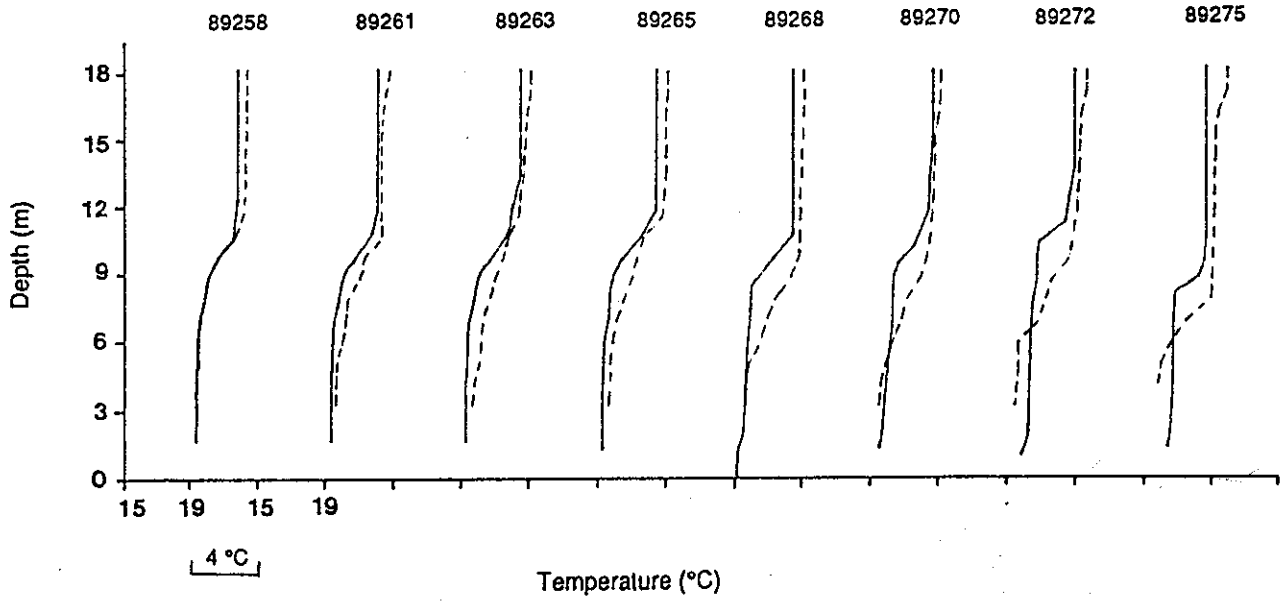

Figure 4.6 Harding Dam: simulated versus observed temperature profiles with aeration from Day 89265 to Day 89275 : $\alpha = 0.0833$.

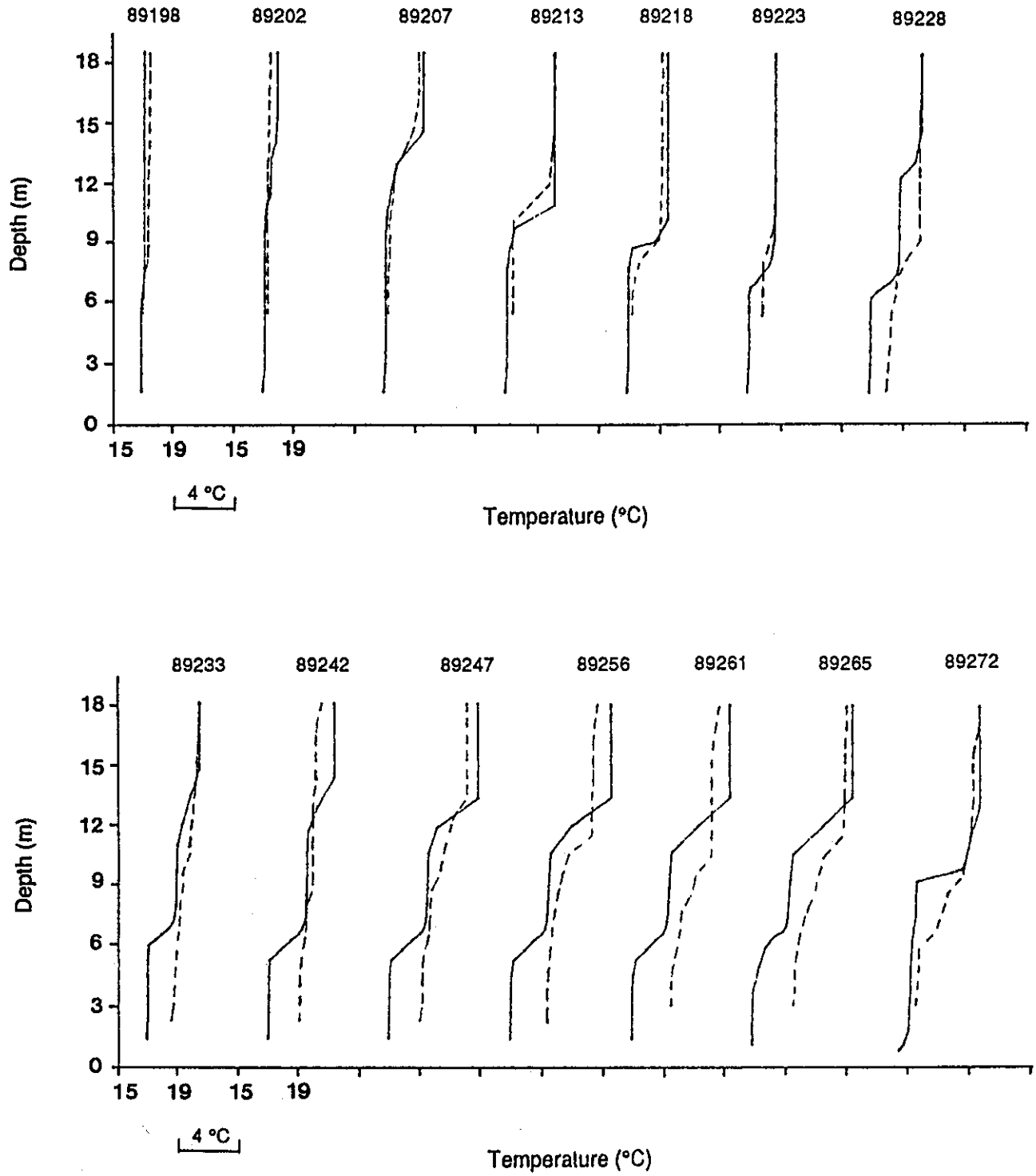

Figure 4.7 Harding Dam: simulated versus observed temperature profiles from weakly to strongly stratified conditions : aerator activated on Day 89265.

CHAPTER 5

STAGE 2B : APPLICATION OF THE AERATION MODEL FOR DESIGN

The final stage of the research project required the application of the modified aeration model to assess the likely long-term performance of the aerator installed in Harding Dam. This assessment process was an essential part of confirming the applicability of the aeration model to practical design situations. Harding Dam was then used as a test case of the model's performance over long simulation periods, thereby also allowing the assessment of operational options for the artificial destratification of the dam in the 1989/90 and future summer periods. For this purpose, the optimal aeration strategy was specified as that which would most effectively maintain fully mixed conditions in the storage over a full summer.

To allow the long term simulation of a range of aeration strategies from winter through early summer, an artificial, yet representative, data set was established. Meteorological data, water balance data and profile information were available in 1989 from mid-July (Day 89198) through early October (Day 89275). Since the simulations were to proceed through December 1989, 1988 data were adopted from Day 88276 (3 October) through Day 88336 (2 December). In this manner, a realistic data set of around 4.5 months duration was available. The data were of reasonably high quality, with only inflow information requiring estimation. Since the period selected was characterised by very low and sporadic inflow, this shortfall was not considered critical.

5.1 Assessment of the Harding Dam Aeration System

The existing aerator was installed in Harding Dam in February 1989. Although designed to deliver 50 Ls^{-1} free air through 100 holes (i.e. 0.5 Ls^{-1} free air per hole), the total measured operating flow was closer to 40 Ls^{-1} (see Section 3.4).

The aerator was switched off in June 1989 and re-started on 22 September 1989 (Day 89265). It was turned back on in response to the increased temperature stratification observed during September, however, the isotherm-depth history plot (Fig. 5.1) indicates that, in hindsight, the aerator should have been re-started up to 10 weeks earlier. The aerator operated continuously from Day 89265 through the 1989/90 summer.

5.1.1 Zero aeration

To quantify the natural response of the storage (i.e. no artificial destratification), the model was first run with zero air input. The results of the simulation are presented in Fig. 5.2 in the form of an isotherm-depth history plot.

The simulation indicated that the stratification in the storage would begin to increase as early as Day 89200 (19 July) with quite strong stratification established by Day 89250 (7 September). The surface layer tended to steadily deepen through Day 89290 (17 October) with the stratification strengthening significantly around Day 89300 (27 October). Although the simulation data set differs from the true 1989 conditions from Day 89275, comparison of the isotherm-depth history plot based on measured data (Fig. 5.1) and the simulated zero aeration isotherm-depth history plot (Fig. 5.2) show a reasonable match up to Day 89265, with the model predicting a somewhat slower heating and deepening of the surface layer after the aerator was started as of Day 89265 (22 September). A 4 °C temperature differential between the surface and bed of the reservoir was predicted by the end of the simulation (Day 89336) if no aeration was employed. With increased surface heating likely through the remainder of the summer, continued and strengthened stratification was then expected.

5.1.2 Aeration at 40 Ls^{-1}

The likely response of the storage to continued aeration at the original design flow rate was simulated by firstly reproducing zero aeration from Day 89198 through Day 89265 (i.e. when the aerator was not operated) and then simulating the impact of a total free air flow rate of 40 Ls^{-1} from Day 89265 through to Day 89336. The result of this simulation is plotted in Fig. 5.3 with the dotted horizontal line denoting the level of the aerator (RL 46.0).

Comparison of Fig. 5.3 with the case of zero aeration over the full design period (Fig. 5.2) clearly shows the positive impact of continuing the existing aeration strategy. The first portion of the simulation (up to Day 89265) was identical, with strong stratification developing by Day 89250. The activation of the aerator on Day 89265 had an immediate influence on the stability of the water column. The deepening mixed layer observed in the zero aeration simulation plunged more rapidly in the aerated simulation, reaching the level of the aerator around Day 89300 as compared to Day 89315 in the non-aerated simulation. This result more closely matched the slope of the measured contours between Day 89265 and Day 89285 (Fig. 5.1).

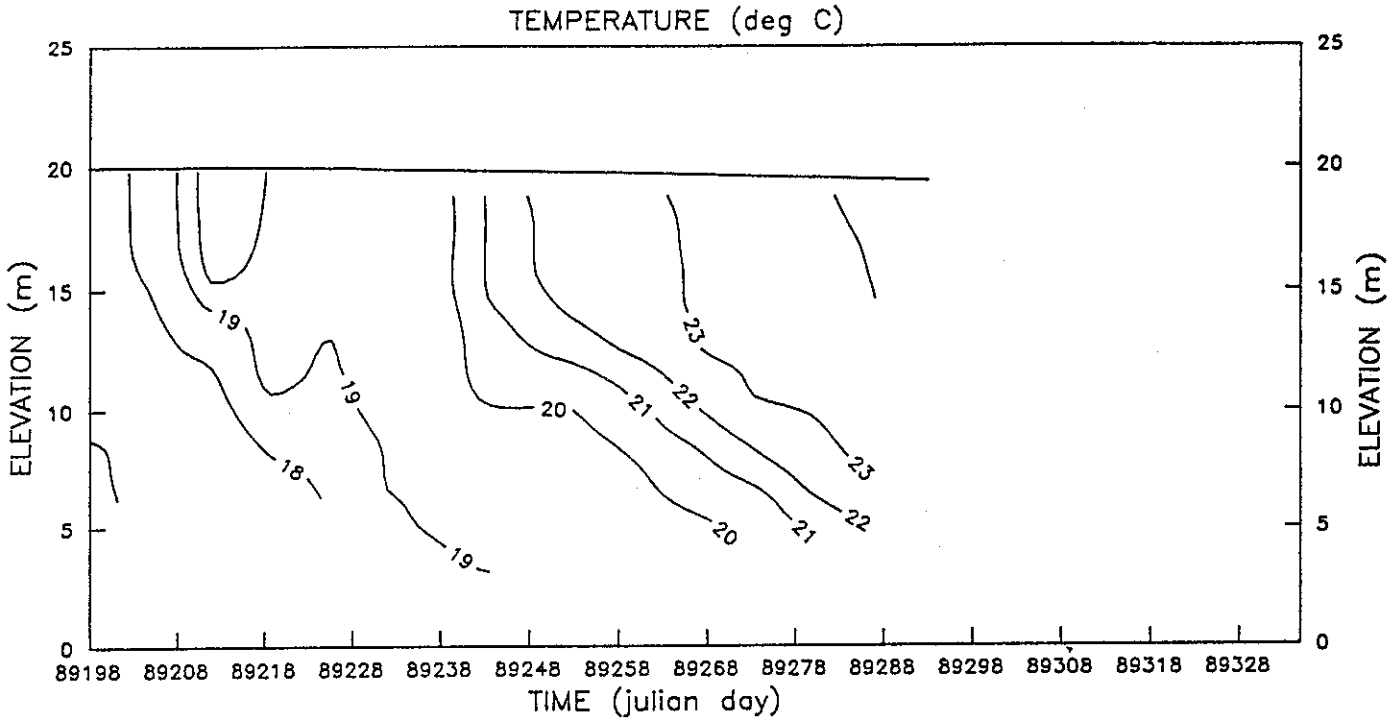

Figure 5.1 Isotherm-depth history plot of 1989 temperature data at station Q7091076 (0.1 km from the dam wall). Aerator activated on Day 89265.

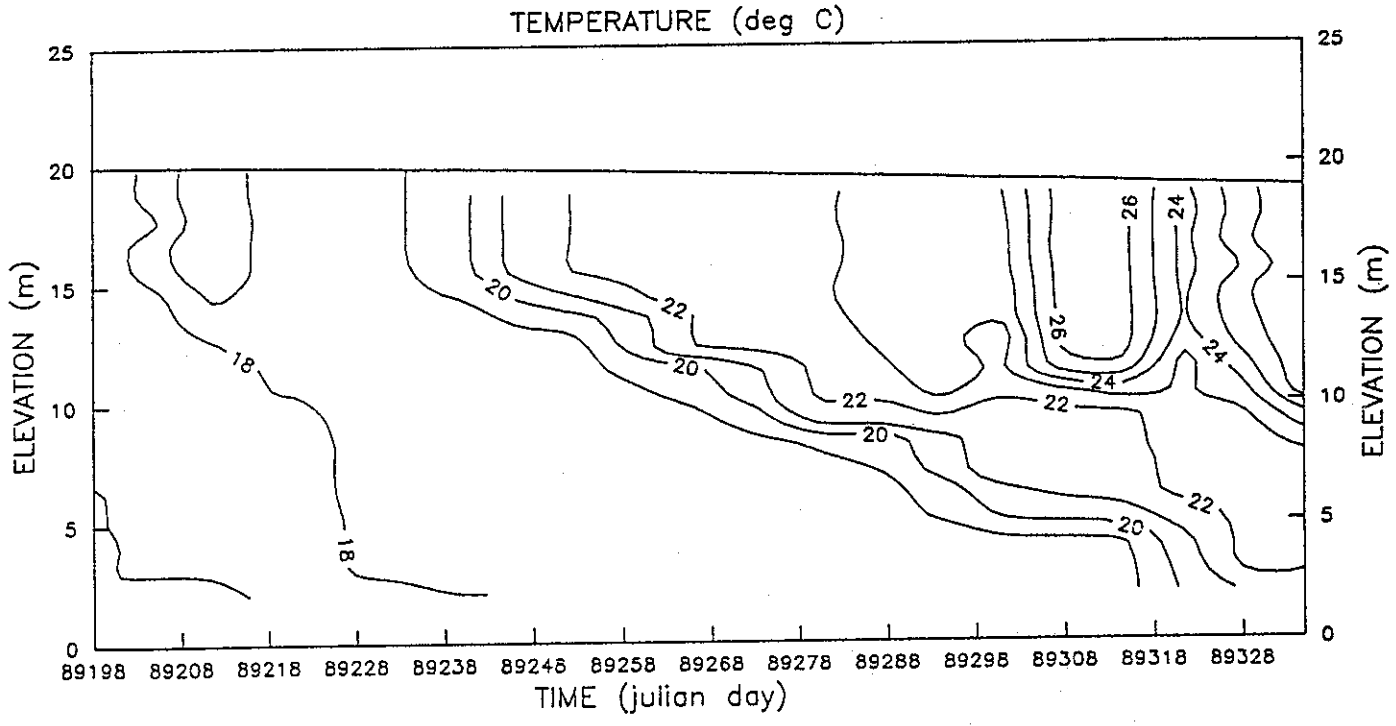

Figure 5.2 Simulated isotherm-depth history plot from July to November 1989 with zero aeration.

As indicated previously, the aerator may have been more effective had it been activated at the onset of stratification of the water column. Although not an option for 1989/90, this simulation should be useful in operational planning for future years. Fig. 5.4 plots the result of aeration at 40 Ls^{-1} over the full simulation period from Day 89198 through Day 89336. Although having a marked impact on the stability of the water column, as compared to the case of zero aeration (Fig. 5.2), it was apparent that the existing aeration strategy was unlikely to maintain fully mixed conditions in Harding Dam over a complete summer period. The aerator will, however, maintain a reasonably well mixed water column above the level of the aerator for a significant portion of the simulated period.

5.2 Improved Destratification of Harding Dam

The results presented above indicated that continued aeration at 40 Ls^{-1} would assist in maintaining a reasonably well mixed water column above the aerator level over the 1989/90 summer. The results also demonstrated the benefits of activating the aerator as early as possible in the stratification cycle. To confirm the applicability of the aeration model as a design/management tool it was then used to assess the available options for improving the artificial destratification of Harding Dam over future summers.

5.2.1 Aeration at 80 Ls^{-1}

The existing aerator line has a maximum flow capacity, in its present configuration, of around 80 Ls^{-1}. To test the impact of increased aeration over the 1989/90 summer, the model was run with the existing air flow to Day 89304 (i.e. 0 Ls^{-1} : Day 89198 to Day 89264; 40 Ls^{-1} : Day 89265 to Day 89304) and 80 Ls^{-1} free air flow from Day 89305 through Day 89336. Figure 5.5 shows that this option would have very little advantage over running the system in its existing form at 40 Ls^{-1} (Fig. 5.3).

To quantify the impact of increased aeration through the existing line over the full simulation period, the model was then run with 80 Ls^{-1} free air flow from Day 89198 through Day 89336 (Fig. 5.6). Although this option has significant benefits compared to the 1989/90 system (Fig. 5.3), the system is only marginally improved when compared to the 40 Ls^{-1} flow over the full simulation period (Fig. 5.4).

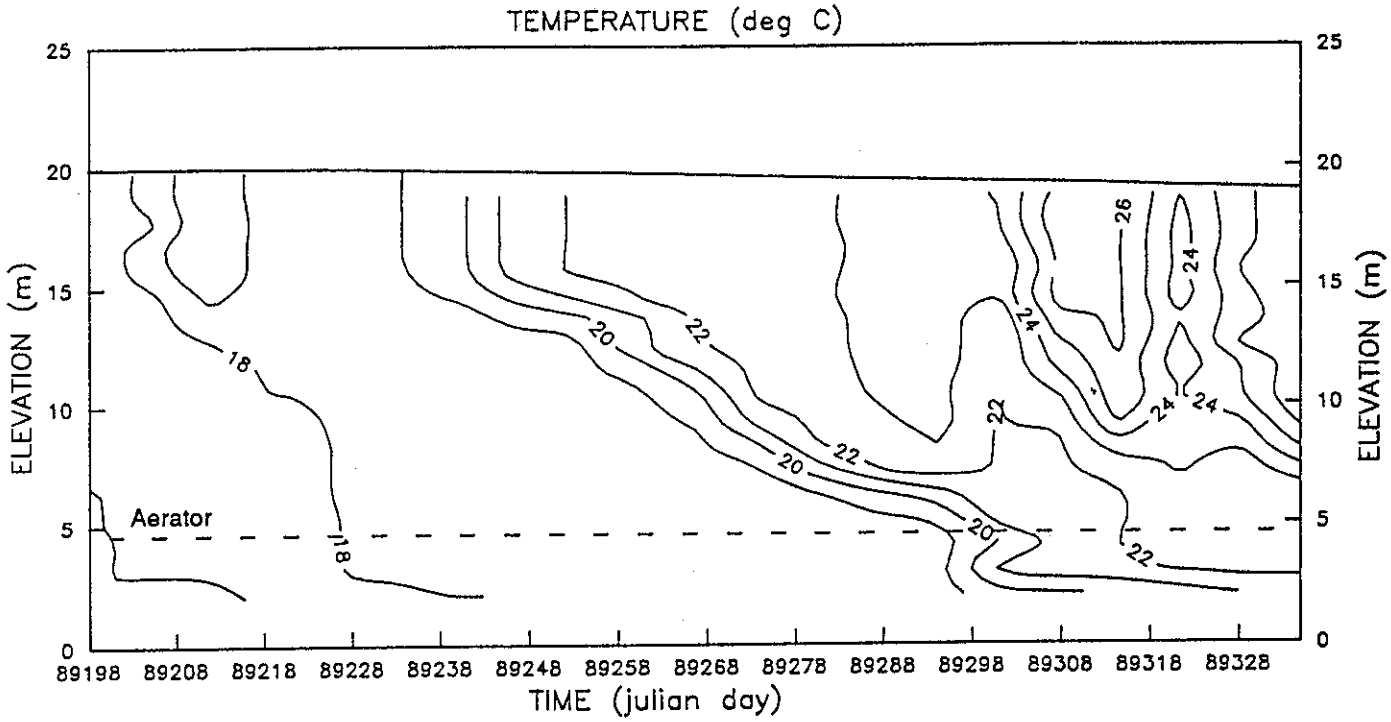

Figure 5.3 Simulated isotherm-depth history plot with a total free air flow rate of 40 Ls^{-1} through 100 holes from Day 89265 to Day 89336.

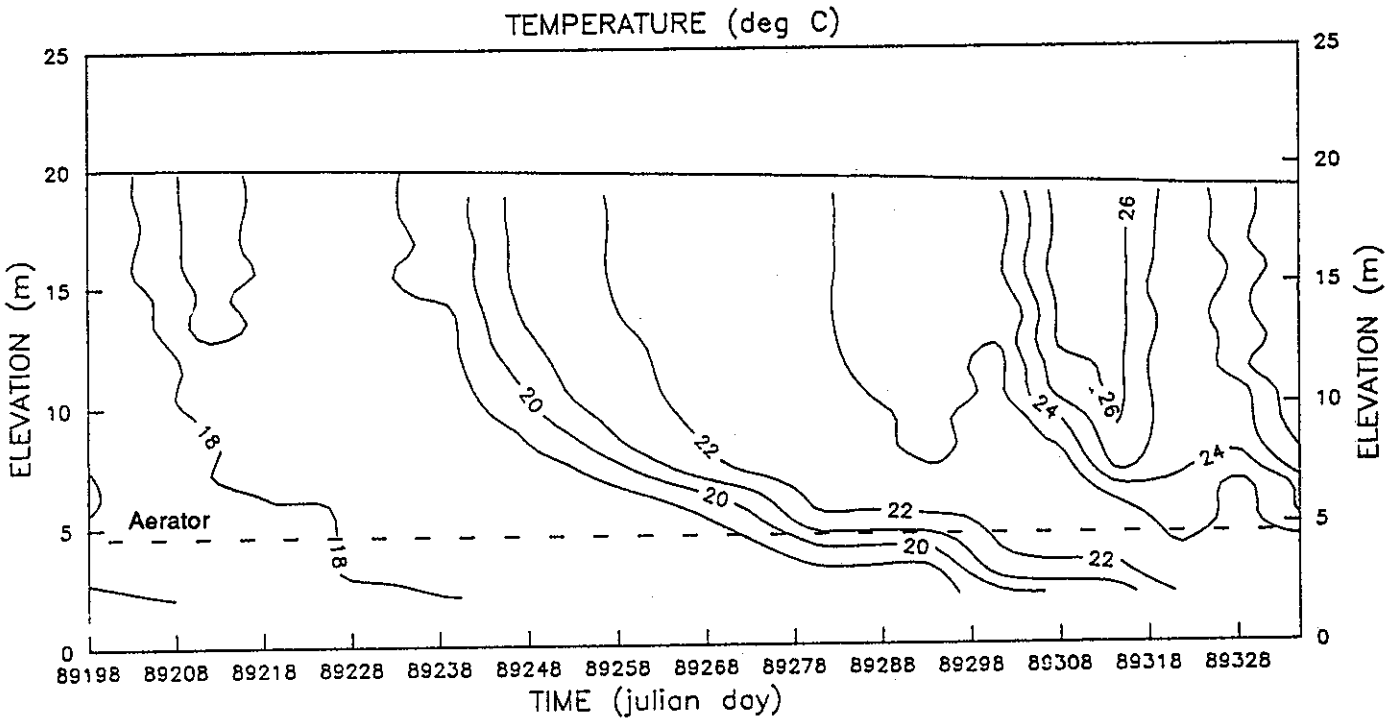

Figure 5.4 Simulated isotherm-depth history plot with a total free air flow rate of 40 Ls^{-1} through 100 holes from Day 89198 to Day 89336.

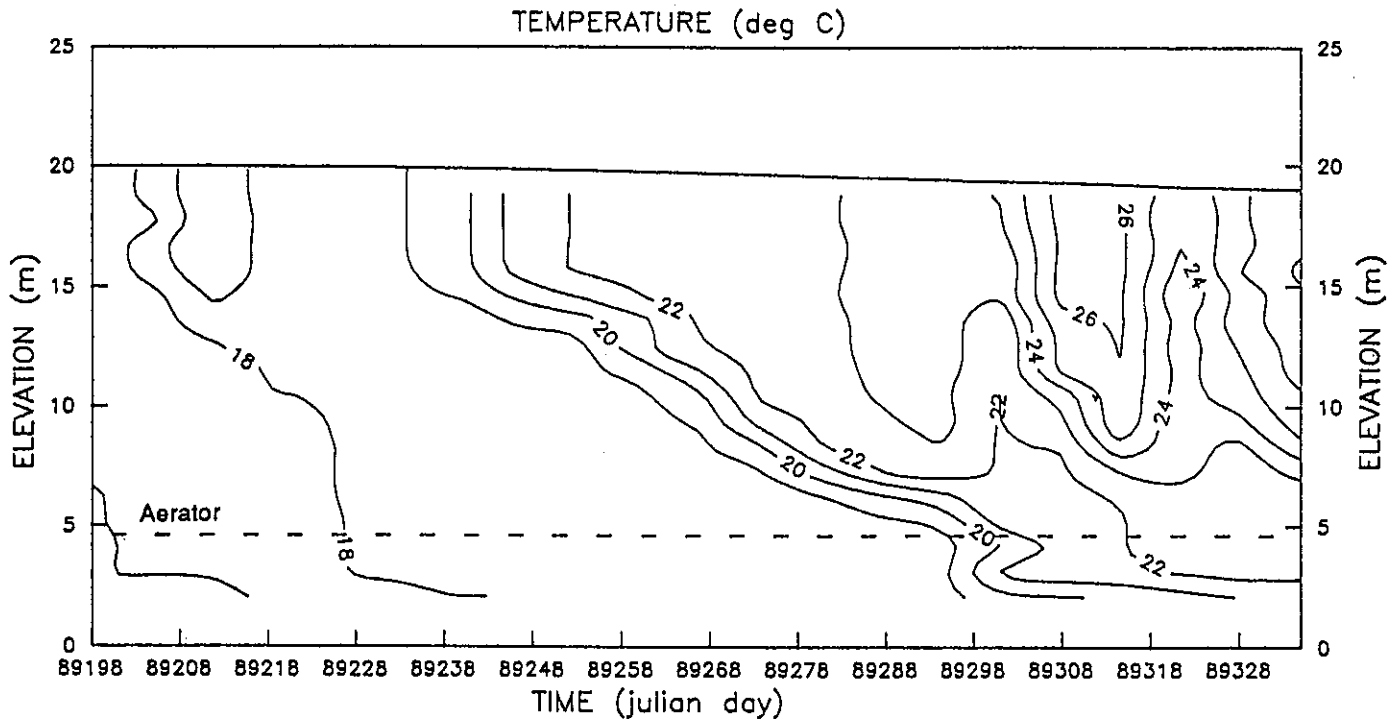

Figure 5.5 Simulated isotherm-depth history plot with a total free air flow rate of 40 Ls^{-1} through 100 holes from Day 89265 to Day 89304, followed by 80 Ls^{-1} through 100 holes from Day 89305 to Day 89336.

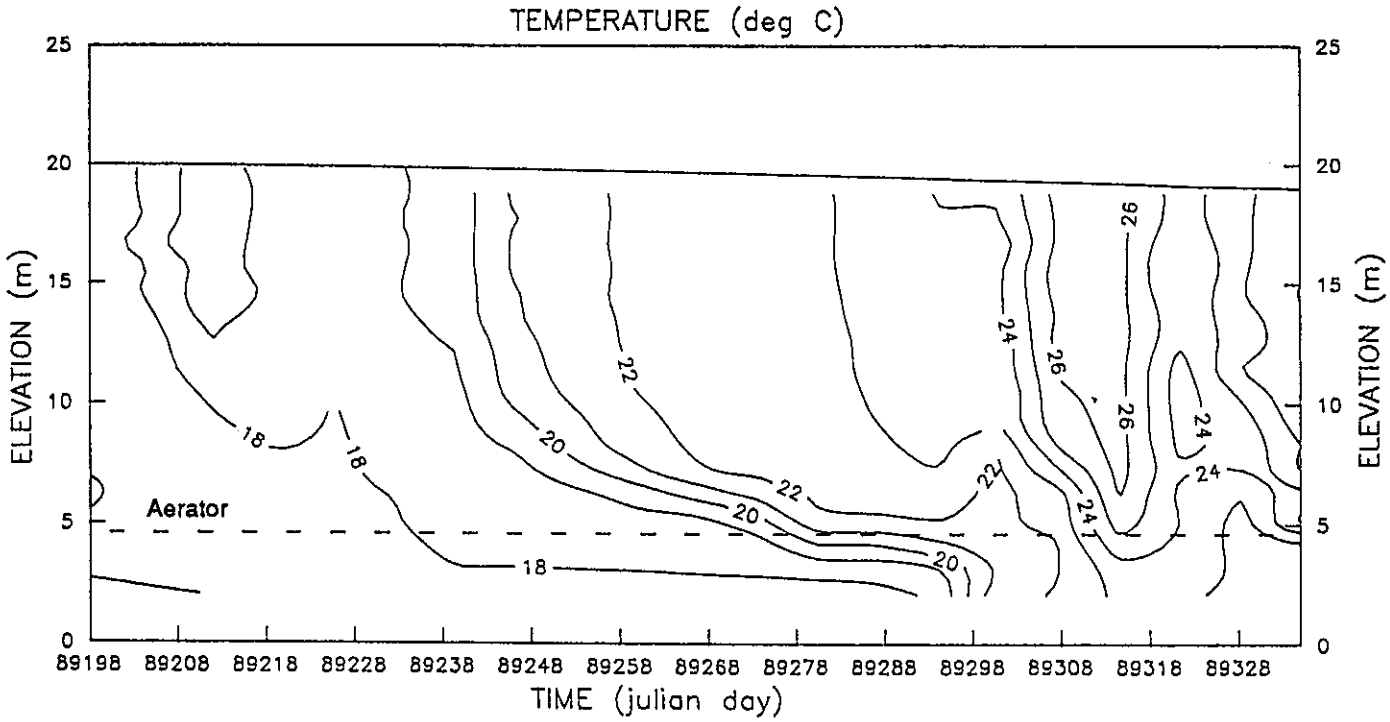

Figure 5.6 Simulated isotherm-depth history plot with a total free air flow rate of 80 Ls^{-1} through 100 holes from Day 89198 to Day 89336.

5.2.2 Aeration at 100 Ls^{-1}

By replacing the existing aerator line as of Day 89304, it would have been feasible to install an aerator capable of delivering any desired air flow. To test the benefits of this option, the model was run with a free air flow of 100 Ls^{-1} from Day 89305 through Day 89336 with the existing air flow up to Day 89304. Figure 5.7 demonstrates that the advantages of upgrading the aerator at this point in the stratification cycle would have only been marginal. It is realistic, however, to consider replacing the aerator for the 1990/91 summer and applying the larger air flow over the full summer period. This option was tested by running the 100 Ls^{-1} air flow through 200 holes from Day 89198 through Day 89336 (Fig. 5.8). This plot clearly shows major advantages in increasing the capacity of the aeration system. The water column is almost fully mixed above the aerator over the full simulation period. The strategy is a significant improvement on operating at either 40 Ls^{-1} (Fig. 5.4) or 80 Ls^{-1} (Fig. 5.6) over the full simulation period.

5.2.3 Aeration at 200 Ls^{-1}

Section 5.2.2 demonstrated the advantage of increasing the free air flow to 100 Ls^{-1}. Figures 5.9 and 5.10 plot similar strategies to those given in Figs. 5.7 and 5.8, except with 200 Ls^{-1} air flow through 200 holes.

Figure 5.9 follows the results described by Fig. 5.7, in demonstrating the limited benefits of increasing the air flow late in the stratification cycle. Figure 5.10, however, confirms the real advantages of increasing the air flow capacity of the aerator provided it is activated at the first evidence of stratification of the water column. The benefit of increasing the total air flow from 100 Ls^{-1} (Fig. 5.8) to 200 Ls^{-1} (Fig. 5.10) over the full simulation period was, however, only marginal.

5.3 Recommendations for the Future Operation of the Harding Dam Aerator

In the work described above, the modified aeration model was used to assess the operational options for the artificial destratification of Harding Dam. In this task, the models' ready application in the design/management environment was also clearly demonstrated. The model was used to assess possible aeration strategies for the 1989/90 summer and future summer periods with the recommendations derived from the modelling work for the improved destratification of Harding Dam as follows:

1989/90 Summer
- continue operation of the existing aerator delivering free air at a rate of 40 Ls^{-1}.

Future Summers
- replace the existing aerator line with a system capable of delivering 100 Ls^{-1},
- commence aeration immediately the stratification cycle commences.

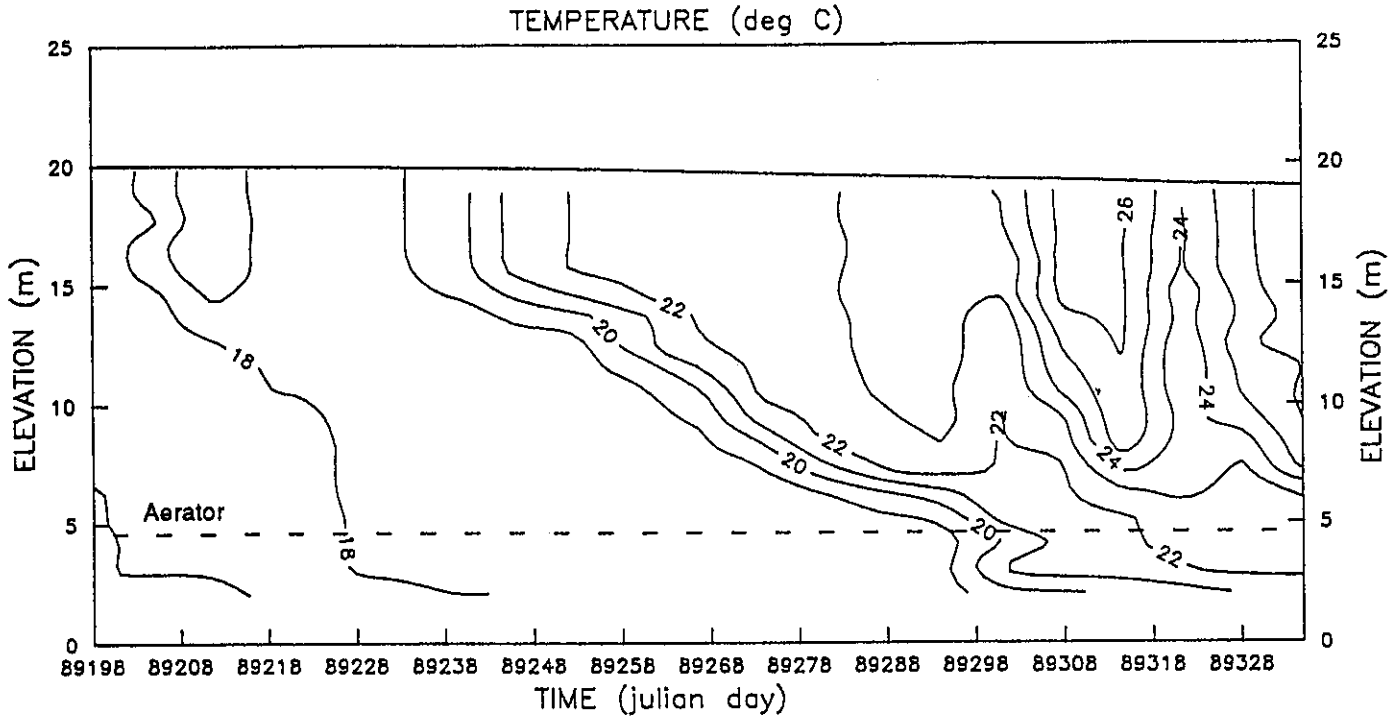

Figure 5.7 Simulated isotherm-depth history plot of simulated data with a total free air flow rate of 40 Ls^{-1} through 100 holes from Day 89265 to Day 89304, followed by 100 Ls^{-1} through 200 holes from Day 89305 to Day 89336.

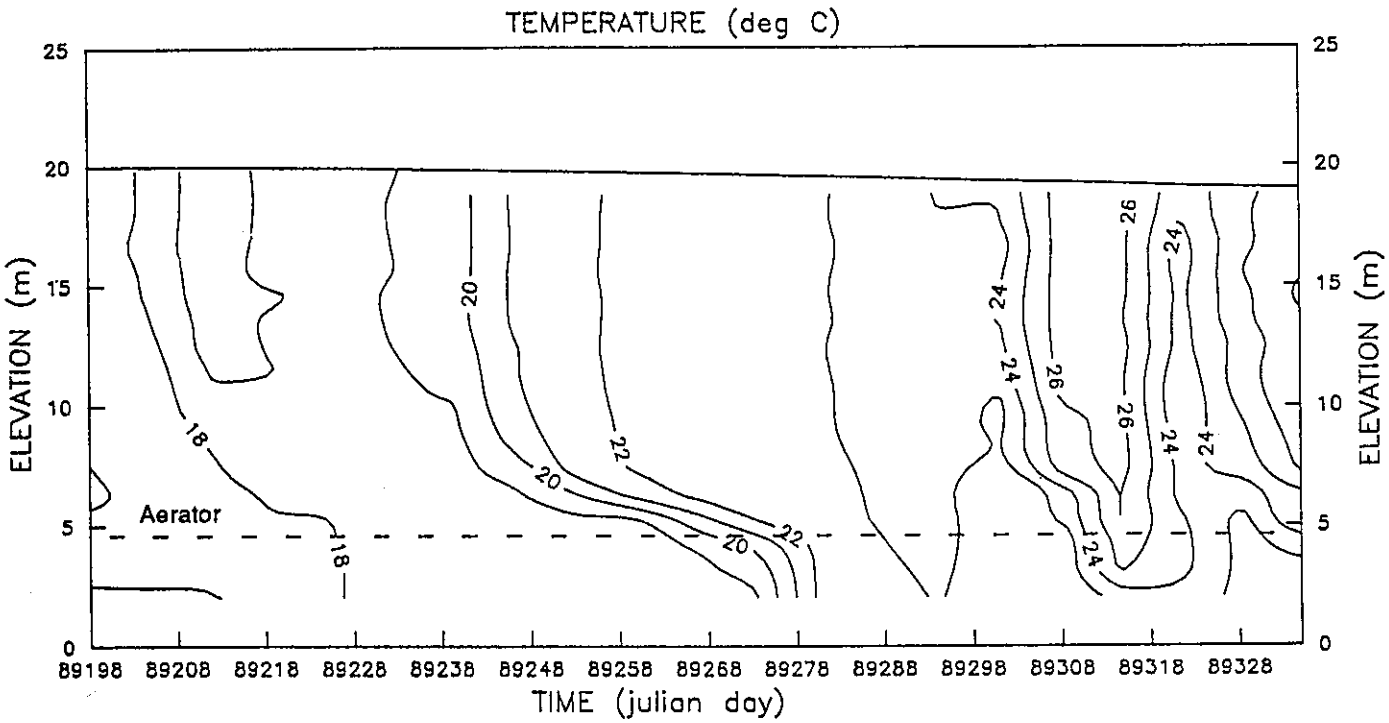

Figure 5.8 Simulated isotherm-depth history plot with a total free air flow rate of 100 Ls^{-1} through 200 holes from Day 89198 to Day 89336.

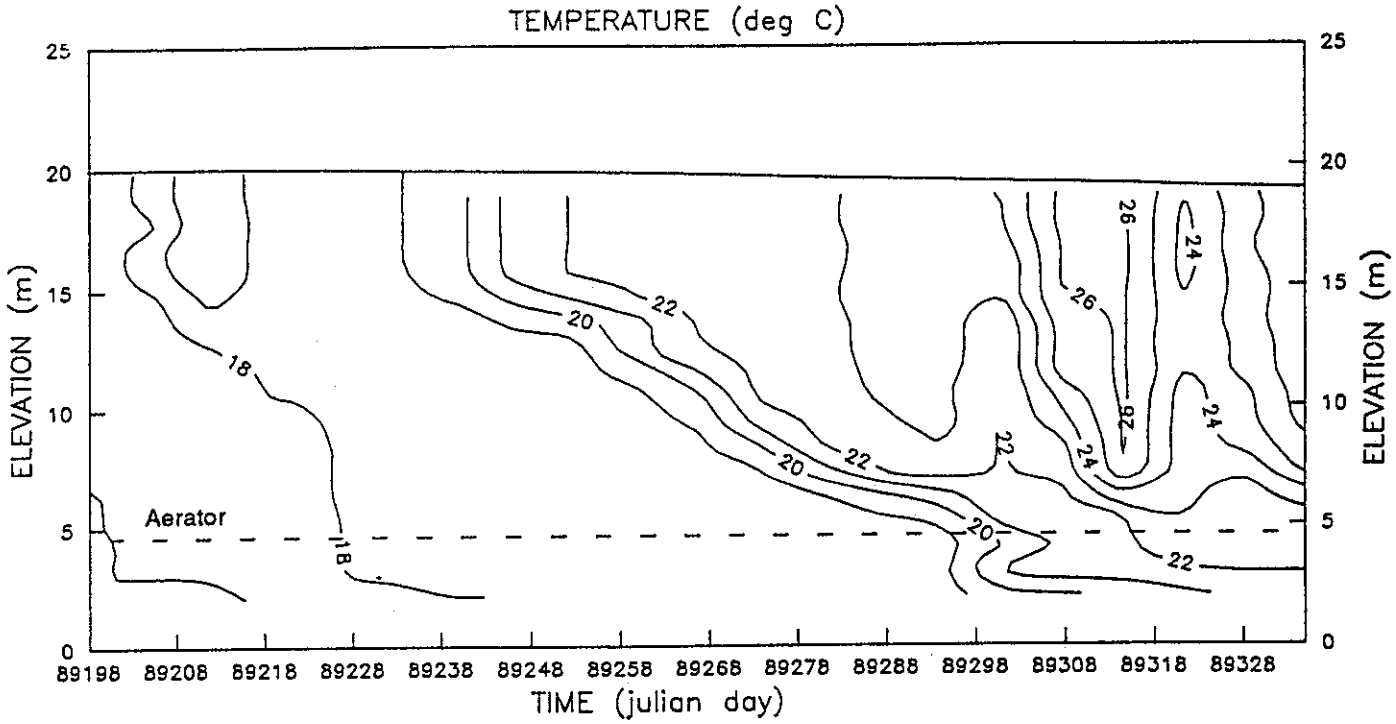

Figure 5.9 Simulated isotherm-depth history plot of simulated data with a total free air flow rate of 40 Ls^{-1} through 100 holes from Day 89265 to Day 89336, followed by 200 Ls^{-1} through 200 holes from Day 89205 to Day 89336.

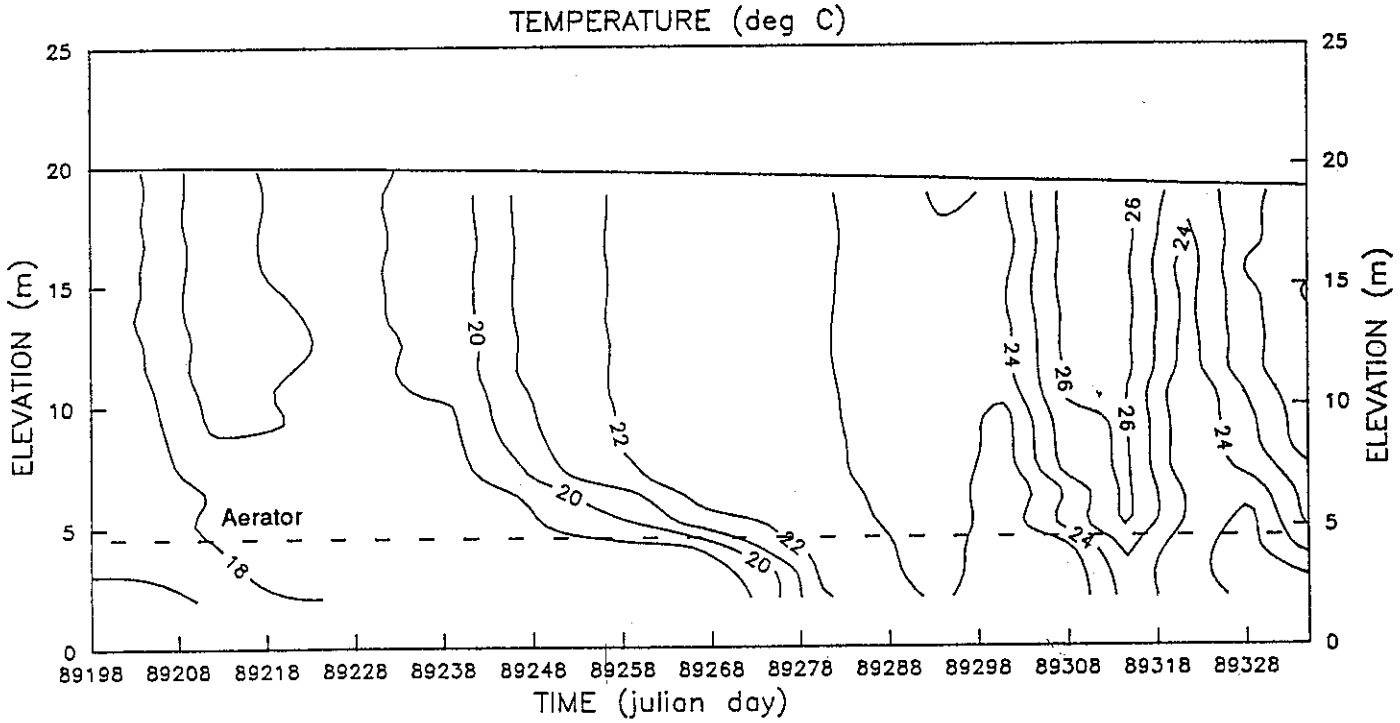

Figure 5.10 Simulated isotherm-depth history plot of simulated data with a total free air flow rate of 200 Ls^{-1} through 200 holes from Day 89198 to Day 89336.

CHAPTER 6

CONCLUSIONS

This report describes the results of a study programme directed at devising improved methods of designing air bubbler destratification systems. The study consisted of several components; laboratory and field programmes intended to improve the understanding of the behaviour of bubble plumes, and to quantify several of the parameters involved in the theoretical description of the plumes; incorporation of this information into the reservoir simulation model DYRESM; testing of the model against field and laboratory data; design of an aeration system for Harding Dam using the model; a field investigation programme to provide information on the bubble plume behaviour and to validate the model performance; and formulation of recommendations regarding the future operation of the Harding Dam aeration system.

The laboratory experiments showed that rising air bubbles entrain surrounding water and carry it up as an air-water mixture. The mixture rises through the decreasing ambient density, driven by the buoyancy of the bubbles but retarded by the negative buoyancy of the entrained water. Ultimately a level is reached at which these two driving forces balance and the entrained water is ejected from the plume. A new plume commences at this point. Within this very broad picture a wide variety of behaviour is observed, depending on the relative values of the air flow rate, the stratification, and the bubble size.

Peak efficiency of destratification occurs when the air flow is just sufficient for the detrainment to occur at the water surface. For a linear stratification, the experiments showed that a maximum efficiency of destratification occurred at a particular value of the plume number P_N. This number includes the effects of the stratification, air flow rate and depth, and was later modified to P_N^* incorporating the effect of bubble expansion. A similar plume number P_Δ is available for the two layer stratification. The efficiency maximum occurs between two extreme conditions where either insufficient air flow is applied for the given stratification (large P_N^*) or an excess of air is applied for the given stratification (low P_N^*).

A bubble plume simulation algorithm was included in the reservoir simulation model DYRESM, based on the assumption that the rising plume could be treated as a simple buoyant plume with a density equivalent to that of the air-water mixture, with an additional source of buoyancy provided by the expansion of the bubbles as they rise through the water column. In the relatively shallow experimental configurations, this latter term was negligible, but extensive numerical tests confirmed the importance of the effect in reservoir situations.

The experiments were run in two series, with 1mm and 4mm diameter bubbles, resulting in different efficiencies for any given plume number. Using the algorithm to simulate these two results indicated that the effect of the different bubble sizes may be incorporated in the model through the value selected for the entrainment coefficient. For simple, single phase buoyant plumes, 0.0833 is usually recommended, and this appears to be appropriate for bubble plumes except in those cases where very large bubbles are formed (in which case the entrainment is reduced). This conclusion is consistent with the sparse data available in the literature.

An aerator design philosophy was proposed. It was founded on two principles; first, that the total entrainment increases as the number of separate plumes increases for a given total air flow rate, assuming that the resulting plumes are independent; and second, that each plume should operate at the optimum plume number. As the stratification in the reservoir is continually changing as the result of destratification and meteorological forcing, the air flow rate and the number of holes require continual alteration, which, in practice, is not feasible. The design procedure developed was then as follows :

(1) select a hole size of about 1.0 mm diameter to ensure that the entrainment coefficient approaches 0.0833,

(2) for a number of different total air flow rates, vary the number of holes in a series of simulations over some predetermined period, and measure the effectiveness of each case, noting that the hole spacing must be sufficient to ensure that the plumes are independent,

(3) select a combination of air flow rate and number of holes which satisfies the specified operational criteria. These criteria may be expressed in terms of the efficiency of energy conversion, temperature difference between the surface and aerator, or time of destratification from some stratified condition. Each of these criteria places different requirements on the aeration system so that the design must be geared to the appropriate criterion.

This procedure was applied to design an aeration system for Harding Dam (W.A.) for operation in the summer of 1988/89. The aerator was designed to maintain a destratified condition over a typical summer period at minimum operating cost. The system was therefore designed to operate only in the presence of a significant stratification whilst minimising the number of days operation required to maintain temperature differences of less than 3°C between the surface and the aerator level. Thus, the aerator was designed to be turned on when the surface to aerator level temperature difference exceeded this amount, and turned off when the difference was less than 1°C. These limits were later changed to 1°C and 0.5°C, resulting in a design air flow rate of 50 L sec^{-1} through 100 holes, spaced 4 metres apart. Each hole was specified to be 1.5mm in diameter.

This design was only partially successful, with field data collected during operation of the aerator indicating that the effectiveness of destratification was somewhat less than that predicted. This was assumed to be caused, at least in part, by the air bubbles being a different diameter to those generated in the experiments with the aerator probably operating with a lower entrainment coefficient than the assumed design value of 0.0833.

The second stage of the project was to evaluate the performance of the bubbler algorithm and to modify the algorithm as required. This involved the assembly of a comprehensive data set for Harding Dam, as well as detailed field investigations of bubble plume characteristics. The field investigations showed that although the overall simplified view of the plume behaviour appeared to be correct, the treatment of the detrained fluid by the algorithm was not completely accurate. Further, the plume was clearly affected by events on time scales shorter than the time step over which the model was implementing the bubble plume algorithm. The algorithm was modified to incorporate these effects and validated against data collected over a two month period.

The resulting model was used to test the likely effectiveness of the Harding Dam aerator for the 1989/90 and subsequent summers. This resulted in the following recommendations for the Harding Dam aerator :

- increase the air flow capacity of the aerator to 100 Ls^{-1}, retaining 100 holes,
- reduce the hole diameter to 1.0 mm to increase the entrainment coefficient,
- commence aeration immediately stratification is observed,
- operate the aerator such that primary plume ejection is at the water surface (i.e. at the plume number corresponding to the peak efficiency of destratification).

In summary, the study showed that the model was capable of realistically reproducing the range of plume behaviour observed in the laboratory and the field, and that the performance of bubble plume aerators depends on the magnitude of the plume number and on the air bubble size. The model was shown to be a useful design tool, given specific operational criteria, as it simulates the dynamic behaviour of the buoyant air-water plume mixture and therefore allows the design to be tested, and the efficiency maximised, under temporally varying meteorological conditions and air flow. The Harding Dam aerator design was partially successful in destratifying the reservoir but, after evaluation and modification of the aeration algorithm, an increased air flow rate was recommended.

Some aspects of the entrainment process are, however, not yet fully understood. At present, no data set exists for any reservoir which will allow complete validation of the aerator model. Such validation requires full meteorological, inflow, outflow and aerator operational data, together with field data which captures the performance of the bubble plume. Only when this validation is complete will the algorithm form a completely reliable design tool for aeration systems.

REFERENCES

ASAEDA, T., IKEDA, H., AND IMBERGER, J. (1990). Influence of bubble size on bubble plumes. University of Western Australia, Centre for Water Research ED 353 TA.

ASAEDA, T. AND IMBERGER, J. (1990) Structures of bubble plumes in stratified environments. University of Western Australia, Centre for Water Research ED-88-250.

BAINES, W.D. AND LEITCH, A.M. (1987). The destratification of a stratified density distribution by a bubble plume. *J. Fluid Mech.*, (submitted)

CALE, G.A. (1979) *Textbook of Limnology*. 2nd Edition. C.V. Mosby Company, St. Louis, USA.

DAVIS, J.M. (1980) Destratification of reservoirs - a design approach for perforated-pipe compressed-air systems. Water Services, **84**: 497-504.

IMBERGER, J. AND LEMCKERT, C. (1990) Bubble plume intrusions. In preparation.

IMBERGER, J. AND PATTERSON, J.C. (1981). A dynamic reservoir and simulation model-DYRESM:5. In *Transport Models for Inland and Coastal Waters*. (H.B. Fischer ed.), pp.310-361.Academic Press, New York

IMBERGER, J. AND PATTERSON, J.C. (1990) Physical Limnology. In: "*Advances in Applied Mechanics*", T. Wu (ed). Academic Press, Boston, **27**: 303-475.

LIST, E.J. (1982) Mechanics of turbulent buoyant jets and plumes. In: "*Turbulent Buoyant Jets and Plumes. HMT: The Science and Applications of Heat and Mass Transfer*". Vol. 6, W. Rodi (ed), Pergamon Press, Oxford.

MCAULIFFE, T. AND ROSICH, R. (1989) A review of the effects of artificial destratification on water quality in Australian water storages. Report to the Urban Water Research Association of Australia. Project No. WS/2. (In press)

MCDOUGALL, T.J. (1978) Bubble plumes in stratified environments. *J. Fluid Mech.*, **85**(4): 655-672.

NORTHCOTE, K.H. *ET AL.* (1967) *Atlas of Australian Soils*. Commonwealth Scientific and Industrial Research Organisation, Melbourne.

PATTERSON, J.C., HAMBLIN, P.F. AND IMBERGER, J. (1984). Classification and dynamic simulation of the vertical density structure of lakes. *Limnol. Oceanogr.* **29**(4): 845-861.

PATTERSON, J.C. AND IMBERGER, J. (1989) Simulation of bubble plume destratification systems in reservoirs. *Aquatic Sciences* **51**(1): 3-18.

ROSICH, R. AND MCAULIFFE, T. (1990) Water quality effects of artificial aeration/destratification at Harding Reservoir in north-western Australia.. Report to the Urban Water Research Association of Australia. Project No. WS 2.

SCHLADOW, G. AND PATTERSON, J.C. (1990) Destratification of lakes: part 1. In preparation.

TENNESSEE VALLEY AUTHORITY, Division of Water Control, Planning and Engineering Laboratory (1972) Heat and mass transfer between a water surface and the atmosphere. Water Resources Lab. Rept. No. 14, Norris, Tennessee.

APPENDICES

APPENDIX A1

PHYSICAL CHARACTERISTICS OF HARDING DAM

	Elevation (R.L.)	Surface Area ($\times 10^3$ m^2)	Storage Volume ($\times 10^3$ m^3)
Maximum flood level	76.0	96 040	838 262
Full supply level	60.0	14 130	63 805
Base of main embankment	40.0	0	0

Table A1.1 *Harding Dam Storage Capacity*

	Height above Foundation (m)	Height above River Bed (m)	Length of Crest (m)
Main Embankment	45	36	320
Auxiliary Embankment	15	-	150

Table A1.2 *Main and Auxiliary Embankment Statistics*

IFF/RDF	Length (m)	Design Cap (m^3/s)	Maximum Cap (m^3/s)	% Flood Level
Main spillway	70	7360	8963	>100%
Auxiliary spillway	0-125	2300	3164	>100%

IFF - Imminent Failure Flood;. RDP - Recommended Design Flood.

Table A1.3 *Harding Dam Main and Auxiliary Spillway Capacities*

Water Elevation (RL)	Storage Volume ($\times 10^3$ m^3)	Surface Area ($\times 10^3$ m^2)
40.00	0.0	0.0
41.00	6.9	100.0
42.00	183.2	150.0
43.00	377.3	245.8
44.00	686.2	375.6
45.00	1130.0	514.0
46.00	1732.1	705.9
47.00	2586.9	1022.1
48.00	3783.2	1358.9
49.00	5270.2	1605.0
50.00	6994.1	1853.8
51.00	8996.4	2156.4
52.00	11329.9	2528.2
53.00	14076.8	2976.3
54.00	17333.4	3577.3
55.00	21288.8	4358.7
56.00	26162.5	5475.3
57.00	32434.5	7151.8
58.00	40592.0	9206.1
59.00	50953.8	11575.8
60.00	63805.0	14125.7
61.00	79185.2	16638.7
62.00	97125.8	19281.9
63.00	117765.7	22005.0
64.00	141307.7	25242.9
65.00	168613.9	29515.9
66.00	200581.7	34545.6
67.00	237908.7	40272.8
68.00	281214.4	46291.0
69.00	330389.9	52046.6
70.00	385257.3	57651.4
71.00	445519.9	62801.8
72.00	510950.8	68221.5
73.00	582361.5	74745.0
74.00	660596.5	81735.6
75.00	745849.0	88804.9
76.00	838262.5	96042.6
77.00	937988.5	103438.4
77.50	990641.8	107175.3

Table A1.4 *Harding Dam Storage Table*

APPENDIX A2

OPERATIONAL DETAILS OF AERATORS I & II

Date	Air Flow Rate ($l\ s^{-1}$)	Water Surface Level (R.L.)	Aerator Level (R.L.)
11 Jun 86	175	53.693	45.0
24 Aug 86	0	52.923	45.0
12 Nov 86	60	51.773	45.0
14 Nov 86	90	51.693	45.0
22 Jan 87	90	60.110	45.0
16 Mar 87	135	59.891	45.0
30 Mar 87	158	59.786	45.0
06 Apr 87	90	59.722	45.0
16 Apr 87	0	59.637	45.0
24 Apr 87	90	59.570	45.0
23 May 87	0	59.401	45.0
25 Sept 87	60	58.558	45.0
21 Dec 87	99	57.512	45.0
06 Jan 88	100	57.297	45.0
07 Jan 88	80	57.279	45.0
08 Jan 88	120	57.296	45.0
09 Jan 88	100	57.255	45.0
28 Jan 88	120	56.986	43.5
13 May 88	100	55.782	43.5
23 May 88	100	56.156	43.5
16 Jun 88	0	55.994	43.5

Table A2.1 *Operational Details of Aerator I on Harding Dam*

Date	Air Flow Rate ($l\ s^{-1}$)	Total Hours Operating (per day)
27 Sept 88	40	6
05 Oct 88	40	6
06 Oct 88	40	24
07 Oct 88	40	24
08 Oct 88	40	24
09 Oct 88	40	24
11 Oct 88	40	24
12 Oct 88	40	24
18 Oct 88	40	6
21 Oct 88	40	24
22 Oct 88	40	24
23 Oct 88	40	24
24 Oct 88	40	24
25 Oct 88	40	24
26 Oct 88	40	24
27 Oct 88	40	24
28 Oct 88	40	24
28 Oct 88	40	24
29 Oct 88	40	24
30 Oct 88	40	24
31 Oct 88	40	24
01 Nov 88	40	24
02 Nov 88	40	24
03 Nov 88	40	24
14 Dec 88	40	6
21 Dec 88	40	6
23 Dec 88	40	6
24 Dec 88	40	6
26 Dec 88	40	6
27 Dec 88	40	6
29 Dec 88	40	6
04 Jan 89	40	6
06 Jan 89	40	6
07 Jan 89	40	6
08 Jan 89	40	6
09 Jan 89	40	6
10 Jan 89	40	6
26 Jan 89	40	6
28 Jan 89	40	6
30 Jan 89	40	6

Table A2.2 *Operational Details of Aerator II on Harding Dam*

APPENDIX A3

Aerator Pneumatic Design

The simulations described in Chapter 3 defined the total free air flow rate required to break down the thermal stratification in Harding Dam over a typical summer period and the number of holes required to efficiently distribute the designated air flow. The physical structure of the aeration system must be designed to deliver and distribute the calculated air flow. This section details the theoretical background used in the design of aeration systems and summarises the application of this theory to the design of the Harding Dam aerator.

A3.1 Gas Flow Through a Hole

The mass rate of flow of gas through any nozzle is defined as (Atlas Copco, 1982) :

$$G = \delta \psi P_1 A[2/(RT_1)]^{0.5} \times 10^{-6} \quad [kg\ s^{-1}] \qquad \text{(A3.1)}$$

where G is the flow rate (kg s^{-1}),
δ is the nozzle efficiency (dimensionless),
ψ is the flow coefficient (dimensionless),
P_1 is the upstream absolute pressure (Pa),
A is the minimum flow area (mm^2),
R is the gas constant (J kg^{-1} K^{-1}),
T_1 is the upstream absolute temperature (K).

The volume rate of free gas flow, Q_{AT}, is then defined by dividing the mass rate of flow, G, by the free gas density, ρ_{AT}. That is,

$$Q_{AT} = \frac{G}{\rho_{AT}} \quad [m^3\ s^{-1}] \qquad \text{(A3.2)}$$

where

$$\rho_{AT} = \frac{P_{AT}}{R\ T_{AT}} \quad [kg\ m^{-3}] \qquad \text{(A3.3)}$$

and P_{AT} is standard atmospheric pressure (101 330 Pa),
T_{AT} is standard atmospheric temperature (293 °K).

For reservoir aeration systems based solely on air delivery (R = 287.1 J kg^{-1} K^{-1}), ρ_{AT} is 1.19 kg m^{-3}.

Most aeration systems are comprised of a single air pipeline laid horizontally near the bottom of the water storage with small diameter holes drilled in the pipe at regular intervals. For a round hole drilled in polyethylene pipe, the nozzle efficiency, δ, approximates the

hole coefficient of discharge, C. Substituting for the gas constant, R, and the nozzle efficiency, δ, in (A3.2), defines the volume free air flow rate through a single hole as

$$Q_{AT} = 0.07\,\psi\frac{CP_1A}{\sqrt{T_1}} \times 10^{-3} \quad [l\,s^{-1}] \qquad \text{(A3.4)}$$

The flow coefficient, ψ, varies between 0 and 0.53 depending upon the value of (P_2/P_1), where P_2 is the downstream pressure (Atlas Copco, 1982). When the pressure ratio (P_2/P_1) exceeds 0.5, the flow through the hole is sub-critical and the free air flow rate, Q_{AT}, is then defined by equation (A3.4) where the flow coefficient, ψ, is dependent upon the pressure ratio. The result must then be derived iteratively, substituting for ψ and P_2. An alternative means of determining the sub-critical free air flow rate is given in the Compressed Air and Gas Data handbook (1980); where :

$$Q_{AT} = 0.13\frac{CP_1A}{\sqrt{T_1}} \cdot \left[\left(\frac{P_2}{P_1}\right)^{1.43} - \left(\frac{P_2}{P_1}\right)^{1.71}\right]^{0.5} \times 10^{-3} \quad [l\,s^{-1}] \qquad \text{(A3.5)}$$

where
- C is the coefficient of discharge (or nozzle efficiency),
- P_1 is the upstream absolute pressure (Pa),
- A is the total hole area $(mm)^2$,
- T_1 is the upstream absolute temperature (K),
- P_2 is the downstream absolute pressure (Pa).

The absolute pressure downstream of any hole, P_2, is given by the water depth, h. When this pressure decreases to a value of less than half the upstream pressure, P_1, the flow through the hole becomes super-critical. Under super-critical conditions, the flow rate is independent of the downstream pressure, ψ tends to 0.53, and the volume free air flow rate becomes :

$$Q_{AT}^{SUPER} = 0.037\frac{CP_1A}{\sqrt{T_1}} \times 10^{-3} \quad [l\,s^{-1}] \qquad \text{(A3.6)}$$

A3.2 DESIGN PARAMETERS

Assuming P_2/P_1 is greater than 0.5 (i.e. sub-critical conditions) the design of a perforated pipe aerator (i.e. regularly spaced small diameter holes) may be derived by substituting $C \approx 0.62$ and $A = \pi D^2/4$ into equation (A3.5), giving :

$$Q_{AT} = 0.063\frac{P_1D^2}{\sqrt{T_1}} \cdot \left[\left(\frac{P_2}{P_1}\right)^{1.43} - \left(\frac{P_2}{P_1}\right)^{1.71}\right]^{0.5} \times 10^{-3} \quad [l\,s^{-1}] \qquad \text{(A3.7)}$$

This equation defines three fundamental variables that must be specified in the design - the free air flow rate per hole, Q_{AT} ; the upstream absolute pressure, P_1 ; and the hole diameter,

D. The free air flow rate per hole is defined by the total air delivery, Q_T, divided by the total number of holes, N, in the aerator pipe.

The minimum pressure upstream of any hole must be greater than the maximum downstream pressure; that is, greater than the maximum absolute hydrostatic pressure. Defining the maximum depth of submergence of the aerator line as h, gives the downstream pressure as :

$$P_2^{MAX} \approx \rho g h + 101\ 300\ Pa \qquad \text{(A3.8)}$$

The minimum absolute delivery pressure upstream of an individual hole is then given as

$$P_1^{MIN} = P_2^{MAX} + \Delta P_0 \qquad \text{(A3.9)}$$

where ΔP_0 is the pressure loss (or over-pressure) across the hole. The true upstream pressure along the aerator pipe will decrease towards the end of the pipe in response to frictional losses (see section A3.3). Substituting (A3.9) into (A3.7) gives the result used to define the over-pressure required to deliver the specified air flow through the final hole of the aerator pipe, given the water depth, h, and the hole diameter, D:

$$Q_{AT} = 63\,(P_2 + \Delta P_o)\,\frac{D^2}{\sqrt{T_1}}\left[\left(\frac{P_2}{P_2 + \Delta P_o}\right)^{1.43} - \left(\frac{P_2}{P_2 + \Delta P_o}\right)^{1.71}\right]^{0.5} \times 10^{-6}\ [ls^{-1}] \qquad \text{(A3.10)}$$

The final design variables then become :

ΔP_0	-	the over-pressure
D	-	the hole diameter
Q_T	-	the total free air flow rate
N	-	the total number of holes.

Work by Asaeda and Imberger (1990) and Knoppert et al. (1970) suggests that small air bubbles produce more efficient entrainment. Previous work has indicated that bubble size is a function of the hole diameter, the over-pressure, the compressed air density at the hole, and the surface tension of the fluid into which the air is released [Van Krevelen and Hoftijzer (1950), Coppock and Meiklejohn (1951)]. On the basis of field experiments on Maarsseveen Lake in Holland, Knoppert et al. (1970) proposed that destratification is most efficient when both the hole diameter, D, and the over-pressure, ΔP_0, are small. This result also implies that destratification is most efficient when the free air flow rate per hole is small (A3.10) and, as a consequence, the total number of holes is large. This conclusion is consistent with the DYRESM simulation runs carried out for the Glennies Creek Reservoir, where large hole diameters, were shown to operate with a very low entrainment coefficient (Lewis, 1989).

A3.3 FLOW AND PRESSURE DISTRIBUTION IN A PERFORATED PIPE

The pressure loss in a straight compressed air delivery pipeline is determined according to the following formula (Atlas Copco, 1976) :

$$P_L = K\, Q_T^{1.85}\, l / \left(d_p^5\, P_I\right) \qquad [kPa] \qquad \text{(A3.11)}$$

where K is a constant (1.6×10^{12}),

Q_T is the total free air flow rate ($m^3\ s^{-1}$),

d_p is the inner diameter of the pipe (mm),

l is the total length of the pipe, including fittings, etc (m),

P_I is the absolute initial line pressure (kPa).

Equation (A3.11) is applicable for most compressed air delivery systems, however, the constant (1.6×10^{12}) may vary somewhat depending on the internal pipe roughness. Pressure losses in polyethylene pipe systems [as calculated by (A3.11)] may be checked using supplier design charts. Given the delivery air flow rate (i.e. free air flow rate/compression ratio) and the pipeline inner diameter, the percent pressure drop per kilometre of pipe may be derived directly from these charts.

The pressure loss in a perforated pipeline, however, is less than that for a non-perforated pipe. The decrease in flow velocity across the holes, as air is discharged into the water storage, generates a static head recharge pressure, P_R^A, along the line :

$$P_R^A = \rho_c/2 \left(V_I^2 - V_{I'}^2\right) \qquad [Pa] \qquad \text{(A3.12)}$$

where ρ_c is the compressed air density ($kg\ m^{-3}$)

V_I is the air flow velocity just upstream of hole I

$V_{I'}$ is the air flow velocity just downstream of hole I.

The net pressure loss between two successive holes in the perforated pipe is then

$$P_L^N = P_L^A - P_R^A \qquad [Pa] \qquad \text{(A3.13)}$$

where P_L^A is the line pressure loss given by (A3.11)

P_R^A is the recharge pressure gain given by (A3.12).

The flow and pressure distribution along the full length of the aerator pipe may be determined by specifying the desired flow through the final hole of the aerator, thereby defining the over-pressure ΔP_o, and then calculating the line pressure loss and recharge between each hole along the length of the aerator pipe back to the compressor. As a first

approximation, however, it is sufficient to analyse the full aerator pipe in a single step. The sequence of design calculations for the Harding Dam aerator is set out in Appendix A3.

It is essential that the aerator distribute the total desired air flow evenly between all holes. Uniform flow distribution is achieved by maintaining a proper balance between (a) the kinetic energy and momentum of the inlet flow, (b) friction losses along the length of the aerator pipe, and (c) the pressure drop across the holes. The Chemical Engineers Handbook (1973) indicates that the ratio of the over-pressure, ΔP_o, to the kinetic energy of the inlet stream, K_I, and to the friction loss along the aerator, P_L^A, should be greater than or equal to 10. That is ,

$$\frac{\Delta P_o}{K_I} \gtrsim 10 \quad and \quad \frac{\Delta P_o}{P_L^A} \gtrsim 10 \tag{A3.14}$$

where

$$K_I \approx \rho \frac{V_I^2}{2} \qquad [Pa] \ . \tag{A3.15}$$

REFERENCES

Asaeda, T. and Imberger, J. (1990)
Structures of bubble plumes in stratified environments. University of Western Australia, Centre for Water Reseach Reference ED 88 250.

Atlas Copco (1976)
Atlas Copco Manual, Second Edition.

Atlas Copco (1982)
Atlas Copco Manual, Fourth Edition.

Chemical Engineers Handbook (1973)
ED. R.H. Perry and C.H. Chilton, Fifth Edition. McGraw-Hill, Tokyo.

Compressed Air and Gas Data (1980)
Ingersoll-Rand Co., Third Edition. Ed. A.W. Loomis.

Coppock, P.D. and Meiklejohn, G.T. (1951)
The behaviour of gas bubbles in relation to mass transfer. Trans. Inst. Chem Engnrs., Vol 29.

Knoppert, P.L. et al. 1970.
"Destratification experiments at Rotterdam." J. Am. Waterworks Assoc. Vol 652, pp. 448-454.

Lewis, D.P. (1989)
Glennies Creek Reservoir Aeration System Design. Report to Department of Water Resources. University of Western Australia, Centre for Water Research Reference WP 328 DL.

Van Krevelen, D.W. and Hoftijzer, P.J. (1950)
Studies of gas-bubble formation. Chemical Eng. Progress, 46(1): 29-34.

APPENDIX A4

HARDING DAM AERATOR PNEUMATIC CALCULATIONS

The general steps in the hydraulic design of an operational aeration system are as follows :

A) Aerator Configuration

1. Define the total free air flow rate, Q_T
2. Select the total number of holes, N
3. Calculate the free air flow rate per hole, Q_{AT}
4. Select an appropriate hole diameter, D_H
5. Specify the aerator pipe diameter, D_A
6. Specify the delivery pipe diameter, D_D
7. Specify the hole spacing, S
8. Calculate the total aerator line length, l_A
9. Specify a realistic aerator layout, defining the delivery line length, l_D
10. Specify the maximum depth of storage, h
11. Estimate the in-line flow temperature, T_I

B) System Pneumatic Calculations

12. Calculate the maximum downstream absolute pressure, P_2
13. Determine the over-pressure, ΔP_o, required to deliver the desired free air flow, Q_{AT}, through the final hole of the aerator
14. Calculate the aerator line pressure losses, P_L^A, along the full aerator length
15. Calculate the static head recharge pressure, P_R^A, along the full aerator length
16. Calculate the pressure loss in the air delivery line, P_L^D
17. Specify the minimum operating in-line absolute pressure, P_{IN}

C) Check Calculations

18. Using DYRESM, check that the given free air flow rate per hole, Q_{AT}, is sufficient to breakdown the stratification in the reservoir. Adjust Q_{AT} as necessary and repeat the design calculations above.
19. For the final design configuration, check that the flow distribution along the aerator is uniform and check that the in-line absolute pressure of the compressor is acceptable.

The "menu" set out above allows a reasonable degree of flexibility in the design of an aeration system. It is worthwhile considering various options and configurations before specifying a final design. In more detailed designs it may be necessary to determine the internal pressure and flow distribution along the full aerator length.

A4.1 Aerator Configuration

An aerator may be constructed either as a series of individual buoyant plumes or as a two dimensional line source of buoyancy. The fundamental difference between these two flow regimes is that in the case of the line source the bubble plumes interact and only entrain the ambient fluid along a plane periphery whilst the individual plumes are free to entrain over a larger conical periphery. It is likely, although yet to be verified, that the line source is somewhat less efficient in entrainment as compared to the individual plume concept.

The simulations suggested the following design parameters based on the assumptions set out in Chapter 3 of this report :

Total free air flow rate	:	Q_T	$= 50\ 1\ s^{-1}$
Total number of holes	:	N	$= 100$
Free air flow rate per hole	:	Q_{AT}	$= 0.5\ 1\ s^{-1}$

The design calculations are detailed below:

A) AERATOR CONFIGURATION :

Assume :	1. Total free air flow rate :	Q_T	=	$50\ 1\ s^{-1}$
	2. Total number of holes :	N	=	100 holes
	3. Free air flow rate per hole :	Q_{AT}	=	$0.5\ s^{-1}$
	4. Hole diameter :	D_H	=	1.5 mm
	5. Diameter of aerator line :	D_A	=	D_D : Diameter of delivery line (6)
	7. Hole spacing :	S	=	4.0 m
	8. Length of aerator line :	l_A	=	400 m
	9. Length of delivery line :	l_D	=	100 metres
	10. Maximum depth above aerator :	h	=	10 metres
	11. In-line temperature :	T_I	=	300 °K

B) SYSTEM PNEUMATIC CALCULATIONS :

5) *Diameter of aerator pipe* :

$$D_A \sim (10\, N\, D_H)^{1/2} \sim 39\ mm$$

- set $D_A = 50$ mm (class 9)

12) *Downstream pressure* :

$$P_2 = \rho g h + 101\,330 \text{ Pa}$$

- set $P_2 \approx 200\,000$ Pa

13) *Determine the over-pressure at the final aerator hole* :

$$Q_{AT} = 63 \times 10^{-6} P_1 \frac{D^2}{\sqrt{T_1}} \left[\left(\frac{P_2}{P_2 + \Delta P_o} \right)^{1.43} - \left(\frac{P_2}{P_2 + \Delta P_o} \right)^{1.71} \right]^{0.5} \left[ls^{-1} \right]$$

For $Q_{AT} = 0.5\ l\ s^{-1}$, $D = 1.5$ mm, $T_1 = 300$ °C :

- $\Delta P_o = 54\,000$ Pa

14) *Line pressure loss along aerator pipe* :

$$P_L^A = 1.6 \times 10^{12}\, Q^{1.85}\, l_A \,/\, \left(D_A^5\, P_{IN} \right)$$

where $Q = Q_T = 0.05\ m^3\ s^{-1}$

$$P_{IN} \approx \left\{ \left(P_2 + \Delta P_0 \right) + P_L^A \right\}$$

i.e. $$P_L^A = 1.6 \times 10^{12} \frac{(0.05)^{1.85}\,(400)}{(50)^5\,(254 + P_L^A)}$$

- $P_L^A \approx 25\ \ kPa$

15) *Static head recharge pressure along aerator pipe* :

$$P_R^A = (\rho_c/2)\,(V_I^2 - V_T^2)$$

where $\rho_c = P/RT$

At the first hole in the aerator :

$\rho_c \sim 3.54\ kg\ m^{-3}$

$V_1 \sim 25.465\ ms^{-1}$

$V \sim 25.210\ ms^{-1}$

and then $P_R^A \sim 22.9\ Pa$

The recharge gain over the full length of the aerator is then of the order of 2 kPa, giving

$$\bullet P_L^N = P_L^A - P_R^A \approx 23\ kPa$$

16) *Line pressure loss in delivery pipe* :

$$P_L^D = 1.6 \times 10^{12}\ Q^{1.85}\ 1_D / \left(D_D^5\ P_{IN}\right)$$

where

$$Q \approx Q_T = 0.05\ m^3\ s^{-1}$$

$$P_{IN} \approx \left\{\left(P_2 + \Delta P_o + P_L^N\right) + P_L^D\right\}$$

$$\text{i.e. } P_L^D = 1.6 \times 10^{12}\ \frac{(0.05)^{1.85}\ (100)}{(50)^5\ (277 + P_L^D)}$$

$$\bullet\ P_L^D \approx 6\ \text{kPa}$$

17) *Minimum operating in-line delivery pressure required* :

$$P_{IN} = P_2 + \Delta P_0 + P_L^N + P_L^D$$

$$\bullet\ P_{IN} \approx 283\,000\ Pa\ (abs) \approx 180\,000\ Pa\ (gauge)$$

C) CHECK CALCULATIONS :

18) *Sufficient flow per hole to destratify the reservoir?* :

$Q_{AT} = 0.5\ 1\ s^{-1}$ (refer Fig. 3.7)

• OK

19) *Uniform flow distribution along aerator pipe? :*

$\Delta P_o / P_L^A = 54\,000 / 25\,000 = 2.16$

• slightly low

20) *Operating in-line pressure acceptable? :*

P_{IN} = 283 000 Pa (abs)

Available compressor : 400 000 Pa (abs)

• OK

A4.2 Operating conditions

The operating conditions of the installed system were checked on February 20, 1989. The total measured air flow was 40 l s^{-1} at an in-line operating pressure of 175 kPa (gauge) and temperature of 341 °C. The depth of water above the aerator was approximately 10 metres. Repeating the calculations set out above:

P_2 = ρgh + 101 330 Pa

200 000 Pa

P_1 = 276 000 Pa (abs)

= 175 000 Pa (gauge)

Assuming $P_L^D \approx 6\ kPa$

$P_L^N \approx 23\ kPa$

then $P_1 = P_I - P_L^D - P_L^N$

$\approx 247\,000\ Pa$

Thus $\frac{P_2}{P_1} = 0.8097$

and $\Delta P_o \approx 47\,000$ Pa

Substituting into (A3.10):

$$Q_{AT} = 63 \times 10^{-6} P_1 \frac{D^2}{\sqrt{T_1}} \left[\left(\frac{P_2}{P_1}\right)^{1.43} - \left(\frac{P_2}{P_1}\right)^{1.71} \right]^{0.5}$$

$$= 63 \times 10^{-6} (247\,000) \frac{(1.5)^2}{\sqrt{341}} \left((0.8097)^{1.43} - (0.8097)^{1.71} \right)^{1/2}$$

$$= 0.39\ l\ s^{-1}$$

This result agrees well with the measured air flow rate.

APPENDIX A5

Water quality contour plots 1986-1988

HARDING DAM

LOCATION: Q7091076 (0.1km from Dam Wall)
PERIOD: 1st Jan–31st Dec 1986
AERATOR: Mark (I) : 11th Jun–31st Dec 1986
FILE: Data86.001

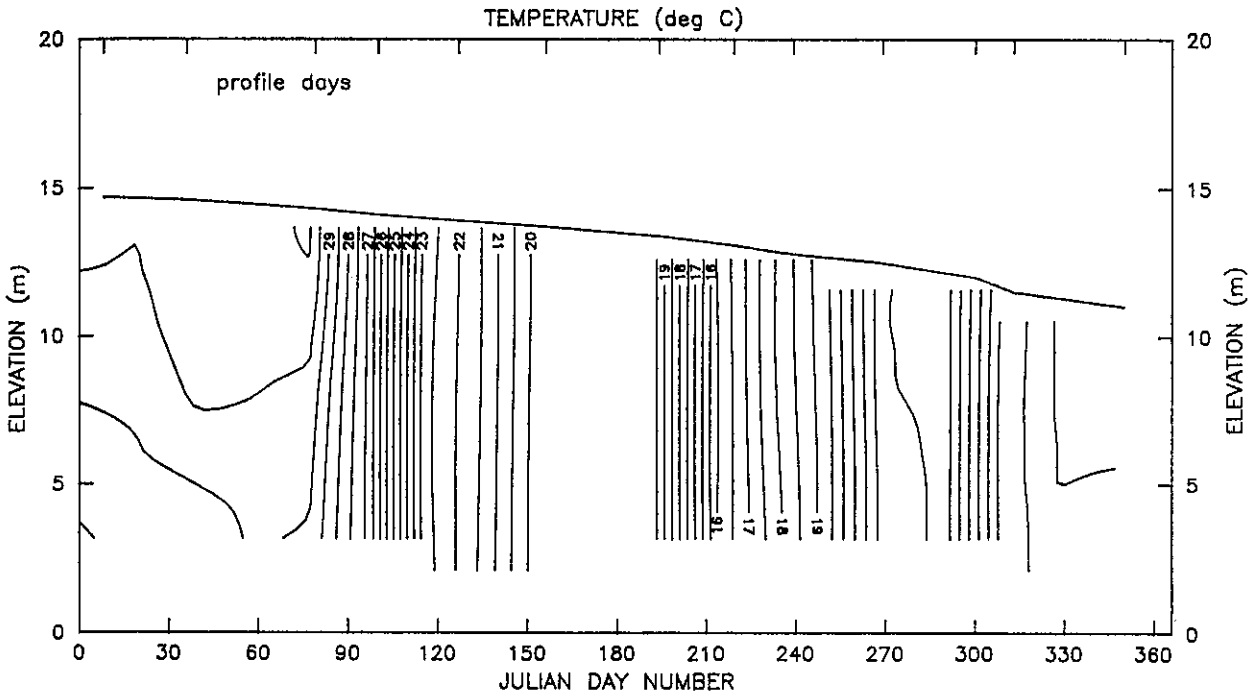

HARDING DAM

LOCATION: Q7091076 (0.1km from Dam Wall)
PERIOD: 1st Jan–31st Dec 1986
AERATOR: Mark (I) : 11th Jun–31st Dec 1986
FILE: Data86.001

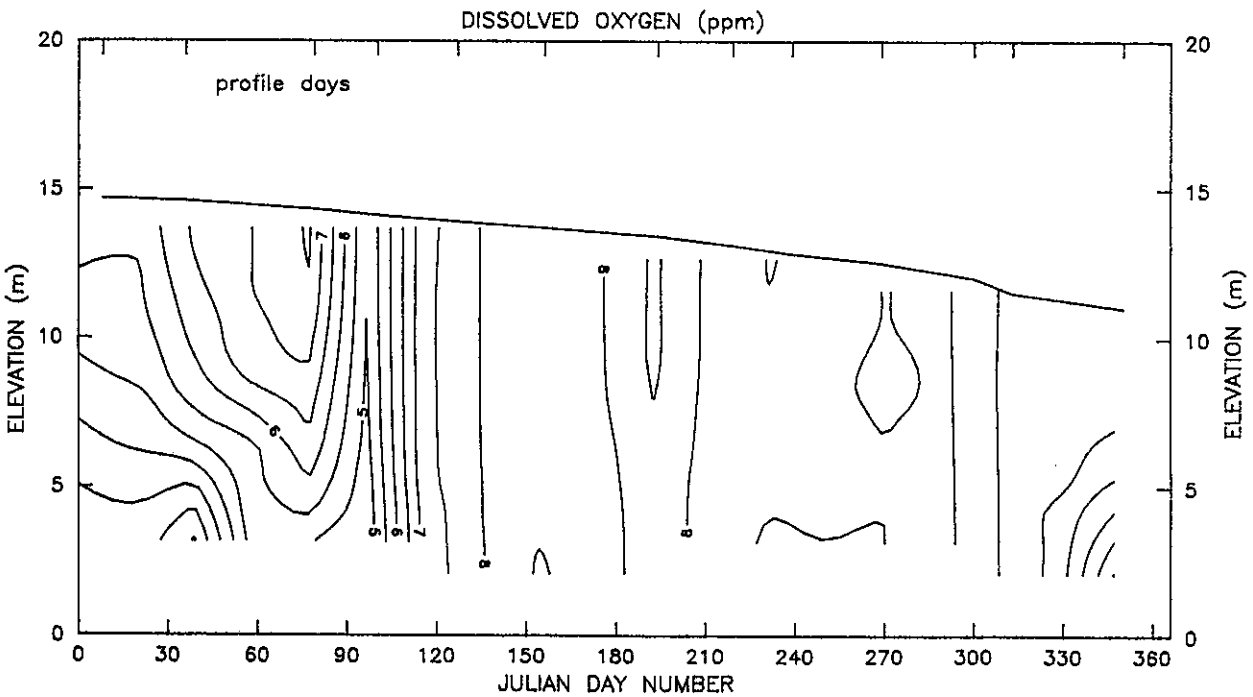

HARDING DAM

LOCATION: Q7091084 (0.5km from Dam Wall)
PERIOD: 1st Jan–31st Dec 1986
AERATOR: Mark (I) : 11th Jun–31st Dec 1986
FILE: Data86.005

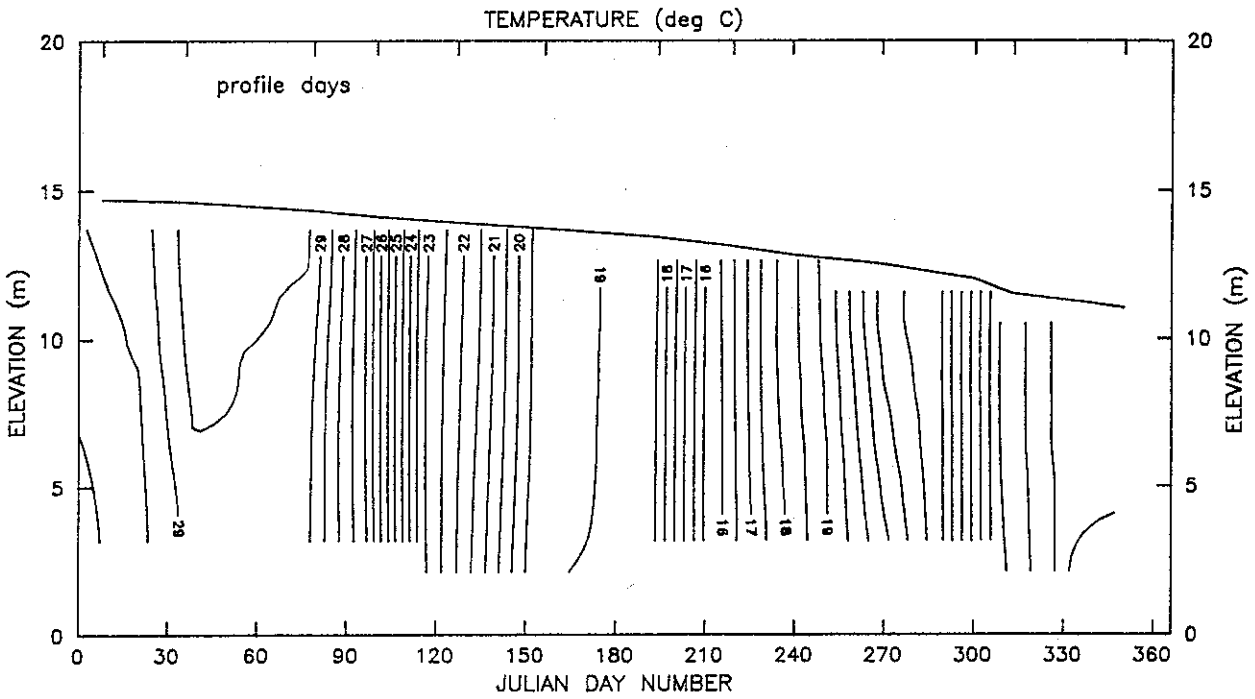

HARDING DAM

LOCATION: Q7091084 (0.5km from Dam Wall)
PERIOD: 1st Jan–31st Dec 1986
AERATOR: Mark (I) : 11th Jun–31st Dec 1986
FILE: Data86.005

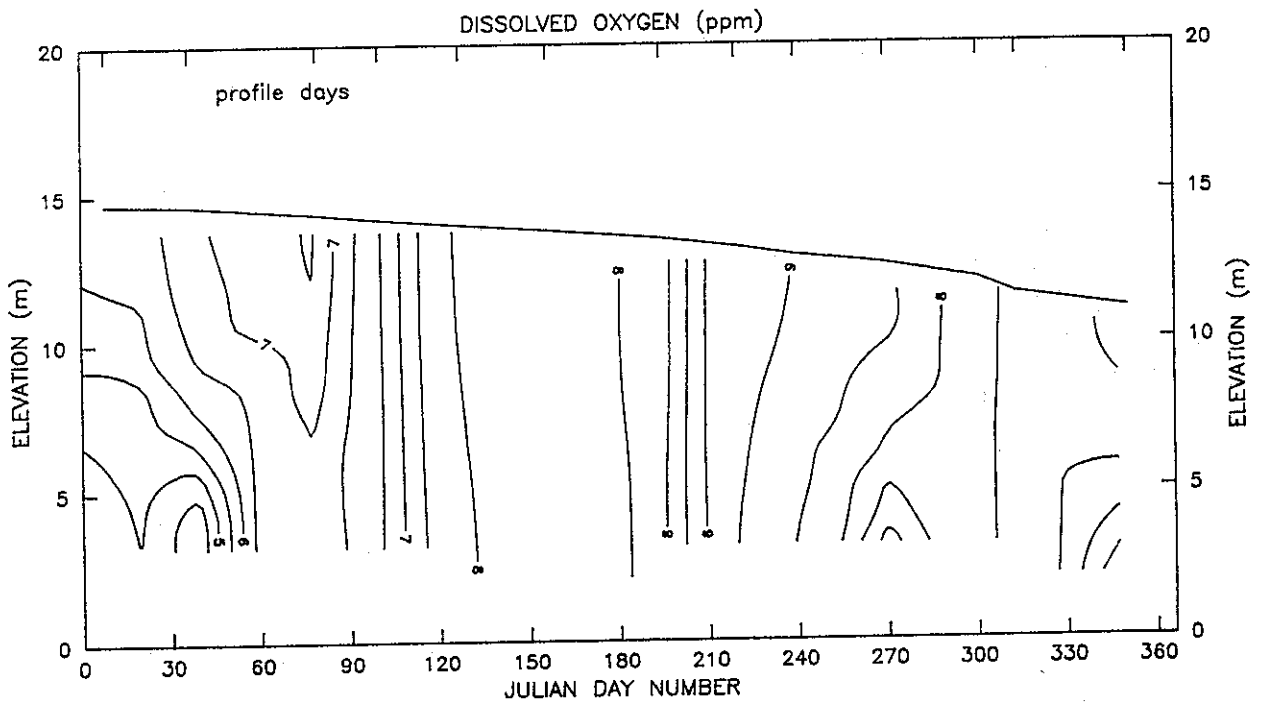

HARDING DAM

LOCATION: Q7091078 (1.5km from Dam Wall)
PERIOD: 1st Jan–31st Dec 1986
AERATOR: Mark (I) : 11th Jun–31st Dec 1986
FILE: Data86.015

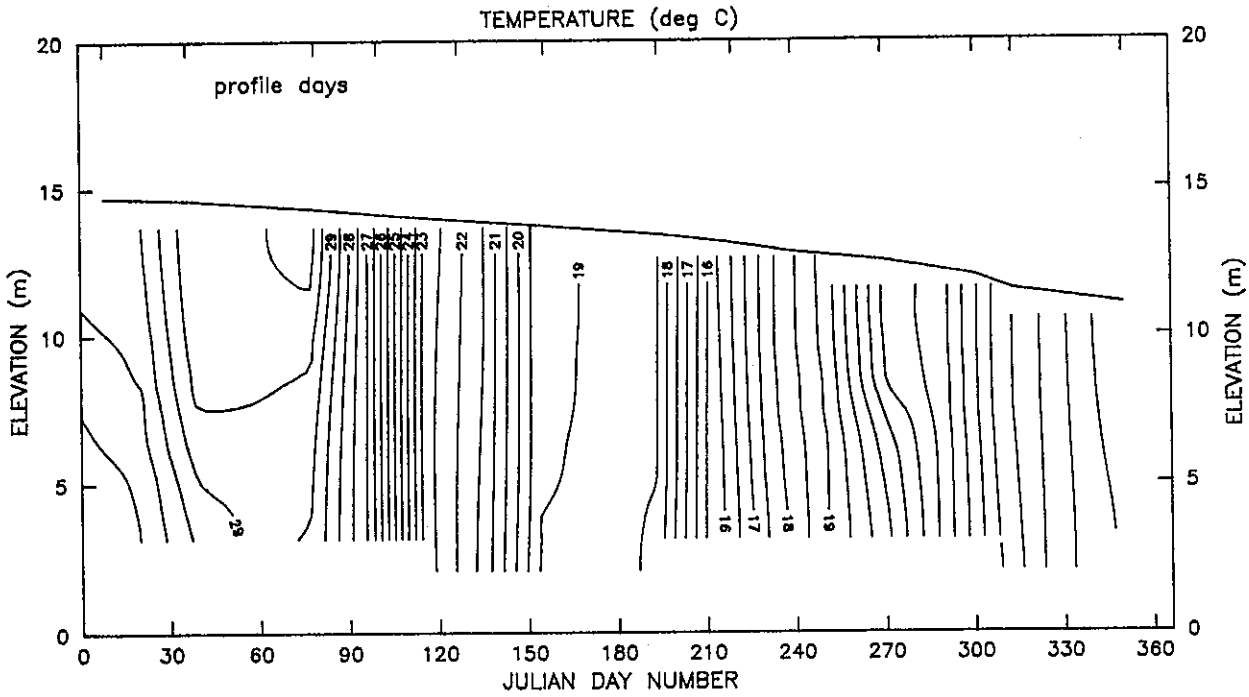

HARDING DAM

LOCATION: Q7091078 (1.5km from Dam Wall)
PERIOD: 1st Jan–31st Dec 1986
AERATOR: Mark (I) : 11th Jun–31st Dec 1986
FILE: Data86.005

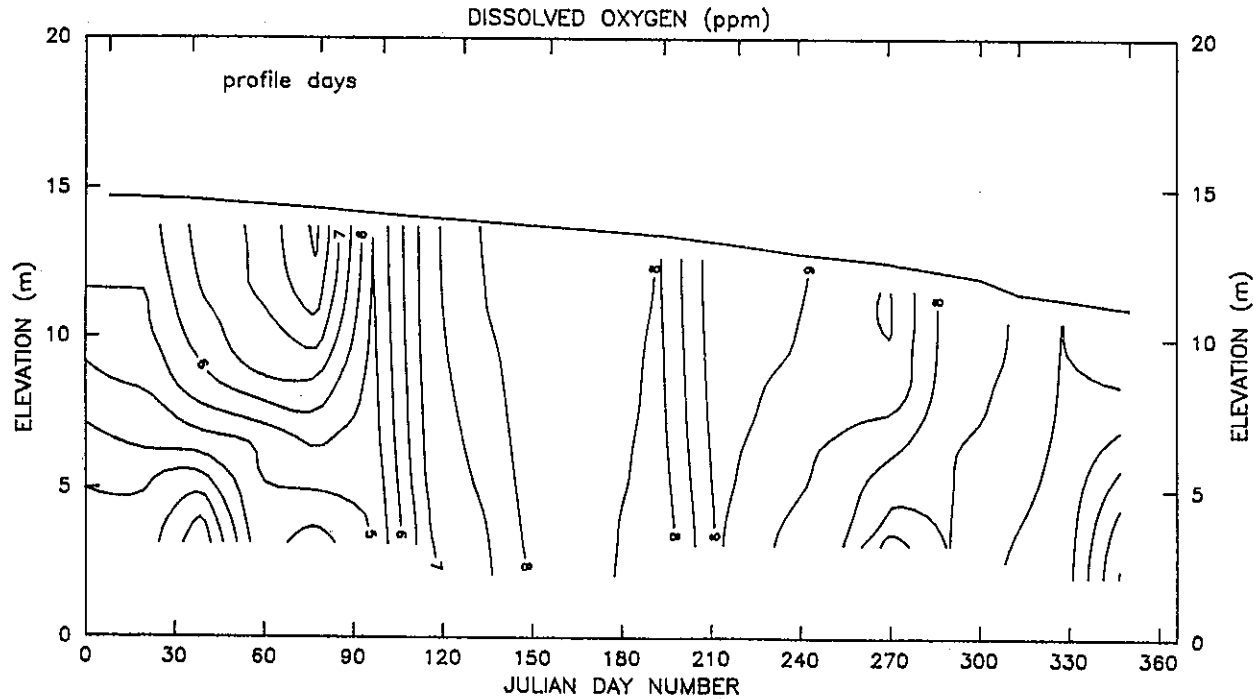

HARDING DAM

LOCATION: Q7091079 (2.5km from Dam Wall)
PERIOD: 1st Jan–31st Dec 1986
AERATOR: Mark (I) : 11th Jun–31st Dec 1986
FILE: Data86.025

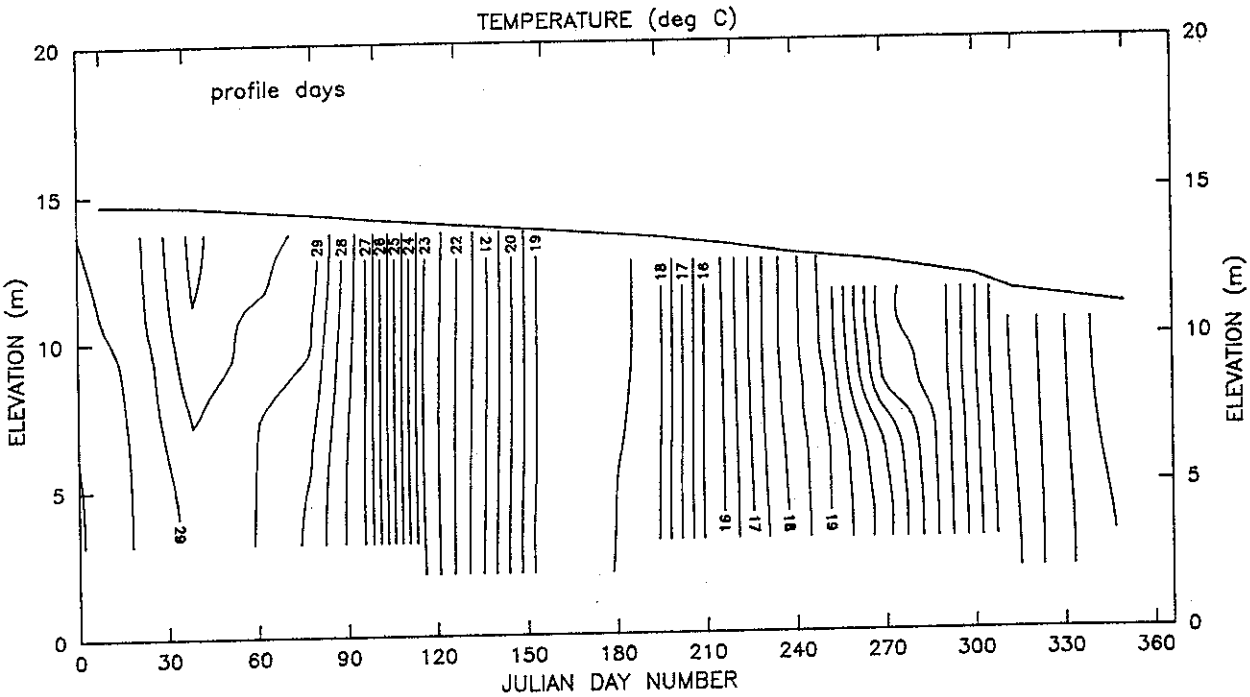

HARDING DAM

LOCATION: Q7091079 (2.5km from Dam Wall)
PERIOD: 1st Jan–31st Dec 1986
AERATOR: Mark (I) : 11th Jun–31st Dec 1986
FILE: Data86.025

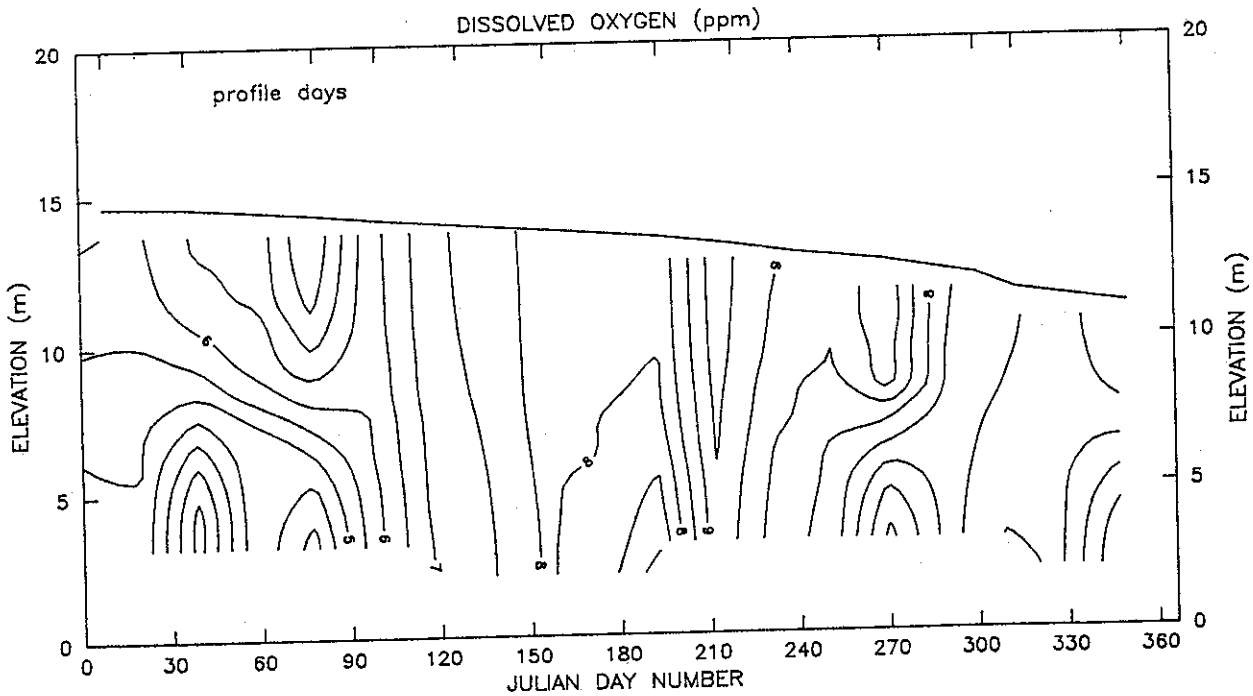

HARDING DAM

LOCATION: Q7091080 (3.5km from Dam Wall)
PERIOD: 1st Jan–31st Dec 1986
AERATOR: Mark (I) : 11th Jun–31st Dec 1986
FILE: Data86.035

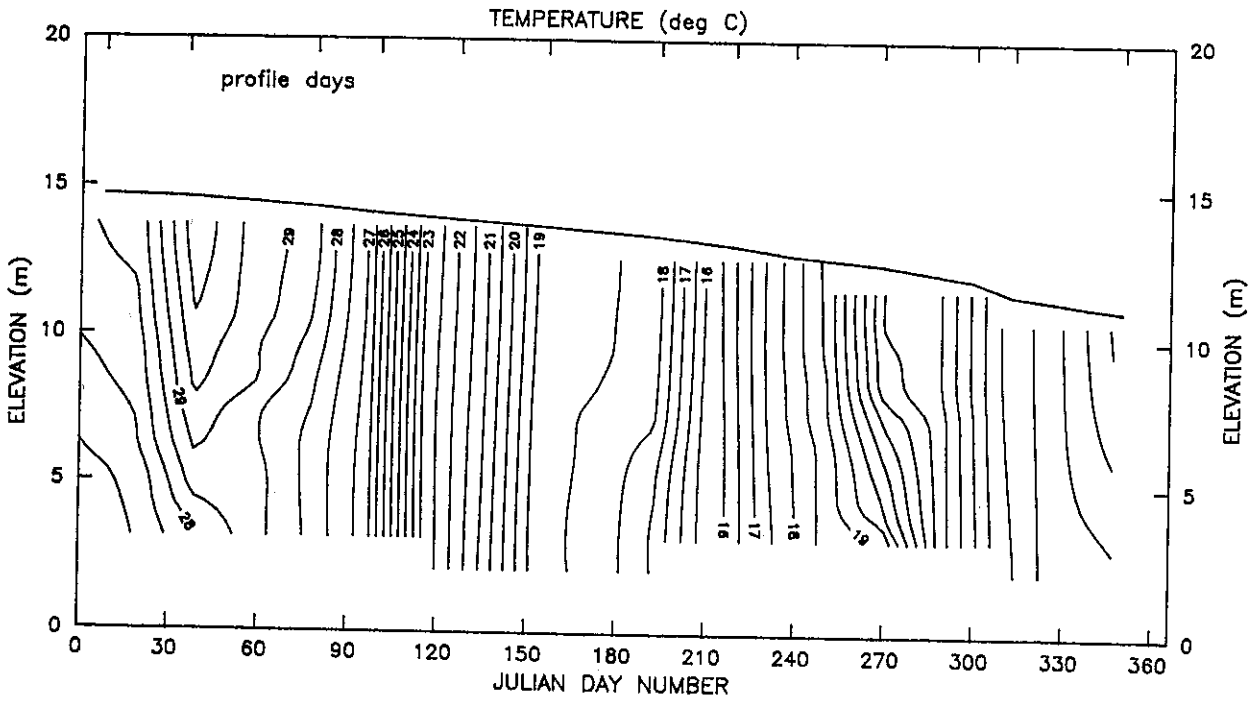

HARDING DAM

LOCATION: Q7091080 (3.5km from Dam Wall)
PERIOD: 1st Jan–31st Dec 1986
AERATOR: Mark (I) : 11th Jun–31st Dec 1986
FILE: Data86.035

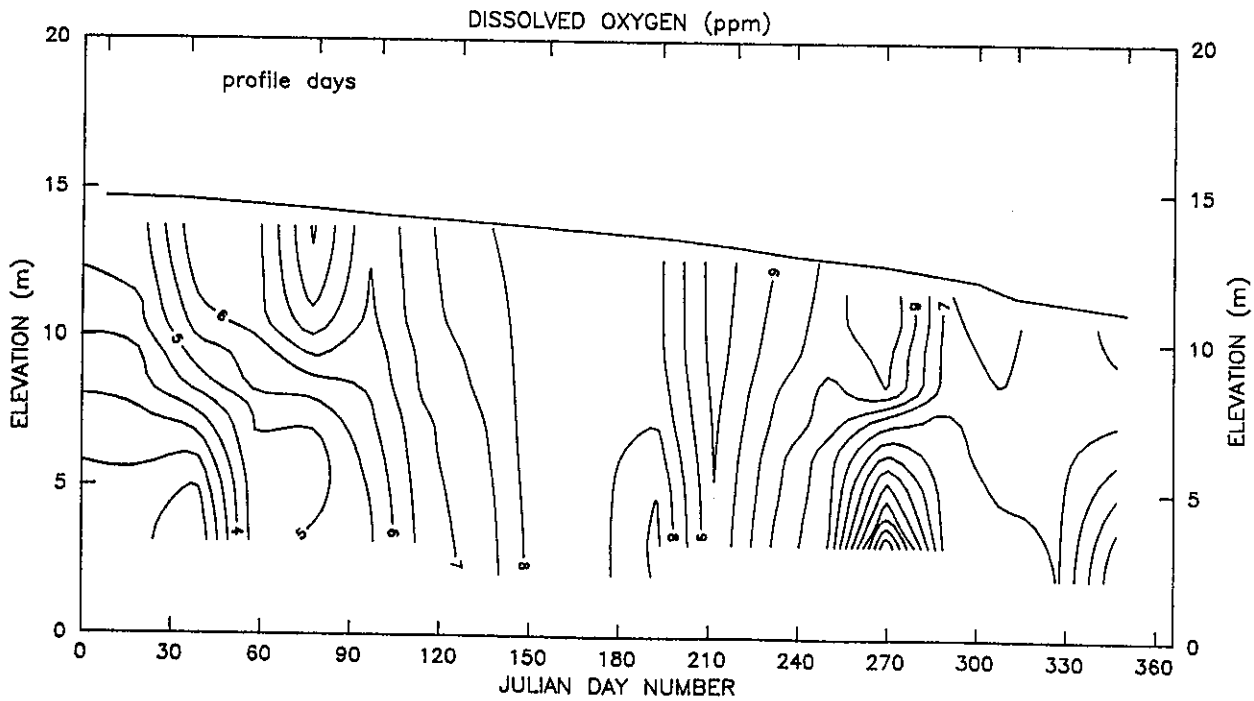

HARDING DAM

LOCATION: Q7091076 (0.1km from Dam Wall)
PERIOD: 1st Jan–31st Dec 1987
AERATOR: Mark (I) : 1st Jan–31st Dec 1987
FILE: Data87.001

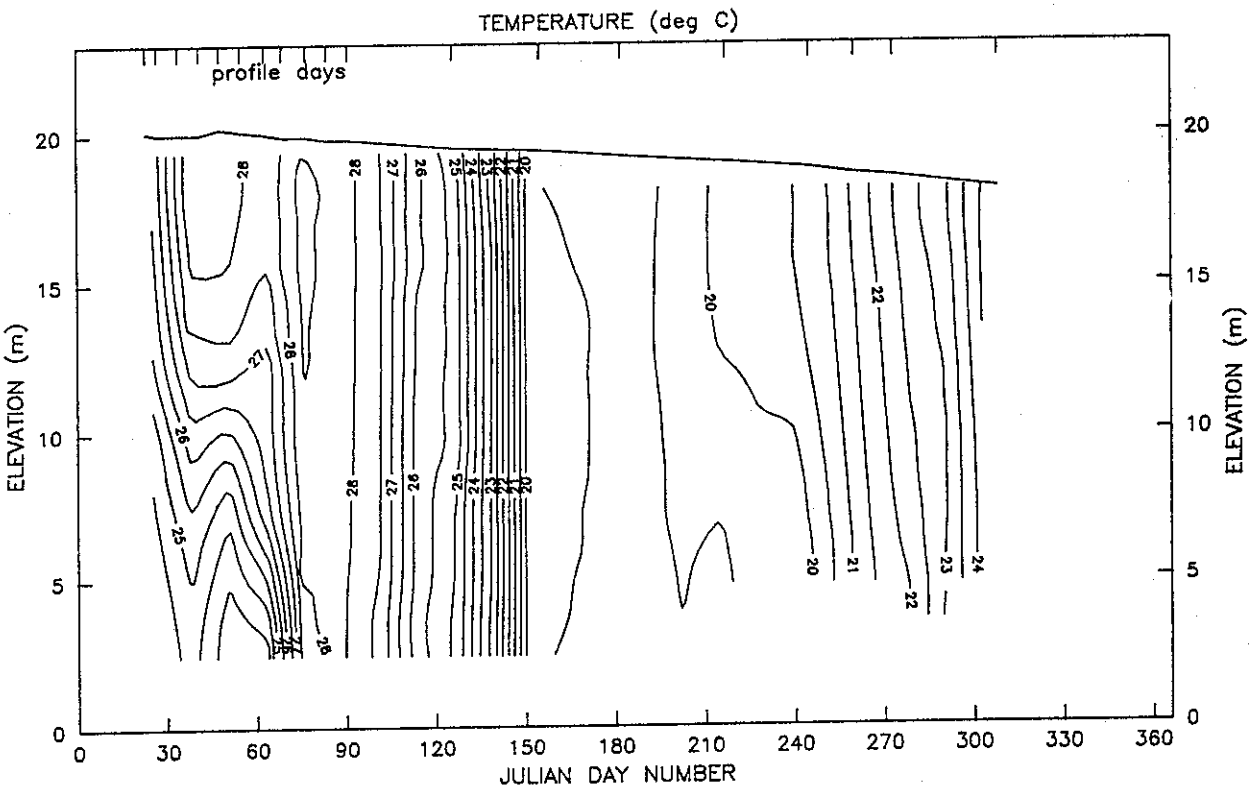

HARDING DAM

LOCATION: Q7091076 (0.1km from Dam Wall)
PERIOD: 1st Jan–31st Dec 1987
AERATOR: Mark (I) : 1st Jan–31st Dec 1987
FILE: Data87.001

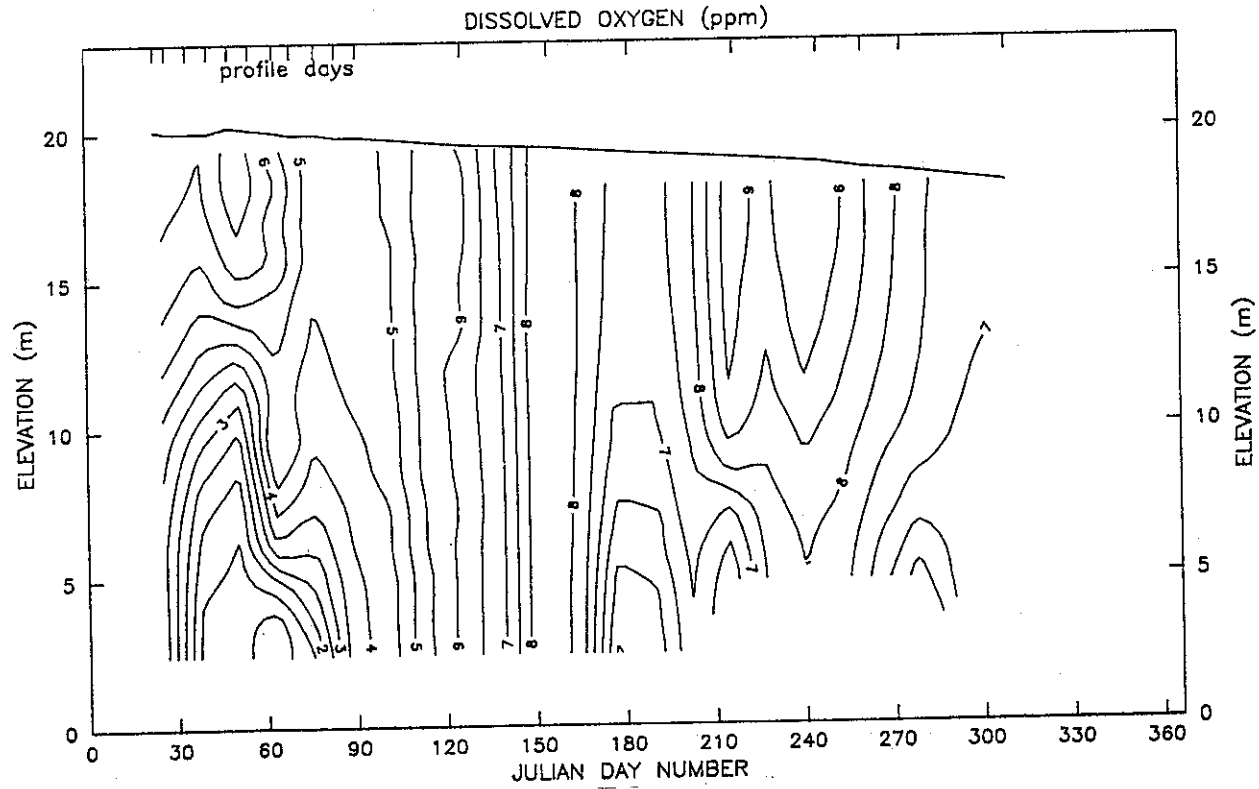

HARDING DAM

LOCATION: Q7091084 (0.5km from Dam Wall)
PERIOD: 1st Jan–31st Dec 1987
AERATOR: Mark (I) : 1st Jan–31st Dec 1987
FILE: Data87.005

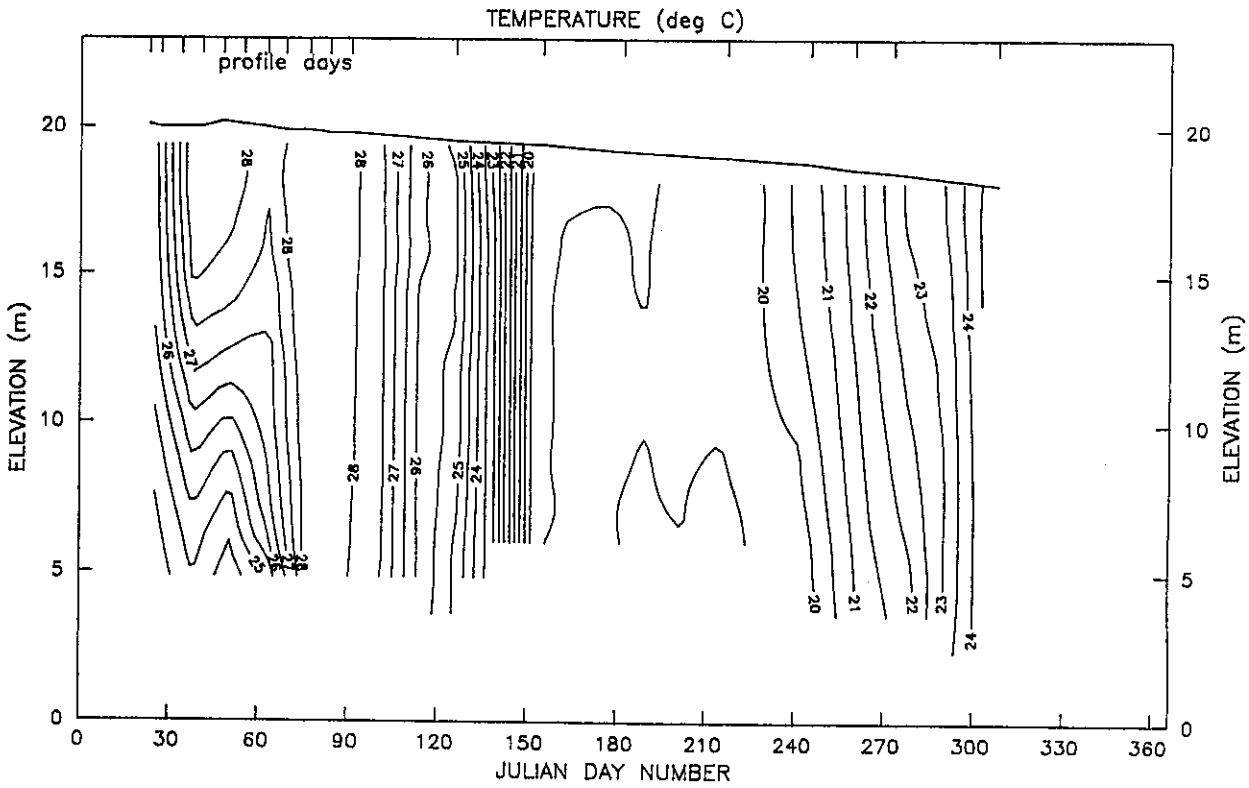

HARDING DAM

LOCATION: Q7091084 (0.5km from Dam Wall)
PERIOD: 1st Jan–31st Dec 1987
AERATOR: Mark (I) : 1st Jan–31st Dec 1987
FILE: Data87.005

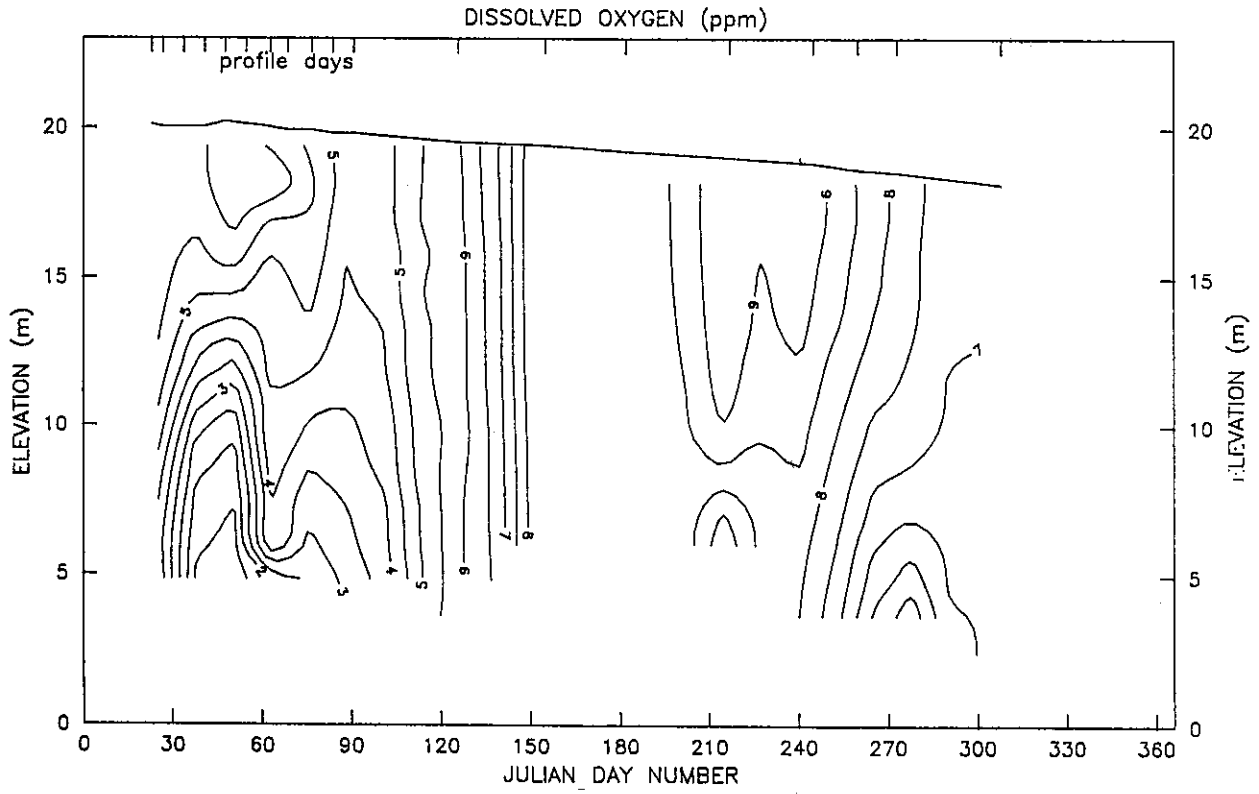

HARDING DAM

LOCATION: Q7091078 (1.5km from Dam Wall)
PERIOD: 1st Jan–31st Dec 1987
AERATOR: Mark (I) : 1st Jan–31st Dec 1987
FILE: Data87.015

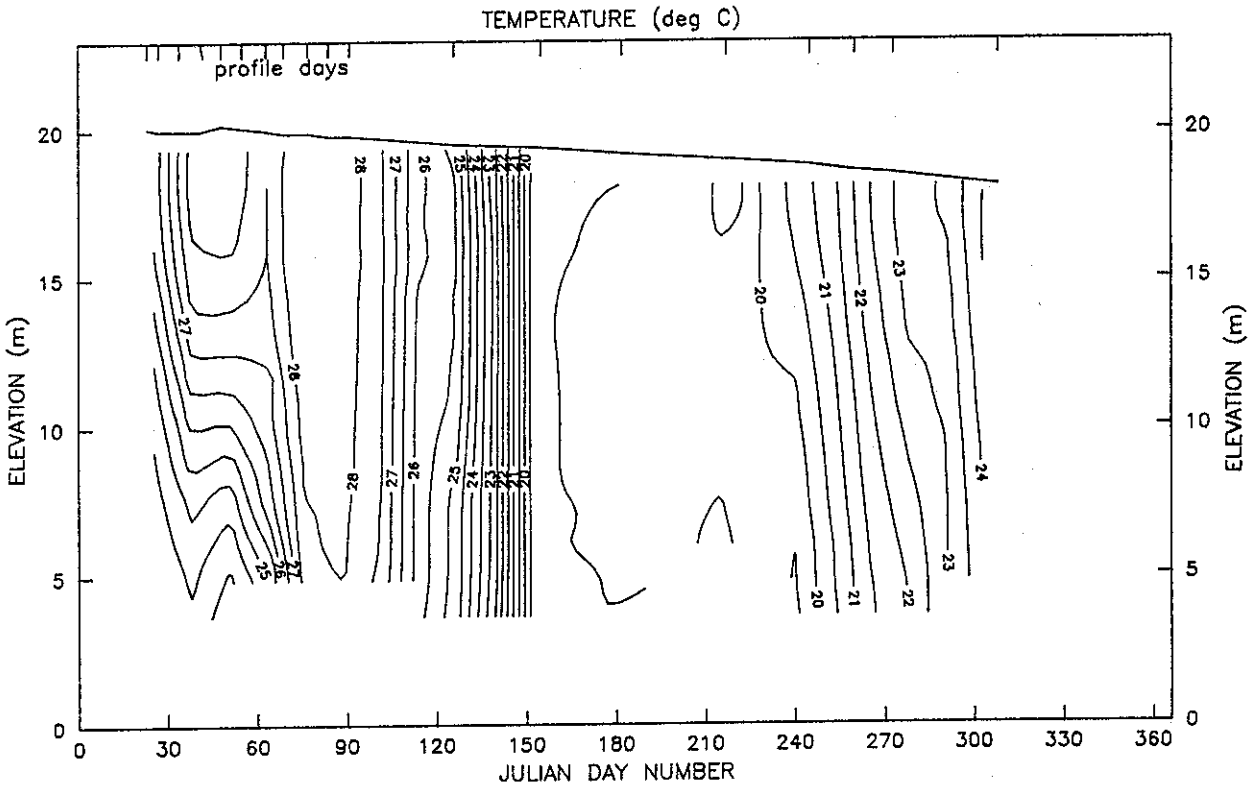

HARDING DAM

LOCATION: Q7091078 (1.5km from Dam Wall)
PERIOD: 1st Jan–31st Dec 1987
AERATOR: Mark (I) : 1st Jan–31st Dec 1987
FILE: Data87.015

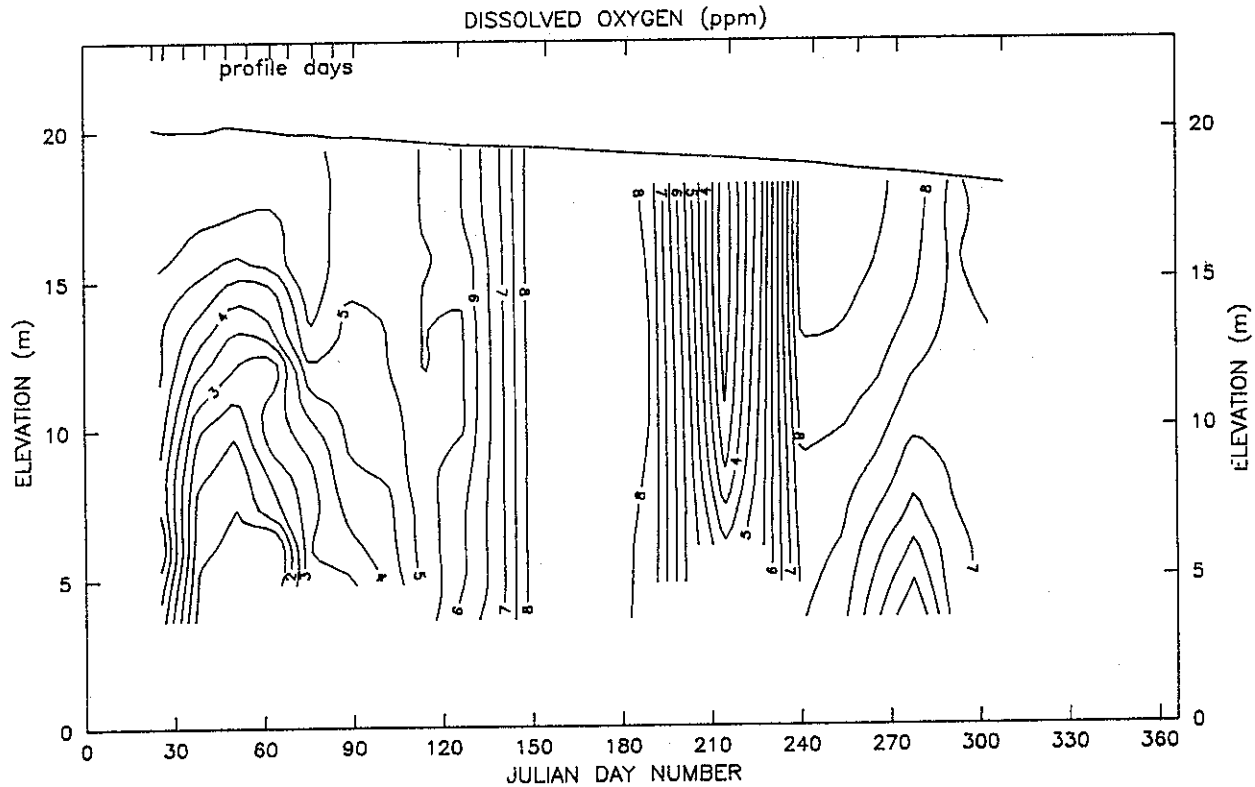

HARDING DAM

LOCATION: Q7091079 (2.5km from Dam Wall)
PERIOD: 1st Jan–31st Dec 1987
AERATOR: Mark (I) : 1st Jan–31st Dec 1987
FILE: Data87.025

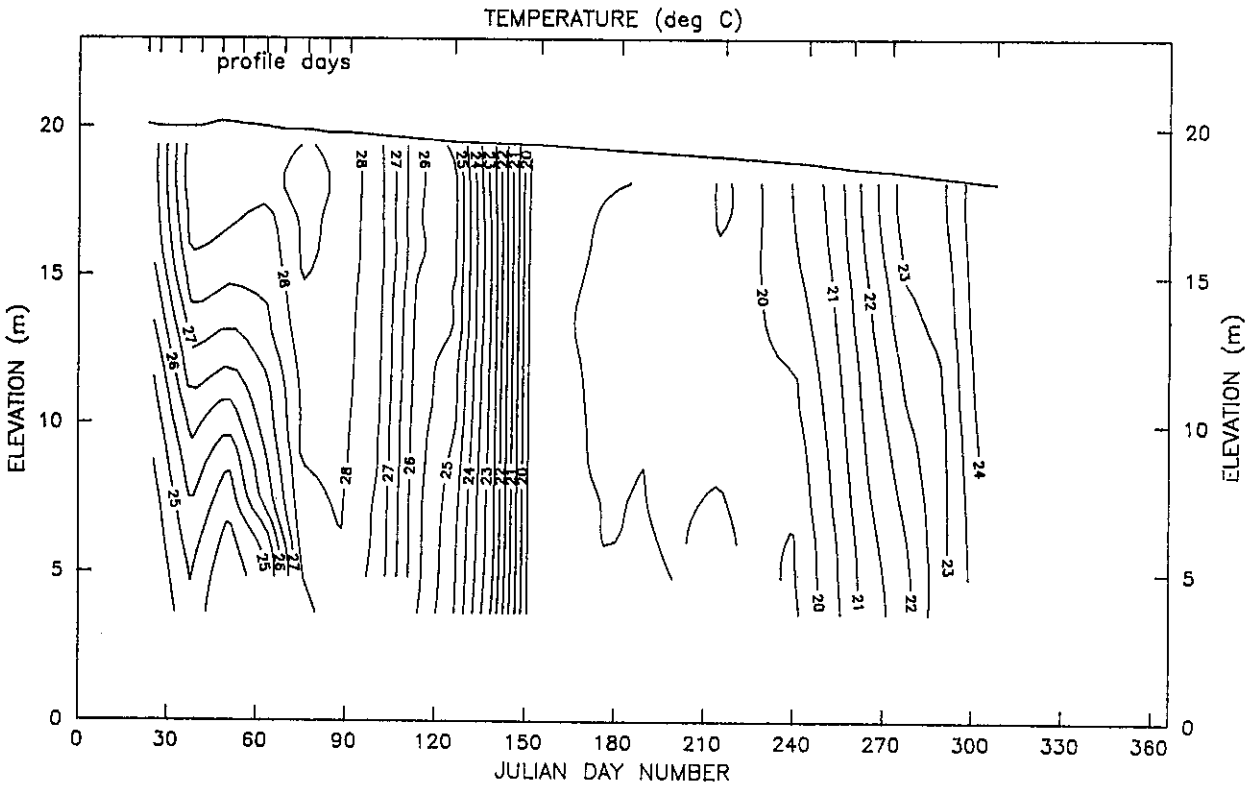

HARDING DAM

LOCATION: Q7091079 (2.5km from Dam Wall)
PERIOD: 1st Jan–31st Dec 1987
AERATOR: Mark (I) : 1st Jan–31st Dec 1987
FILE: Data87.025

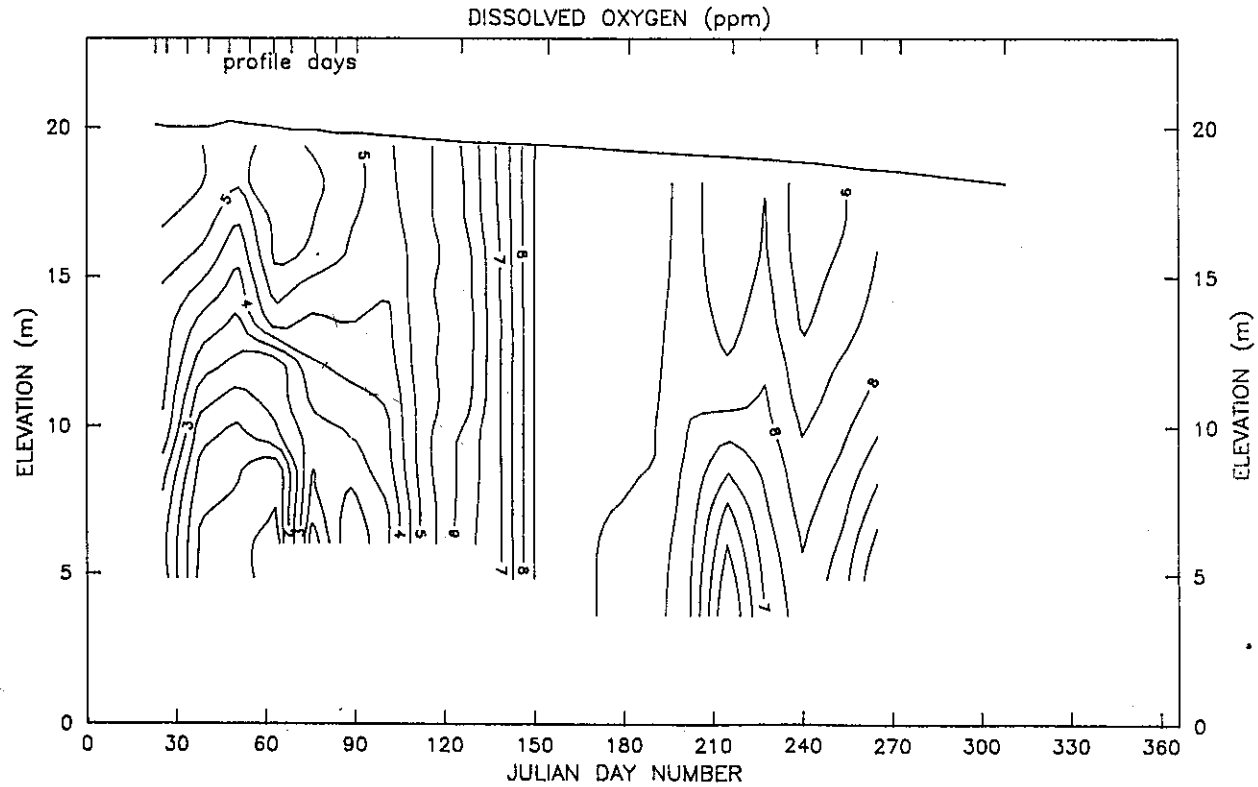

HARDING DAM

LOCATION: Q7091080 (3.5km from Dam Wall)
PERIOD: 1st Jan–31st Dec 1987
AERATOR: Mark (I) : 1st Jan–31st Dec 1987
FILE: Data87.035

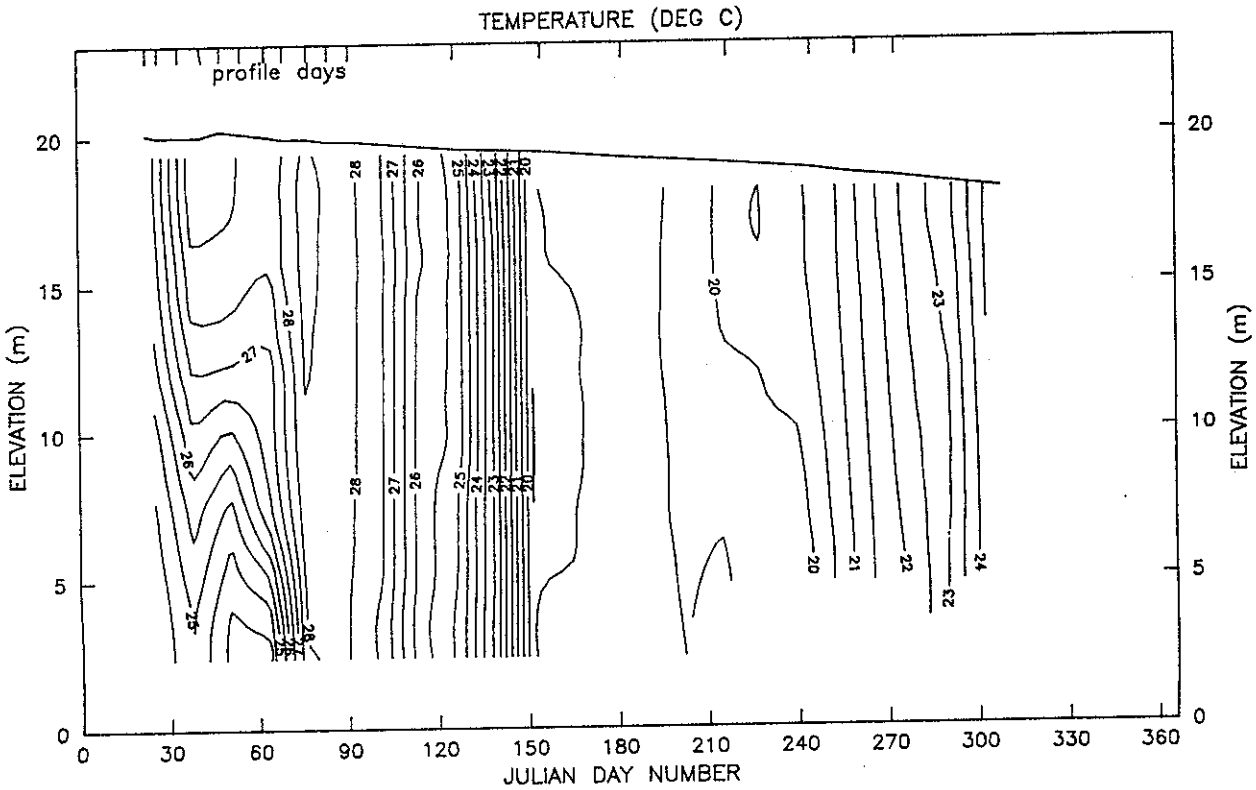

HARDING DAM

LOCATION: Q7091080 (3.5km from Dam Wall)
PERIOD: 1st Jan–31st Dec 1987
AERATOR: Mark (I) : 1st Jan–31st Dec 1987
FILE: Data87.035

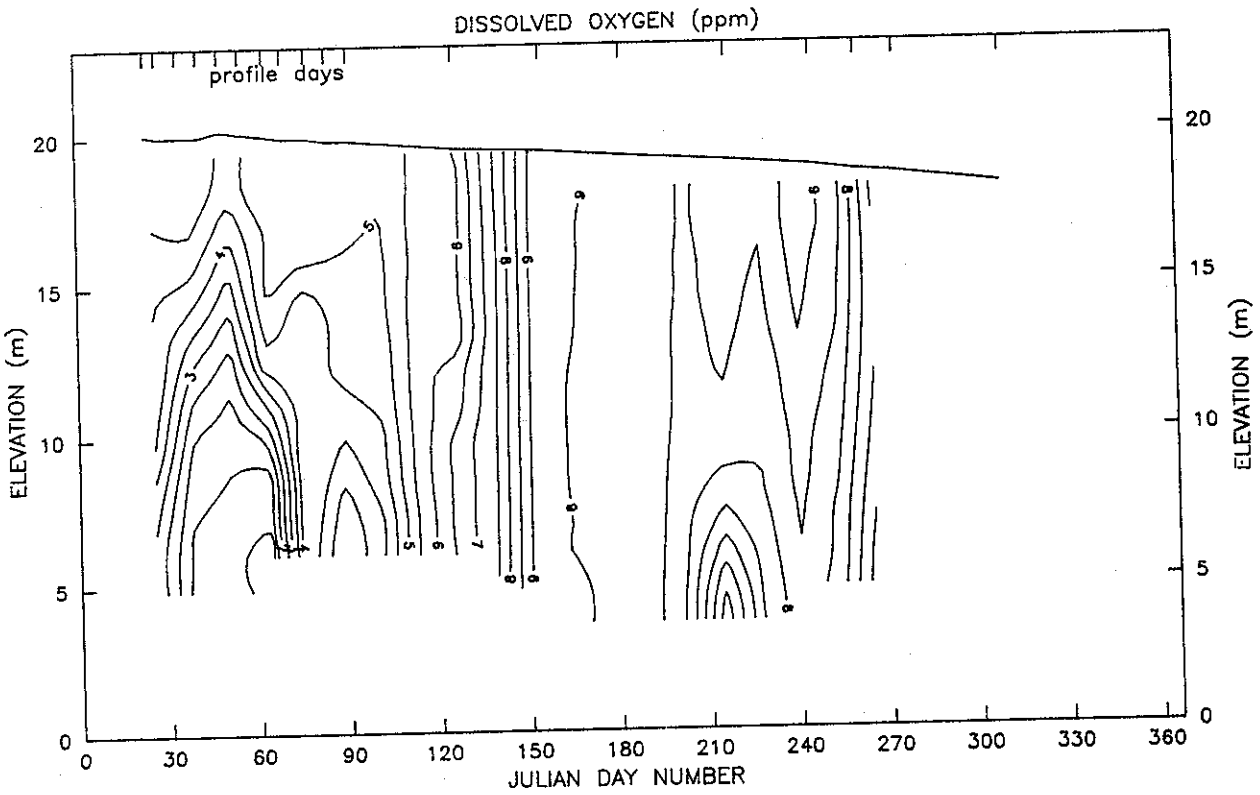

HARDING DAM

LOCATION: Q7091076 (0.1km from Dam Wall)
PERIOD: 1st Jan–31st Dec 1988
AERATOR: Mark (I) : 1st Jan–16th Jun 1988
Burn's : 27th Sept–31st Dec 1988
FILE: Data88.001

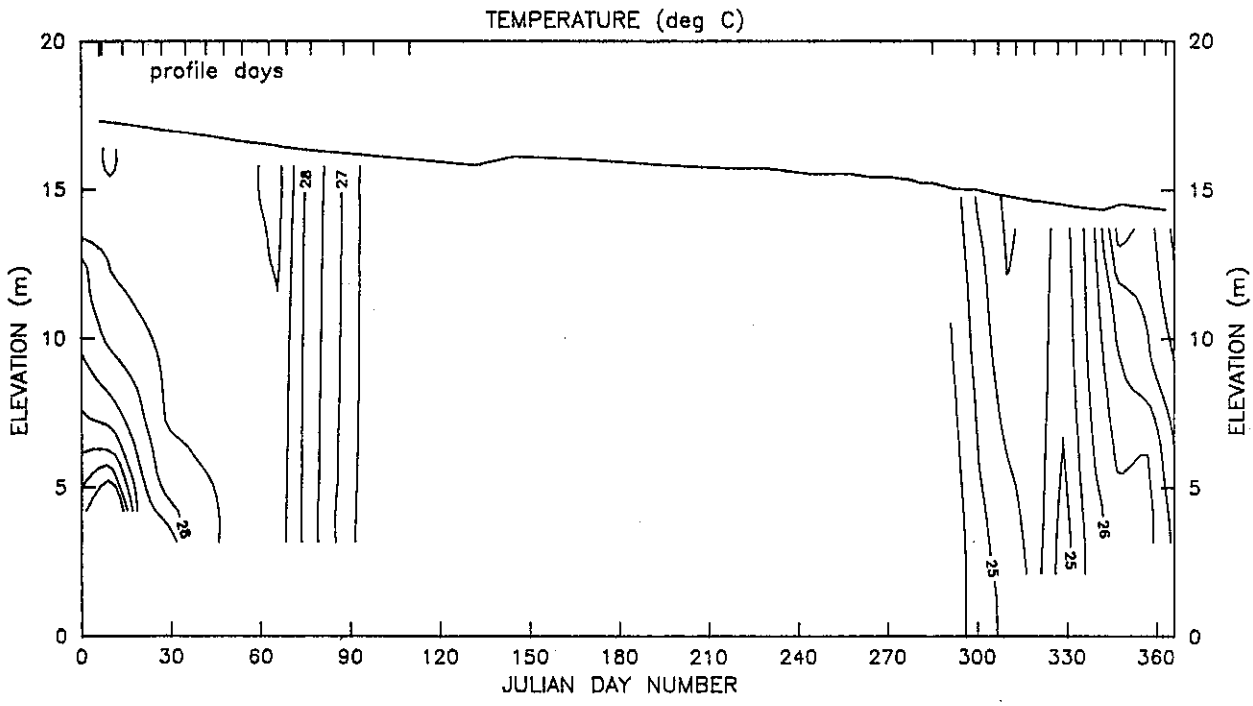

HARDING DAM

LOCATION: Q7091076 (0.1km from Dam Wall)
PERIOD: 1st Jan–31st Dec 1988
AERATOR: Mark (I) : 1st Jan–16th Jun 1988
Burn's : 27th Sept–31st Dec 1988
FILE: Data88.001

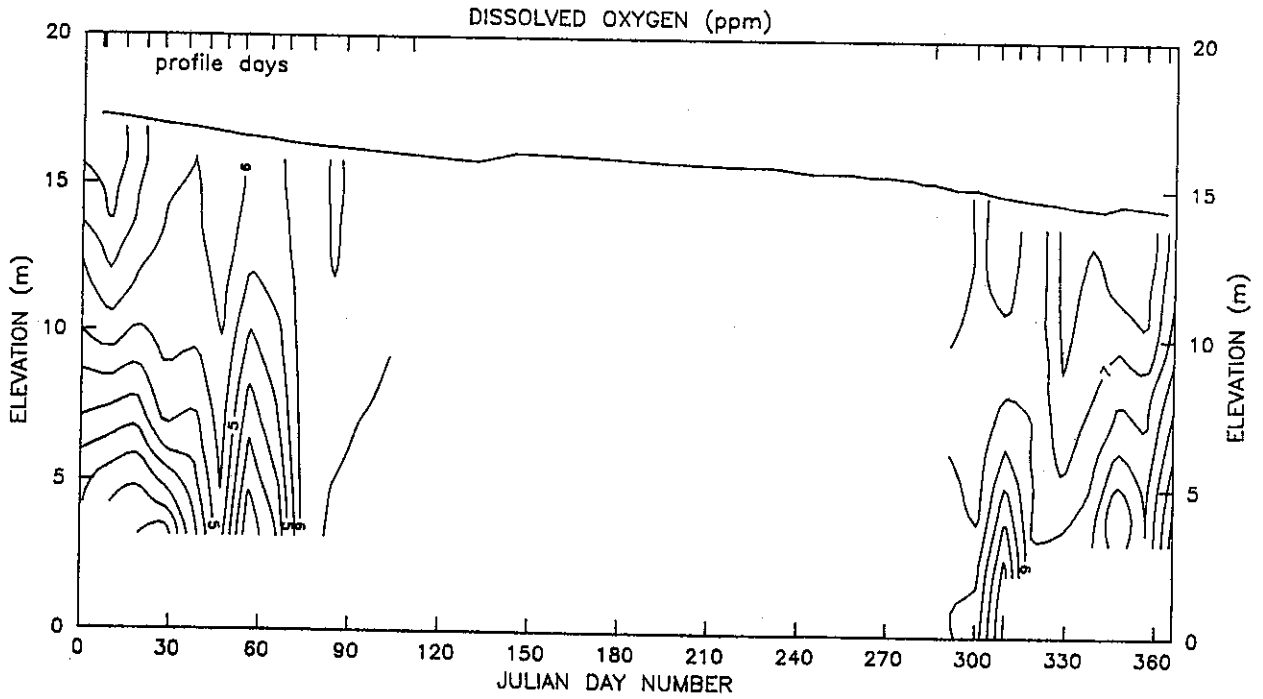

HARDING DAM

LOCATION: Q7091084 (0.5km from Dam Wall)
PERIOD: 1st Jan–31st Dec 1988
AERATOR: Mark (I) : 1st Jan–16th Jun 1988
Burn's : 27th Sept–31st Dec 1988
FILE: Data88.005

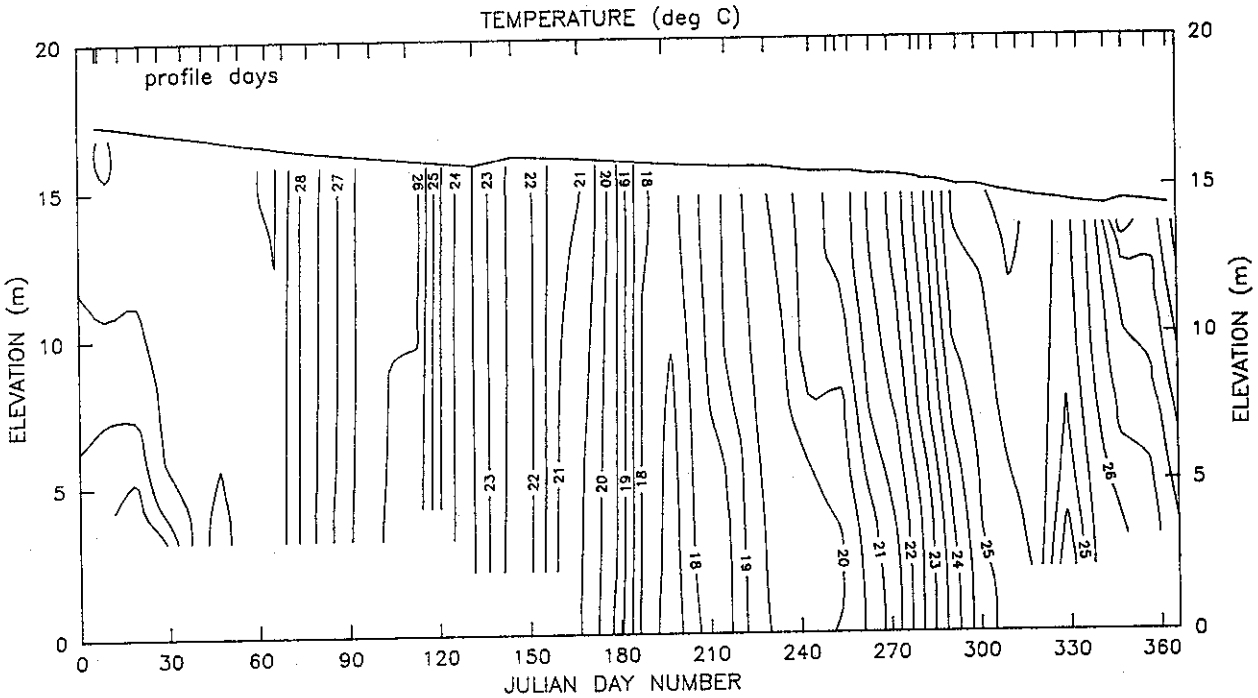

HARDING DAM

LOCATION: Q7091084 (0.5km from Dam Wall)
PERIOD: 1st Jan–31st Dec 1988
AERATOR: Mark (I) : 1st Jan–16th Jun 1988
'Burn's : 27th Sept–31st Dec 1988
FILE: Data88.005

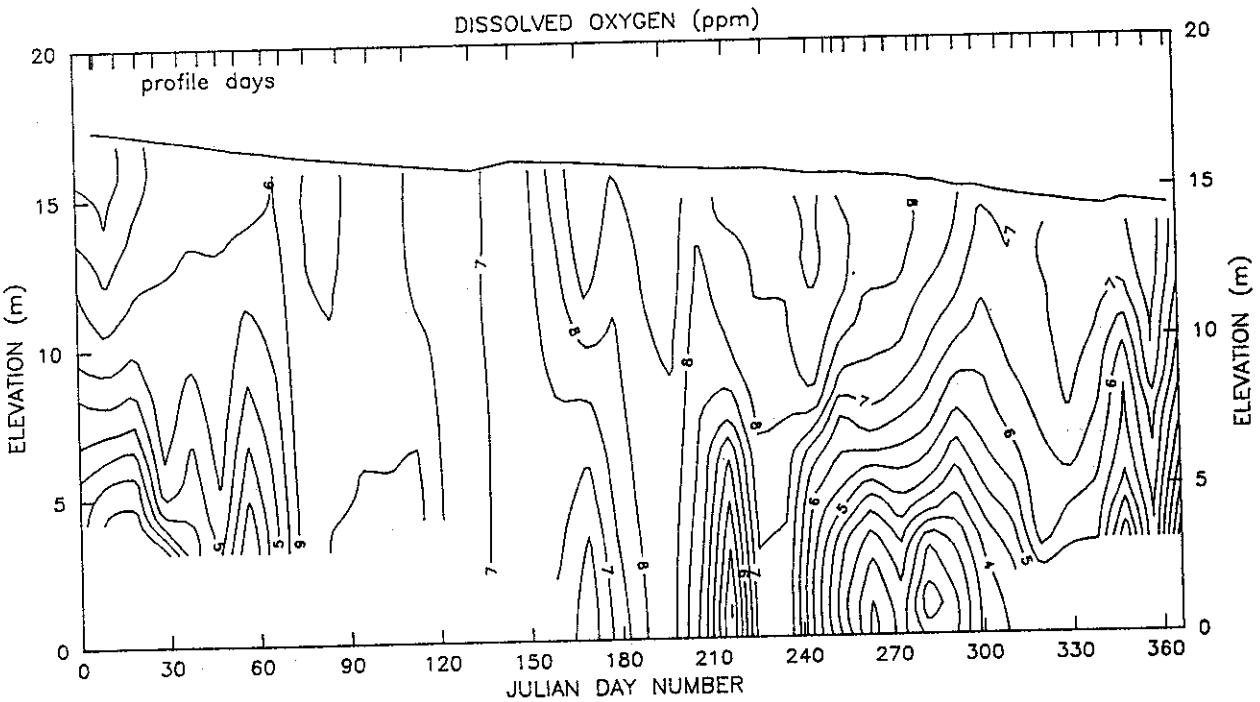

HARDING DAM

LOCATION: Q7091078 (1.5km from Dam Wall)
PERIOD: 1st Jan–31st Dec 1988
AERATOR: Mark (I) : 1st Jan–16th Jun 1988
Burn's : 27th Sept–31st Dec 1988
FILE: Data88.015

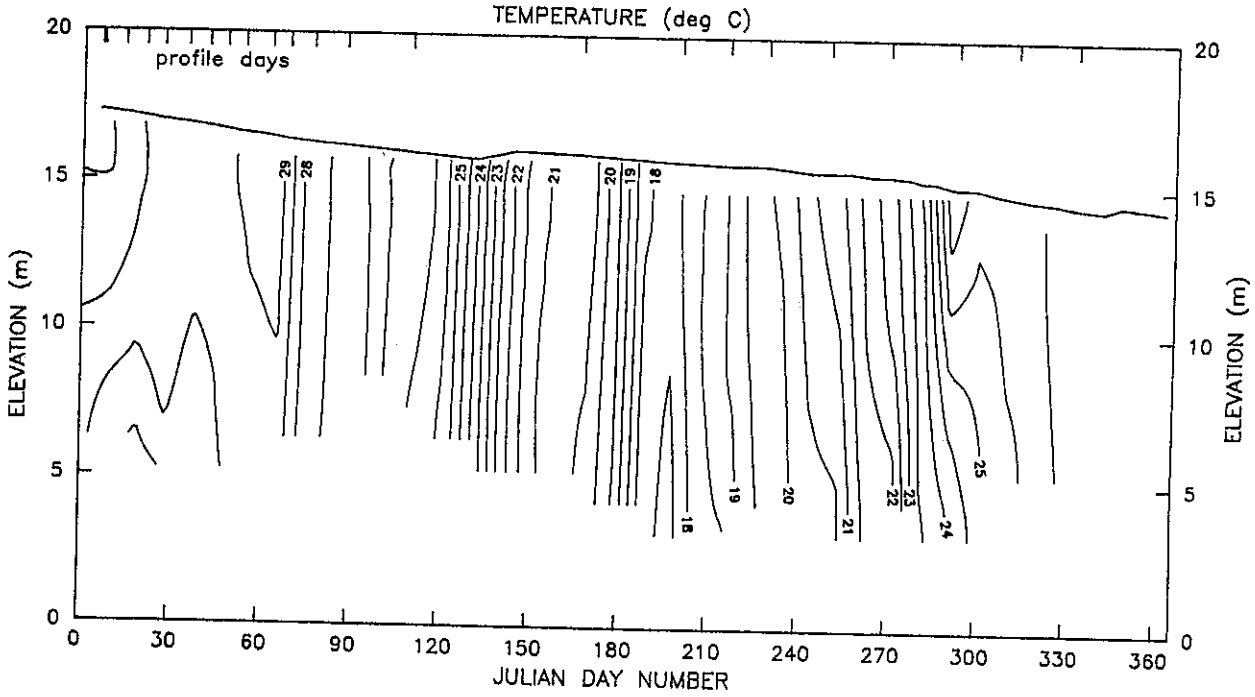

HARDING DAM

LOCATION: Q7091078 (1.5km from Dam Wall)
PERIOD: 1st Jan–31st Dec 1988
AERATOR: Mark (I) : 1st Jan–16th Jun 1988
Burn's : 27th Sept–31st Dec 1988
FILE: Data88.015

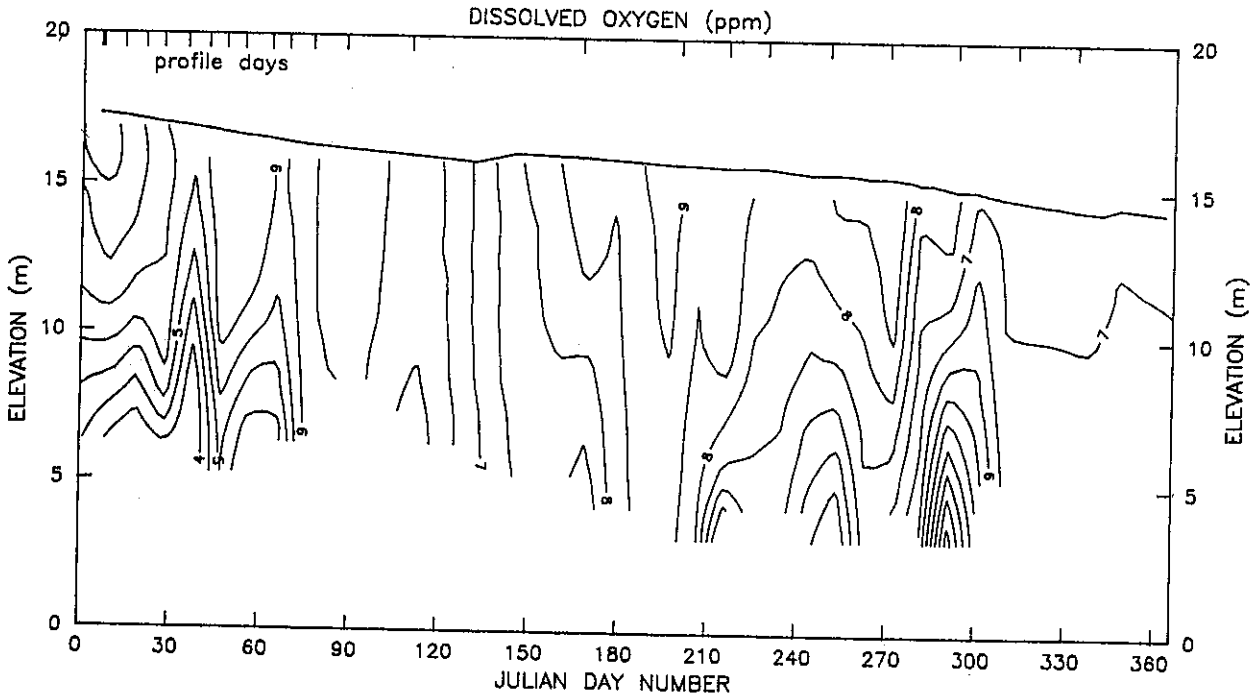

HARDING DAM

LOCATION: Q7091079 (2.5km from Dam Wall)
PERIOD: 1st Jan–31st Dec 1988
AERATOR: Mark (I) : 1st Jan–16th Jun 1988
Burn's : 27th Sept–31st Dec 1988
FILE: Data88.025

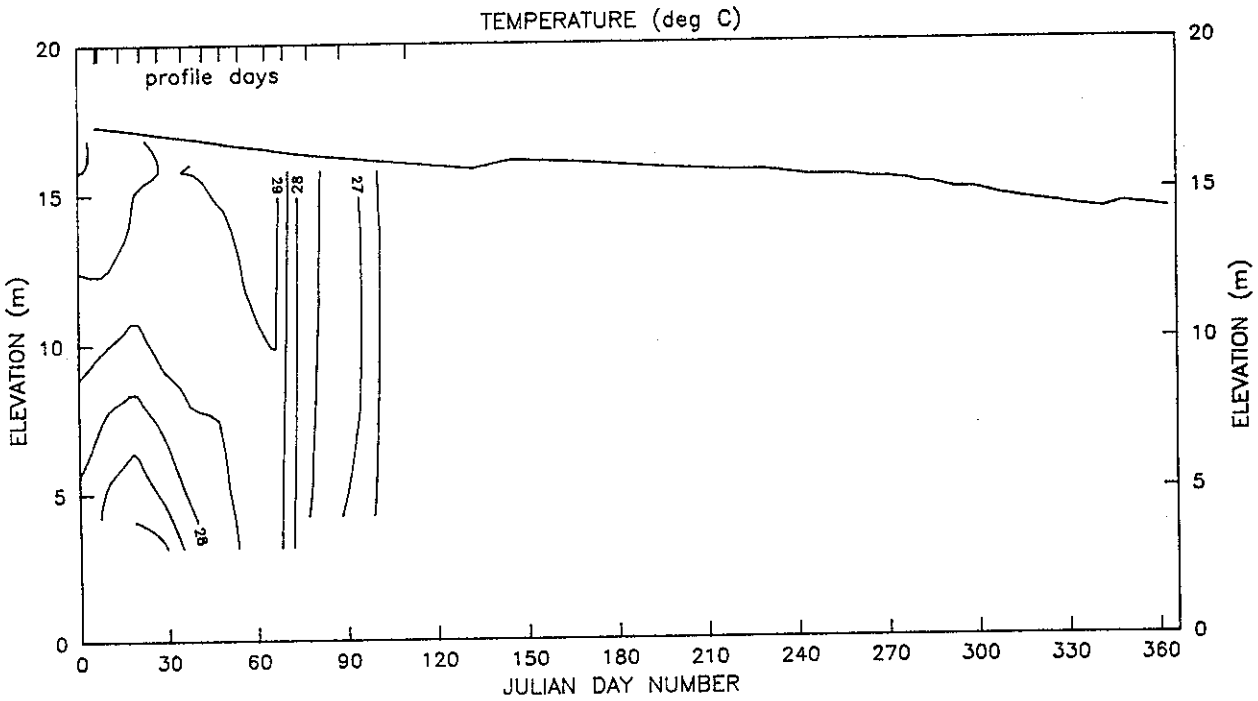

HARDING DAM

LOCATION: Q7091079 (2.5km from Dam Wall)
PERIOD: 1st Jan–31st Dec 1988
AERATOR: Mark (I) : 1st Jan–16th Jun 1988
Burn's : 27th Sept–31st Dec 1988
FILE: Data88.025

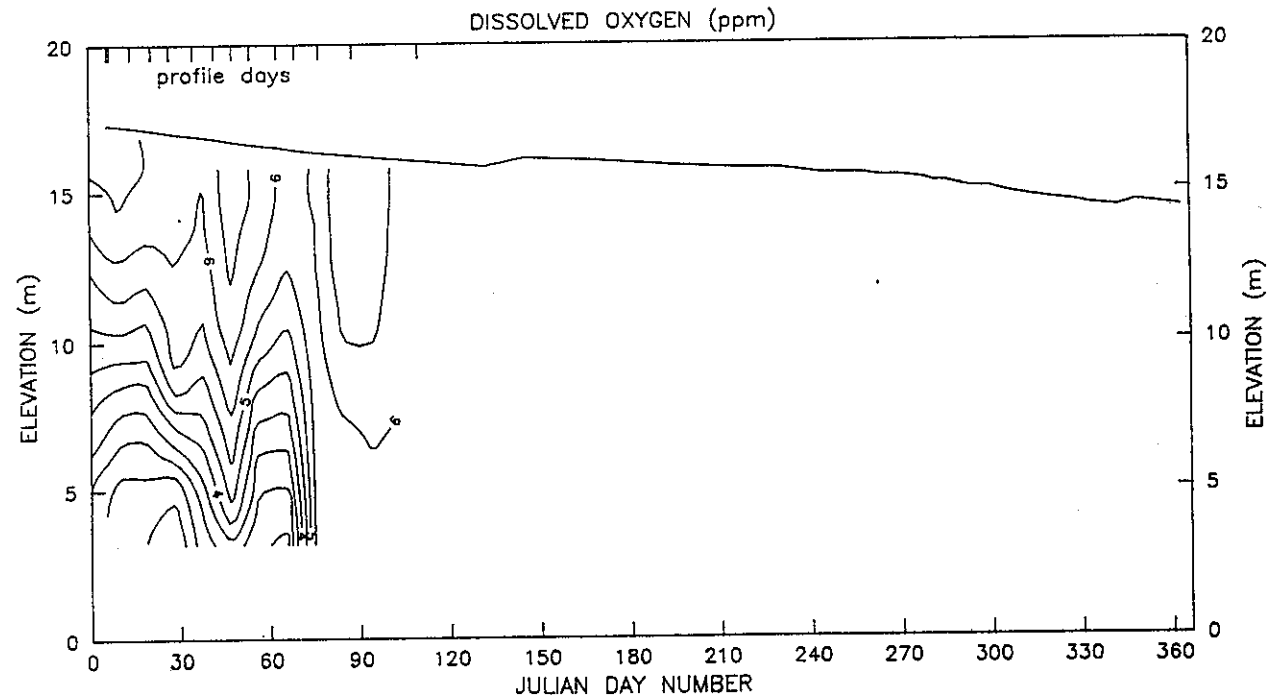

HARDING DAM

LOCATION: Q7091080 (3.5km from Dam Wall)
PERIOD: 1st Jan–31st Dec 1988
AERATOR: Mark (I) : 1st Jan–16th Jun 1988
Burn's : 27th Sept–31st Dec 1988
FILE: Data88.035

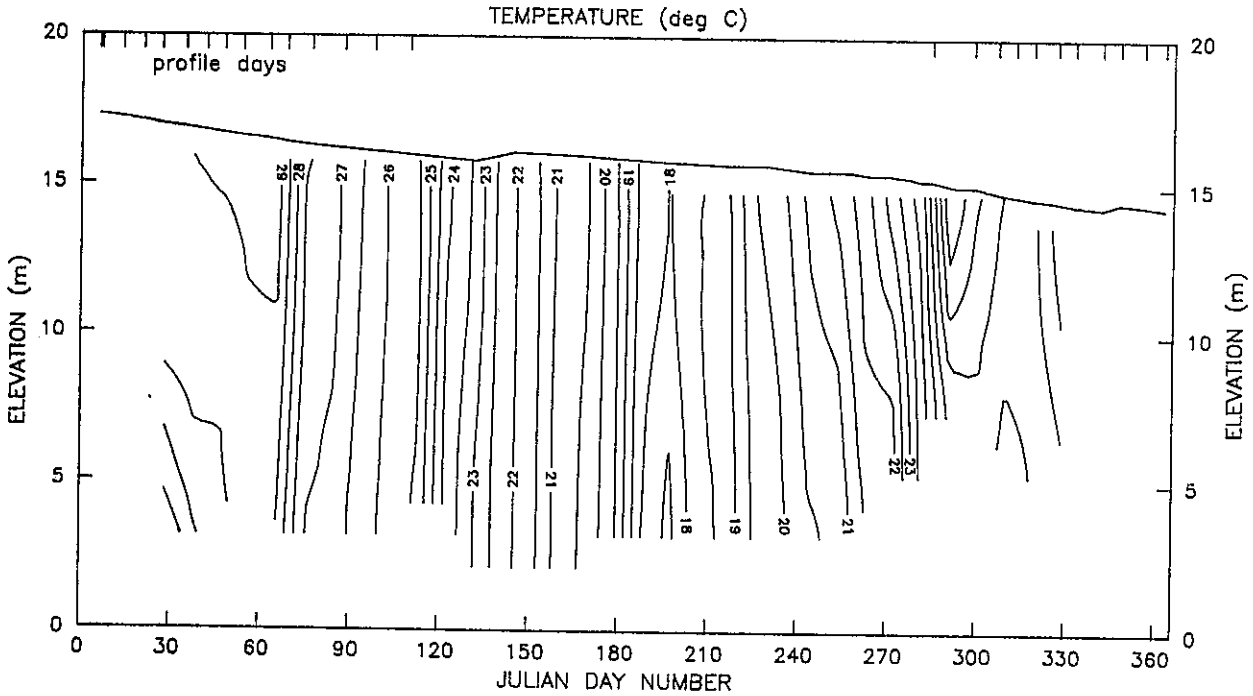

HARDING DAM

LOCATION: Q7091080 (3.5km from Dam Wall)
PERIOD: 1st Jan–31st Dec 1988
AERATOR: Mark (I) : 1st Jan–16th Jun 1988
Burn's : 27th Sept–31st Dec 1988
FILE: Data88.035

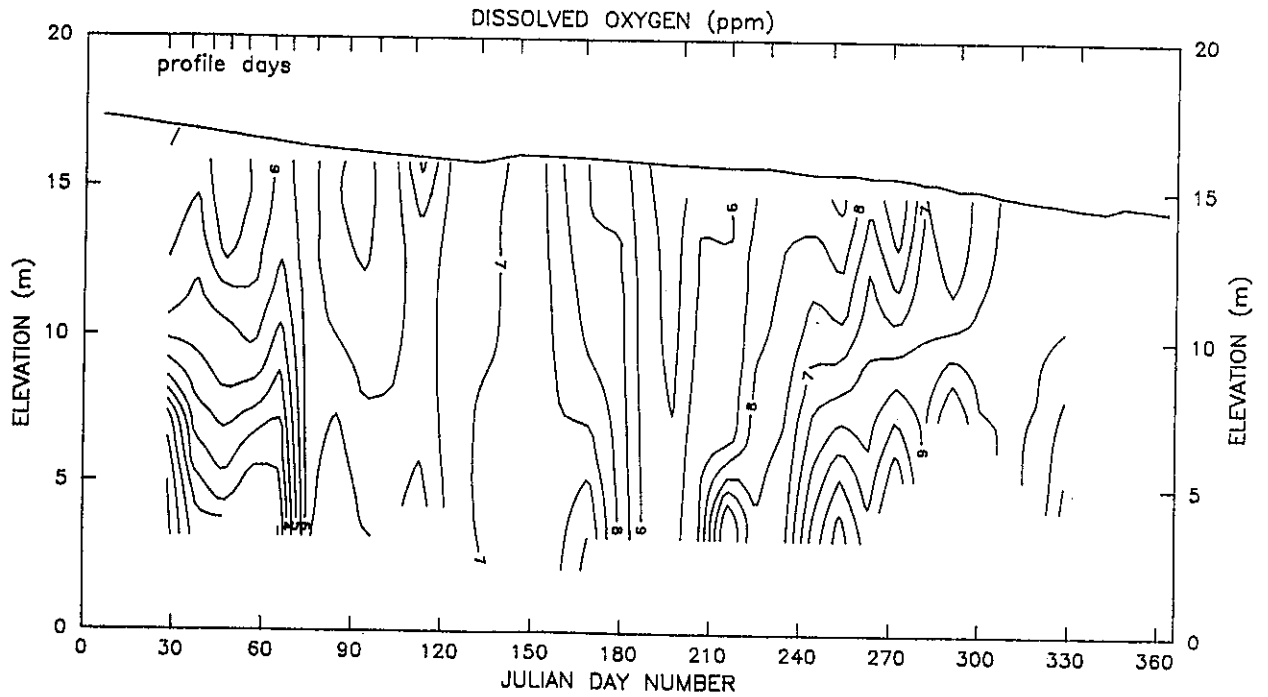

UWRAA RESEARCH REPORTS

Report No.	Title	Author
1	Trickling filter - solids contact process: Pilot plant studies.	M. Laginestra
2	A model of water pricing for Melbourne, Sydney and Perth	P.B. Dixon P.M. Norman
3	Taste generation associated with chloramination	M. Kerslake
4	Bacterial regrowth in water supplies	K. Power L.A. Nagy
5	Leakage management: Assessing the effect of pressure reduction on losses from water distribution systems	B. Horvath
6	Improving communication with the public on water industry policy issues	B.E. Nancarrow G.J. Syme
7	Water use efficiency of domestic appliances	I.J. Beith D.J. Horton
8	Pilot plant study of fermentation units to increase degradable COD fraction in sewage.	P.J. Bliss D. Barnes P.R. Evans I. Law
9	Artificial destratification of water storages in Australia.	T.F. McAuliffe R.S. Rosich
10	Taste thresholds of monochloramine and chlorine in water	R. O'Halloran C. Veres
11	Chromatographic analysis of chloramines using electro-chemical detection	R. O'Halloran Hai Lin Ge P. Spizziri
12	Glass reinforced plastic bore casing for large diameter and deep bores	R. Bowyer
13	A guide to improving communication with the public on water industry policy issues	B.E. Nancarrow G.J.Syme
14	Fouling and cleaning of fine bubble ceramic dome diffusers	K.J. Hartley
15	Chloramination of Water Supplies	P.M. Thomas (ed)
16	The 1988 Australian Winter Storms Experiment: Report on aircraft observations	J.B. Jensen
17	Pipeline assets: Life cycle management and economic life	R. Vass M. Anderson R. Lewis D. Samson
18	Development of empirical model for trade waste discharges to small treatment plants	Camp Scott Furphy
19	PRELIM users guide (Amended): Australian Version	Camp Scott Furphy
20	Chemical regeneration of activated carbon: Preliminary studies	G. Newcombe
21	Management and display of dam surveillance data	D.M. Stirling G.L. Benwell A.B. Murnane
22	Evaluation and demonstration facilities for primary sensors	J.A. Lanaway M. Cavey